

Electronic Thesis and Dissertation Repository

---

3-24-2017 12:00 AM

## Wall Pressure Coefficients for Low- to High-Rise Buildings

Emilio S. Hong, *The University of Western Ontario*

Supervisor: Gregory A. Kopp, *The University of Western Ontario*

A thesis submitted in partial fulfillment of the requirements for the Master of Engineering  
Science degree in Civil and Environmental Engineering

© Emilio S. Hong 2017

Follow this and additional works at: <https://ir.lib.uwo.ca/etd>



Part of the [Civil Engineering Commons](#)

---

### Recommended Citation

Hong, Emilio S., "Wall Pressure Coefficients for Low- to High-Rise Buildings" (2017). *Electronic Thesis and Dissertation Repository*. 4488.

<https://ir.lib.uwo.ca/etd/4488>

This Dissertation/Thesis is brought to you for free and open access by Scholarship@Western. It has been accepted for inclusion in Electronic Thesis and Dissertation Repository by an authorized administrator of Scholarship@Western. For more information, please contact [wlsadmin@uwo.ca](mailto:wlsadmin@uwo.ca).

## Abstract

Currently, the design of wall cladding and components are based on provisions provided in building codes, such as ASCE 7 for the United States. These codes provide pressure coefficients based on the tributary area, position on the building and the building category. For ASCE 7, low-rise and high-rise buildings are separated by an artificial boundary at 60 ft. (18.2 m). The reasoning for this artificial boundary is unclear. This work investigates the wall pressure coefficients for various buildings, based on aspect ratios, motivated by the large differences in design pressure coefficients for low-rise and high-rise buildings.

For this study, a systematic wind tunnel study was performed examining a square plan building with different aspect (i.e., height-to-width ratio) ratios. The wind profile and turbulence intensities were examined to determine the model-scale appropriate for the multiple building heights. Once the model-scale was selected, height configurations of low-rise ( $H/W < 1$ ) and high-rise ( $H/W > 1$ ) buildings were tested. A statistical analysis was performed on these pressure coefficients and these values were converted to  $GC_p$  (gust factored pressure coefficients) values, as a function of (full-scale) area. The pressure coefficients were compared to studies found in the literature to ensure the reliability of the data. Pressure patterns were observed and the impact of the wind directions was analyzed. Cladding element position and pressure coefficients were compared for the different buildings. The pressure coefficients were compared to ASCE 7.

This study concluded that the aspect ratio affected the length of the wall separation bubble, with smaller aspect ratios having more compressed separation bubbles. For positive pressure coefficients, low-rise buildings have different zones of pressure while high-rise buildings are more uniform. For negative pressure (i.e., suction) coefficients, the patterns continually vary with the different aspect ratios. The study showed that there were some aspects of ASCE 7 that were not in good agreement with the data.

**Keywords:** Low-Rise Buildings, High-Rise Buildings, Walls, Pressure Coefficients, Wind Tunnel

## Acknowledgements

First and foremost, I would like to thank Dr. Greg Kopp. I started working with Dr. Kopp in the summer of 2014, since then I feel I have grown considerably as a person and researcher through his advice and mentorship. Outside of his knowledge as a researcher, he has created a great work environment and provided many opportunities to succeed. I have enjoyed my time working with him and look forward to continuing to work with him in the future.

Throughout my studies, I have had the pleasure of sharing a small office with Rahul, Sarah, Anant, Aaron and Arif. I have been fortunate to have such officemates and have enjoyed the numerous days that we have spent together in this cramped space and our discussions on various topics. They have provided some excellent company during this degree, such as the late night with assignments or the summer afternoons enjoying the weather. I would like to acknowledge the other research group members, particularly Chieh-Hsun for his help, I do not know how many more hours I would have spent on MATLAB without his assistance. I would also like to thank the Boundary Layer Wind Tunnel Laboratory staff and technicians for their help with the experimental portions of this project.

Finally, I would like to thank my family and friends for their support during this degree. I appreciate the efforts people have made to look at everything I have asked them to, despite how difficult the material may be or how urgently I asked. I would like to thank my father, for providing me with an additional mentor and for giving his full support throughout these graduate studies.

# Table of Contents

Abstract.....	i
Acknowledgements.....	ii
List of Figures.....	v
List of Tables.....	vii
Nomenclature.....	viii
Chapter 1 Introduction.....	1
1.1 Background and Literature Review.....	1
1.1.1 Preface.....	1
1.1.2 Pressure Coefficients and Wind Characteristics.....	2
1.1.3 Literature Review.....	3
1.1.4 Building Codes: Past and Present ASCE 7.....	9
1.2 Objectives.....	15
1.3 General Approach.....	16
1.4 Scope of Project.....	17
1.5 Overview of Thesis.....	18
Chapter 2 Methodology and Analysis Procedure.....	20
2.1 Geometry of the Building Model.....	20
2.2 Wind Tunnel Test Parameters.....	24
2.3 Scaling.....	29
2.3.1 Definitions.....	30
2.3.2 Scaling Method.....	31
2.4 Data.....	37
2.4.1 Area Averaging.....	38
2.4.2 Extreme Value Analysis.....	39
2.4.3 Conversion Factor for ASCE 7.....	41
Chapter 3 Analysis of Wall Pressure Coefficients.....	43
3.1 Reliability of Data.....	43
3.1.1 Comparisons between Measured Test Results.....	43
3.1.2 Comparisons with External Data Sets.....	45
3.2 Pressure Distributions.....	48
3.2.1 Peak Pressure Coefficients.....	48

3.2.2 Wind Direction Effects .....	50
3.2.3 Mirroring the Pressure Coefficients and Normalizing .....	56
3.3 Cumulative Distribution Functions .....	62
3.3.1 Distributions for Different Aspect Ratios.....	62
3.3.2 Comparing Different Tributary Areas .....	64
3.4 Pressure Coefficients vs Position .....	67
3.4.1 Comparison of Vertical Position on Building .....	67
3.4.2 Comparisons of Horizontal Position on Building.....	68
3.4.3 Comparisons of Position Away from Edges.....	71
3.5 Current ASCE Building Code Comparison .....	73
3.6 Implications .....	81
Chapter 4 Conclusion and Recommendations .....	83
4.1 Conclusions .....	83
4.2 Recommendations .....	85
References .....	86
Appendices.....	90
Appendix A .....	90
Appendix B .....	91
Appendix C .....	92
Curriculum Vitae .....	93

## List of Figures

Figure 1-1: Zoning for ASCE 7-88 (1988) with low-rise on the left and high-rise on the right. The zones for the low-rise are a length of 10% of building width and high-rise zones are a length of 5% of building width. ....	11
Figure 1-2: Pressure coefficients for ASCE 7-88 (1988) for walls of low-rise and high-rise buildings. This shows the pressure coefficients for positive and negative pressure coefficients based on the size of the cladding and component. The zones are given in Figure 1-1. ....	12
Figure 1-3: Zoning for high-rise building from ASCE 7-95 to present. ....	13
Figure 1-4: Pressure coefficients for ASCE 7-95 (1995) for walls of low-rise and high-rise buildings. This shows the pressure coefficients for positive and negative pressure coefficients based on the size of the cladding and component. The zones are given in Figure 1-1 for low-rise and Figure 1-3 for high-rise. This figure has remained unchanged for later iterations of the ASCE 7 building provisions. ....	14
Figure 1-5: Three building shapes depicting the three categories based on H/W ratios. ....	18
Figure 2-1: Picture of wind tunnel model at tallest H/W configuration with the pressure tap panel 3 <sup>rd</sup> from the bottom. ....	20
Figure 2-2: Elevation of the building model used displaying the ten panels and the bottom line shows the floor (ground plane). The dimensions shown indicate the side length and panel lengths. The figure shows the units in mm inside the square brackets and inches. ....	21
Figure 2-3: Drawing of the high resolution of pressure taps on instrumented panel used on the wind tunnel building model. Square brackets indicate mm dimensions, other dimensions are in inches. ....	23
Figure 2-4: Wind tunnel model in configuration of a 5 panel tall building with the pressure tap panel at the top of the building. This yields a H/W ratio of 1.32. ....	24
Figure 2-5: Photograph of the wind tunnel with the model inside facing a 180 degree angle. This image shows the exposure used in the background. This terrain configuration involved the barriers, block heights, scattered nuts and spires. The model is set in a 6 panel high configuration (H/W = 1.66). ....	25
Figure 2-6: Wind tunnel model with 0°, 90° and 180° indicated on the figure. During testing, the turn table rotated so the wind would be coming from the indicated direction. ....	26
Figure 2-7: Wind profile for a building of H/W ratio of 2.58. Displaying turbulence intensity and mean wind speeds. ....	34
Figure 2-8: Power spectral density for high-rise building at a model-scale height of 0.67m. ....	35
Figure 3-1: Maximum pressure coefficient values, $G_{Cp}$ , for H/W = 1.83, enveloped over the measured wind directions, for two separate and independent tests, (a) Set 1, (b) Set 2. ....	43
Figure 3-2: Minimum pressure coefficient values, $G_{Cp}$ , for H/W = 1.83, enveloped over the measured wind directions, for two separate and independent tests, (a) Set 1, (b) Set 2. ....	44
Figure 3-3: Individual pressure tap comparison for H/W=2.58 with the panel at the top most position. The comparison shows Set 1 in red and Set 2 in blue for three different pressure tap locations. The location is indicated by the tap position indicated in Chapter 2. ....	45
Figure 3-4: Adaptation Castro and Robins (1977), the convention used for their test of the Silsoe Cube with the wind direction indicated by the arrow. For the comparison, 0 to 1 will be represented by line A going upwards along the height and 2 to 3 will be represented by line C going downwards along the height. ....	46
Figure 3-5: a) Comparison of mean pressure coefficients along the windward wall taken for a wind direction of 0°. The vertical coordinate system is with 0 at the bottom of the wall and 1 at the top of the wall, following the nomenclature of Castro & Robins (1977). b) Comparison of mean pressure coefficients along the windward wall taken at a wind direction of 180°. The lengths are taken with 3 at the bottom of the wall and 2 at the top of the wall, following the nomenclature of Castro & Robins. ....	47
Figure 3-6: Peak positive pressure coefficients for low-rise building (a) and high-rise building (b). ....	49
Figure 3-7: Peak negative pressure coefficients for low-rise building (a) and high-rise building (b). ....	49
Figure 3-8: Wind direction definition based on the wind flow of the wind tunnel. The initial position of the pressure tap panel faces the wind flow and rotates with the turn table. The presented configuration is of a wind direction of 90°. ....	50

Figure 3-9: Distribution of the critical wind directions causing highest positive pressures for H/W=0.28 (a) and H/W=2.58 (b). The colour legend is for the wind directions. ....	51
Figure 3-10: Distribution of angles causing the worst suction pressure coefficients for low-rise of H/W=0.28 (a) and H/W=0.56 (b). The colour axis is for the different wind directions. ....	52
Figure 3-11: Distribution of angles causing the worst suction pressure coefficients for high-rise of H/W=1.2 (a) and H/W=2.58 (b). The colour axis is for the different wind directions. ....	53
Figure 3-12: Pressure coefficients for low-rise building (H/W=0.28) at wind directions of 90° (a) and 120° (b). ....	54
Figure 3-13: Pressure coefficients for high-rise building (H/W=2.58) at wind directions of 90° (left) and 120° (right). ....	55
Figure 3-14: Positive pressure coefficients for cladding size of 4.48 m <sup>2</sup> for a) H/W=0.28 b) H/W=0.52 c) H/W=0.80 d) H/W=1.08 e) H/W=1.83 and f) H/W=2.58. ....	58
Figure 3-15: Negative pressure coefficients for cladding size of 4.48 m <sup>2</sup> for a) H/W=0.28 b) H/W=0.52 c) H/W=0.80 d) H/W=1.08 e) H/W=1.83 and f) H/W=2.58. ....	59
Figure 3-16: Positive pressure coefficients for H/W=2.58 a) 1.12 m <sup>2</sup> cladding size b) 4.48 m <sup>2</sup> cladding size c) 17.90 m <sup>2</sup> cladding size d) 71.62 m <sup>2</sup> cladding size e) 286.47 m <sup>2</sup> cladding size. ....	60
Figure 3-17: Negative pressure coefficients for H/W=2.58 a) 1.12 m <sup>2</sup> cladding size b) 4.48 m <sup>2</sup> cladding size c) 17.90 m <sup>2</sup> cladding size d) 71.62 m <sup>2</sup> cladding size e) 286.47 m <sup>2</sup> cladding size. ....	61
Figure 3-18: Cumulative distribution functions at different H/W ratios for cladding size 4.48 m <sup>2</sup> for positive pressure coefficients. ....	63
Figure 3-19: Cumulative distribution functions at different H/W ratios for cladding size 4.48 m <sup>2</sup> for negative pressure coefficients. Zoomed in view of 0.9 to 1.0. ....	64
Figure 3-20: Cumulative distribution function for the different cladding sizes of H/W=0.52 for a) positive and b) negative pressure coefficients. ....	65
Figure 3-21: Cumulative distribution function for the different cladding sizes of H/W=2.58 for a) positive and b) negative pressure coefficients. ....	66
Figure 3-22: Pressure coefficients for H/W=2.58 comparing the pressure coefficients of cladding size 4.48 m <sup>2</sup> along the height of the building for a) positive pressures b) suction. ....	68
Figure 3-23: Pressure coefficients for H/W=1.08 comparing the pressure coefficients of cladding size 4.48 m <sup>2</sup> along the width of the building for a) positive pressures b) suction. ....	69
Figure 3-24: Negative pressure coefficients for cladding size 4.48 m <sup>2</sup> along the width of the building a) H/W=0.52 and b) H/W=2.58. ....	70
Figure 3-25: Pressure coefficients for H/W=1.08 comparing the pressure coefficients of cladding size 4.48 m <sup>2</sup> compared by the distance away from the edge of the wall for a) positive pressures b) suction. ....	71
Figure 3-26 Negative pressure coefficients for cladding size 4.48 m <sup>2</sup> along the width of the building a) H/W=1.83 and b) H/W=2.58. ....	72
Figure 3-27 Negative pressure coefficients for cladding size 4.48 m <sup>2</sup> along the width of the building a) H/W=0.52 and b) H/W=0.28. ....	73
Figure 3-28: Comparison between the code and collected pressure coefficient values for high-rise buildings. The code values are from ASCE 7-10. ....	74
Figure 3-29: Comparison between the code and collected pressure coefficient values for low-rise buildings. The code values are from ASCE 7-10. ....	75
Figure 3-30: Comparison of the code provisions and observed data for H/W=0.28. The code values are from ASCE 7-10. ....	75
Figure 3-31: Comparison of the code provisions and observed data for H/W=0.52. The code values are from ASCE 7-10. ....	76
Figure 3-32: Code comparison for high- and low-rise compared with the cube configuration (H/W=1.08). The code values are from ASCE 7-10. ....	76
Figure 3-33: Comparison of positive pressure coefficients for low-rise buildings between ASCE 7, Gavanski and Uematsu (2014) and the current study (H/W=0.28, H/W=0.58, H/W=0.80). ....	78
Figure 3-34 Comparison of interior zone negative pressure coefficients for low-rise buildings between ASCE 7 (Zone 4), Gavanski and Uematsu (2014) and the current study (H/W=0.28, H/W=0.58, H/W=0.80). ....	78

Figure 3-35: Comparison of edge zone negative pressure coefficients for low-rise buildings between ASCE 7 (Zone 5), Gavanski and Uematsu (2014) and the current study (H/W=0.28, 0.58, 0.80).....79

Figure 3-36: Comparison of edge zone negative pressure coefficients for low-rise buildings between ASCE 7 (Zone 5), Gavanski and Uematsu (2014) and H/W=0.28.....80

## List of Tables

Table 1-1: Papers only concerned with wall pressure coefficients, listed by aspect ratio. ....4

Table 2-1: Configuration heights and H/W ratios.....22

Table 2-2: Height configurations and positions tested and corresponding set that the testing was performed.....27

Table 2-3: Full-scale areas used in the analysis, assuming a length scale of 1:200. ....39

Table 2-4: Factors used for Lieblein BLUE. ....40

Table 2-5: Velocity conversion factors for all height configurations .....42



## Nomenclature

$A$	Total tributary area
$a$	Edge length distance used in ASCE 7
$a_{ij}$	Tributary area for each tap
$a_i$	Factor used in Lieblein analysis
$b_i$	Factor used in Lieblein analysis
$b'_n$	Parameter used in Lieblein analysis
$C_p$	Pressure coefficient
$F_{WT}$	Factor from model scale to full scale for $GC_p$ values
$f$	Frequency
$f_0$	Coriolis parameter
$GC_p$	Pressure coefficient with gust factor
$GC_{pf}$	Peak pressure coefficient
$H$	Height of building
$I_u$	Turbulence intensity
$k_d$	Directionality factor
$k_h$	Velocity pressure exposure factor
$k_{zt}$	Terrain factor
$L$	Characteristic length
$L_t$	Integral time scale
$L_x$	Longitudinal integral length scale
$n$	Number of samples
$p$	Recorded pressure
$p_{ASCE}$	Design pressure
$p_o$	Static pressure
$U_r$	Reference height wind speed
$U_z$	Wind speed at a particular height $z$
$U_{zx}$	Local wind speed at a particular height $z$
$U_{10m, model}$	Wind speed at the model scale equivalent of 10 m
$U_{10}$	Wind speed at 10 m
$u$	Wind speed
$u_H$	Roof height wind speed
$u_i$	Wind speed at a particular time
$u'_n$	Parameter used in Lieblein analysis
$\bar{u}$	Mean wind speed
$u_*$	Friction velocity
$u_{10 m oc 3 sec gust}$	3 second gust at reference height of 10 m in open terrain
$W$	Width of building
$x_f$	Parameter for determining power spectrum
$z$	Height from ground
$z_r$	Reference height
$z_0$	Roughness length

$\alpha$	Coefficient used in calculation for power law
$\Delta$	Segment length
$\eta$	Parameter from ESDU 85 (1985)
$\lambda_B$	Scaling parameter for width of building
$\lambda_L$	Scaling parameter for length scale
$\nu$	Kinematic viscosity of air
$\rho$	Density of air
$\rho_{uu}$	Autocorrelation
$\sigma$	Standard deviation
$\sigma_u$	Streamwise standard deviation
$\sigma_{ux}$	Local streamwise standard deviation
$\tau$	Time lag
$\phi$	Latitude of location on Earth
$\omega$	Speed of the rotation of the Earth

# Chapter 1 Introduction

## 1.1 Background and Literature Review

### 1.1.1 Preface

There have been many developments in wind engineering as a practice over the last several decades. Experimental wind simulations have developed significantly over this time period. Wind tunnel approaches have advanced; there are now laboratories that can replicate non-synoptic winds such as tornadoes (Natarajan and Hangan, 2010). Wind engineering has become multi-disciplinary, involving the fields of statistics, meteorology, fluid mechanics and structural dynamics (Holmes, 2015). The wind forces on structures can often be determined using the velocity pressure, the drag coefficient and local pressures. The responses of a structure can be summarized by the Davenport Chain, described by five links: the climate factor, exposure factor, aerodynamic shape, influence factor and dynamic amplification factor (Davenport, 2002).

Buildings have long been an interest of wind engineering. Early studies of low-rise buildings can be dated back to the late 1800s by Baker (1895). High-rise buildings have been studied in wind engineering with famous examples such as the World Trade Center and the CN Tower (Davenport, 2002). Many different building scenarios have been tested in wind tunnels to determine possible wind effects. The design of these buildings is important and many new buildings are being built every year. Estimations are that billions of dollars will be invested in infrastructure over the next several years in Canada alone (Globe and Mail, 2016). Companies are not only building more buildings, but push the limits of design including building taller and skinnier buildings (Higgins, 2015).

With all this infrastructure in place, there are the risks associated with these structures due to wind hazard. Cladding and components receive wind forces directly and are often one of the first failures in intense wind events. Failures of cladding and components cause additional problems, such as wind-borne debris, internal water damage, structural damage and internal pressure forces. As a result, the proper design of cladding and components for wind is important as small losses can turn into much larger losses and these details influence overall resilience of a structure in a given wind event.

The focus of this thesis is to examine the wind loads on wall cladding and components for low- and high-rise buildings. This work will aim to characterize different wind loading characteristics based on several different geometric factors.

### 1.1.2 Pressure Coefficients and Wind Characteristics

A pressure coefficient is a dimensionless value that describes relative pressures. For structural engineering, pressure coefficients are used to describe the aerodynamic effects on a structure. Additionally, aerodynamic effects can be tested in model-scale using wind tunnels. A pressure coefficient is defined as:

$$C_p = \frac{(p-p_o)}{0.5\rho U_H^2} \quad (1-1)$$

where  $C_p$  is the pressure coefficient,  $p$  is the recorded pressure,  $p_o$  is the static pressure of the atmosphere,  $\rho$  is the density of air and  $U_H$  is the wind speed, for the wall pressure coefficient,  $U_H$  was taken at the roof height. In building codes, pressure coefficients are used to determine the pressures that will be applied to tributary areas.

Pressure coefficients primarily characterize the geometry of the building, although they do depend on turbulence (i.e. terrain). To determine the wind loading on a structure, other factors affect the magnitude of these forces. When examining a structure, the wind climate that the structure is placed in affects the potential loading. This ranges from the expected wind speeds to the terrain roughness coefficients surrounding the area, referred to as exposure. These characteristics are used to determine the wind loads on a structure.

### 1.1.3 Literature Review

The pressure coefficients of walls have been investigated in many studies. Past studies have examined low-rise and high-rise buildings; however these studies often did not study both types of buildings. Larger scale tests have been performed such as the Silsoe Cube (e.g., Castro and Robins, 1977), testing at a larger scale, and full-scale tests for low-rise buildings (Kopp et al., 2012). The cube,  $H/W=1$ , where  $H$  is the building height and  $W$  is the side length, has been studied on multiple occasions due to its simple geometry (e.g., Uematsu and Isyumov, 1999). Wall pressure coefficient studies vary in tap densities used for measurements. Most of these studies have not been focused on analysis of pressure coefficient for codification purposes, instead examining different phenomena that may occur on a building's walls. Some of these studies have used computational fluid dynamics to assist or replicate results determined experimentally. Table 1-1 lists some of the published papers concerning wall cladding pressure coefficients. This table indicates the number of pressure taps used for the study, the  $H/W$  ratios examined and the building category observed (low-rise, high-rise or cube-like).

Table 1-1: Papers only concerned with wall pressure coefficients, listed by aspect ratio.

Authors	H/W	Building Category	Number of Taps	Comments
Tielmann et al. (1997)	0.30	Low	23	Turbulence intensity for replicating full-scale wind loads
Tielmann et al. (1998)	0.30	Low	50	Parameters for wind tunnel study of low-rise buildings
Uematsu and Isyumov (1999)	0.30	Low	30	Examination of peak factors
Tamura et al. (2001)	0.25	Low	416	Peak factors and pressure distributions
Zisis and Stathopoulos (2009)	0.33	Low	38	Full scale testing of pressure coefficients
Gavanski et al. (2014)	0.20	Low	366	Area averaging used to compare code values
Castro and Robins (1977)	1.00	Cube	45	Effects of turbulent and smooth flow
Richardson et al. (1997)	1.00	Cube	77	Reliability of wind tunnel tests and the effects of varying parameters
Hölscher et al. (1998)	1.00	Cube	189	Comparing multiple wind tunnels
Richards et al. (2007)	1.00	Cube	88	Re-examination of the Silsoe cube
Irtaza et al. (2012)	1.00	Cube	61	Sheet cladding on cube building
Kim et al. (2012)	1.00	Cube	25	Low rise building study, focus on neighbouring effects
Ramponi et al. (2014)	1.00	Cube	60	Other factors affecting pressure coefficients
Maruta et al. (1988)	3.00	High	202	Effects on glass cladding
Lin et al. (2005)	3.00-4.00	High	120	Characteristics of wind forces acting on tall buildings
Zhang and Gu (2008)	6.00	High	100	Staggered arrangement effects
Dagnew et al. (2009)	4.00	High	150	Comparison between numerical modeling and wind tunnel

Cóstola et al (2009)	2.10	High	30	Complexity of wind tunnel studies and the variation between different wind tunnels
Kim et al. (2011)	4.00	High	252	Interference effects on local peak pressures between two buildings
Hui et al. (2012)	4.00	High	252	Mutual interference effects between two high-rise building models with different shapes on local pressure coefficients
Hui et al. (2013)	4.00	High	252	Pressure and flow field investigation of interference effects on external pressures between high-rise buildings

*1.1.3.1 Studies on Low-Rise Buildings*

Most of the buildings in the world are low-rise buildings. Low-rise buildings are generally defined to be lower than wide. Stathopoulos et al. (1979) performed tests on low-rise buildings to determine the pressure coefficients for walls and roofs. The study examined the codification approach along with the magnitudes of pressure coefficients. Observations were made for many different factors affecting pressure coefficients on low-rise buildings such as dynamic loads, terrain roughness, scale and local wind effects. Uematsu and Isyumov (1999) studied peak effects for determination of pressure coefficients for design purposes. Wind tunnel data collected in the study showed different characteristics compared to the current provisions. This study showed that the current code provisions need to be updated, such as the current approach of evaluating design wind loads for cladding. Tamura et al. (2001) examined peak wind effects on members in low-rise buildings systems, for various loading combinations. One

observation from this study was that higher tap resolution would allow for better understanding of peak effects.

In recent years, the focus has shifted from determining wind pressure coefficients to other external effects that influence pressure coefficients. Some studies have focused on the aerodynamic effects that buildings may have on surrounding buildings. Tests have been performed regarding the neighbourhood effects on wall pressure coefficients (Kim et al., 2012) and the results on the pressure coefficients from different groupings of low-rise buildings (Hussain and Lee, 1980). Many studies have focused on the roof of low-rise buildings, as opposed to examining the walls, because of the significant financial losses associated with roof failures (Lee and Rosowsky, 2005).

Studies have been performed to examine what factors are necessary for proper replication of wind forces at model-scale. Tieleman et al. (Tieleman et al., 1997 and Tieleman et al., 1998) observed parts of the wind profile that affect pressure coefficients. The fluctuations (rms) and peak pressure coefficients are replicated by properly duplicating the turbulence intensities (Tieleman et al., 1997). This is especially important when observing the corners of the building, as incorrect replication of the turbulence intensities will have a greater effect on this location of the building since the corners of the building often have the largest pressure coefficients. The study examined additional parameters such as the replications of small- and large-scale turbulence and integral scales (Tielemann et al., 1998). A study performed by Zisis and Stathopoulos (2000) evaluated the replication of such parameters by comparing the wind data collected from a full-scale test and a model test at 1:200. Gavanski and Uematsu (2014) examined various building parameters and found that some of the current code provisions may be too low for low-rise buildings. The study involved area averaging to determine the pressure



coefficients across the walls. Comparisons were made to ASCE 7-10, with suction coefficients in the code being found to be too high for larger tributary areas and too low for smaller tributary areas. The positive pressure coefficients were found to be relatively uniform across the walls, implying that zoning would only be needed for the suction coefficients.

### *1.1.3.2 Cube-Shaped Buildings*

Cube-shaped buildings are a special case because, with  $H/W=1$ , aerodynamically they are a transition between low-rise and high-rise buildings. The aerodynamics are different for  $H/W$  greater and lower than 1 (as will be seen). For higher aspect ratios ( $H/W$ ), the flow tends to go more around the sides of the building, whereas for lower aspect ratios the flow tends to go over the top of the building. Cubes have been extensively studied; Hölscher et al. (1998) established that wind tunnels could duplicate results if the flow parameters and model geometries are carefully taken into account, similar to the studies by Tieleman et al. described earlier.

Castro and Robins (1977) analyzed the effects from smooth and turbulent flows, on the spatial variations of the pressures. Richards et al. (2007) compared results from the full-scale Silsoe cube to wind tunnel tests. This study found that matching the turbulence spectra is required in addition to matching the mean wind speed profile for proper full-scale results, since the turbulence spectra have a significant effect on the observed peak pressure coefficients. Irtaza et al. (2012) did further comparisons with the Silsoe cube and wind tunnel tests, re-testing the model with a focus in the sheet-clad scaffolds. This helped to further validate the use of wind tunnels to determine pressure coefficients.

Ramponi et al. (2014) studied different external effects that affect the pressure coefficients on the model. Richardson et al. (1997) used the cube case to determine the reliability of wind tunnels and observed that various parameters such as the scale factors, wind profiles and tapping position are required for proper analysis.

### *1.1.3.3 High-Rise Buildings*

The number of high-rise buildings has increased for many large cities. These structures are pushing past previous records, with buildings being built taller and with thinner aspect ratios. Due to their general size, it is difficult to do full-scale testing of such structures. For design, these buildings are often tested in wind tunnels while studies using computer models are emerging.

There have been many academic studies of wind effects on high-rise buildings. High-rise buildings often focus on different phenomena. These include effects such as instantaneous peak pressure coefficients (Maruat et al., 1998), staggered arrangement effects (Zhang and Gu, 2008), interference effects (Kim et al., 2011 and Hui et al. 2013) and neighbouring effects (Hui et al. 2012). Zhang and Gu used a similar tap position at different heights along the building and made comparisons of the pressure coefficients at different positions. The effects of future building on existing buildings was studied by Irwin et al. (1998) for cladding pressures. Lin et al. (2005) studied the wind characteristics of several wind tunnel models. The study found that the side ratio, the aspect ratio and elevations affected local wind force coefficients, spectra and span wise cross correlation.

Cóstola et al. (2009) used computation fluid dynamic simulations to observe the different results from different wind tunnels, attempting to realize the complexity of wind tunnel

simulations. Cóstola et al. study focused on the different factors (building geometry, exposure/sheltering, wind speed and direction) that influence wind pressure coefficients that should be replicated for proper comparisons. Cóstola et al. used collected primary pressure coefficient data as well as for pressure coefficients from external sources on identical building configurations.

#### *1.1.3.4 Overview of Literature*

The literature gives several different considerations for testing and analysis. These studies did not study pressure coefficients for code purposes, primarily focused on different phenomena for low-rise to high-rise buildings. Many of these studies used relatively low numbers of pressure taps. In fact, many studies used single taps to determine pressure coefficients for tributary areas (Kumar et al., 2000). Table 1-1 showed a wide range in the densities of pressure taps used. These different studies illustrated the validity of using wind tunnels for analyzing pressure coefficients on structures. There were multiple different parameters that should be taken into consideration for proper simulations such as turbulence, terrain roughness, scale factors, etc. There have been a wide range of aspect ratios studied. It is advantageous for the current study that there are multiple past studies that can be used for validation and comparison with the current data.

#### 1.1.4 Building Codes: Past and Present ASCE 7

For wind design, many countries have their own set of provisions. For the purpose of this study, the ASCE (American Society of Civil Engineers) standard will be used. This is because ASCE has a larger global impact and many building codes around the world, such as Canada's

National Building Code of Canada (NBCC), are influenced by it, to some extent. Mehta et al. (2010) observed the evolution of the wind portions of ASCE 7 and the effects of the changes. In general, the wind portions continue to have similar design philosophies for all ASCE editions, while taking into account new information.

In ASCE 7-10, the pressure coefficient,  $GC_p$ , values are given for cladding and component design. The  $GC_p$  values are used to determine the pressure using the formula:

$$P_{ASCE} = (GC_{pF}) \frac{1}{2} \rho U_{10m\ oc,3\ sec\ gust}^2 k_{zt} k_d k_h I \quad (1-2)$$

where  $P_{ASCE}$  is the design pressure,  $GC_{pF}$  is the peak pressure coefficient,  $\rho$  is the density of air,  $V_{10m\ oc,3\ sec\ gust}^2$  is the 3-sec gust velocity at a reference height of 10 m for an open terrain,  $k_{zt}$  is the terrain factor,  $k_d$  is the directionality factor,  $k_h$  is the velocity pressure exposure factor and  $I$  is the importance factor. The other factors; wind velocity, terrain coefficient, directionality factor, exposure factor and importance, can be grouped together as:

$$q_z = \frac{1}{2} \rho U_{10m\ oc,3\ sec\ gust}^2 k_{zt} k_d k_h I \quad (1-3)$$

which represents the design wind speed at the roof height of the building.

The first versions of ASCE 7 were developed in the late 1980s from the earlier ANSI predecessors. Throughout the iterations of this standard, there have been multiple changes in both the zones to which the pressures are applied and the magnitude of the pressures. This work will only examine the provisions related to the design of walls and ignore the provisions for design of cladding and components of roofs. The current study focuses on the walls, while there have been many studies performed observing the pressure coefficients for various roof shapes. One of the constants throughout these iterations is the formula used to determine the cladding

coefficients, presented above. Other similarities between the different iterations are the separation of low-rise and high-rise buildings, boundary at 18.3 m, reduction due to roof angle and the edge zone length size characteristic. Positive pressure coefficients do not have different zones for all iterations.

ASCE 7-88 (1988) was one of the earlier provisions involving cladding and components. The zoning requirements for low-rise and high-rise buildings were different in this version. Figure 1-1 shows the zoning used. The low-rise zoning has remained consistent for all iterations of ASCE 7, while the high-rise zoning changed after ASCE 7-88.

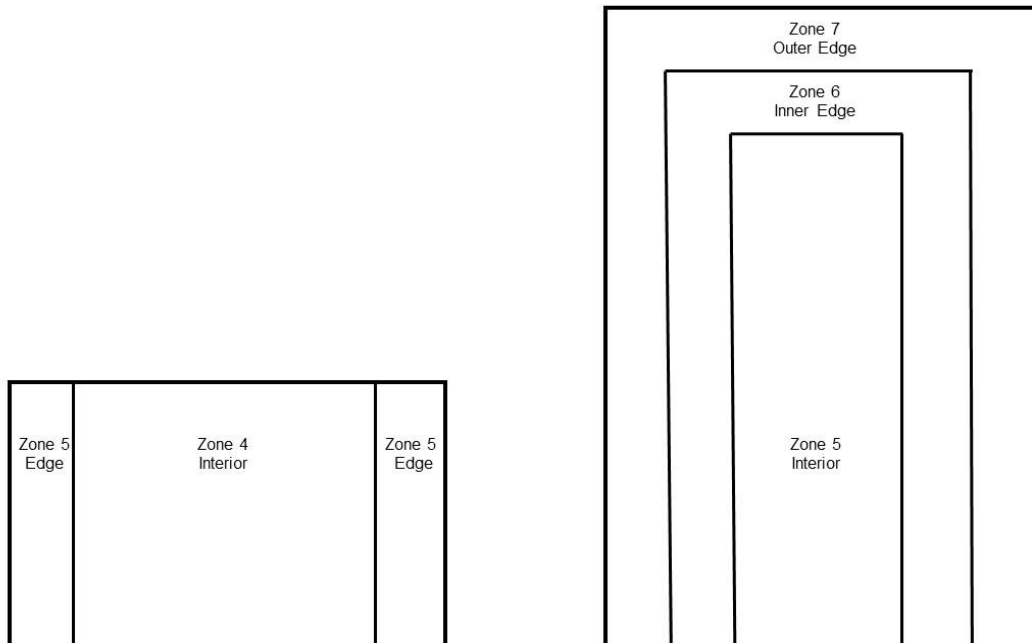


*Figure 1-1: Zoning for ASCE 7-88 (1988) with low-rise on the left and high-rise on the right. The zones for the low-rise are a length of 10% of building width and high-rise zones are a length of 5% of building width.*

For the zoning of zones 4 through 7 shown in Figure 1-1, the width of the zone is given as a parameter  $a$ . This parameter is determined the lower of 10% of the shorter horizontal dimension or 40% of the height for low-rise buildings and 5% of the least horizontal dimension for high-rise buildings. The minimum  $a$  can be is 4% of the least horizontal dimension or 3 ft. (0.91m).

Figure 1-2 shows the pressure coefficients for low-rise and high-rise buildings in ASCE 7-88. The negative pressure coefficients (i.e., suction) decrease in magnitude for zones further from the building edges. There are significant drops in pressure coefficient with the interior zone being less than half of the most exterior zone for high-rise buildings.

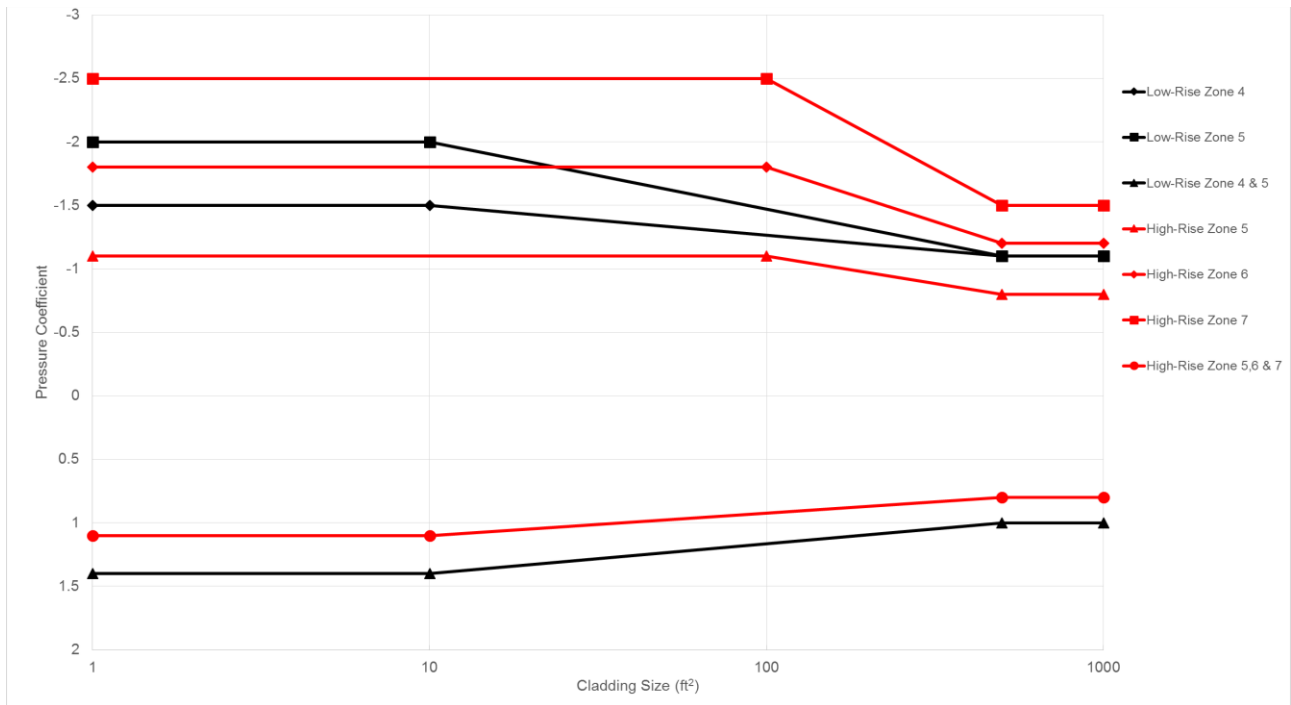
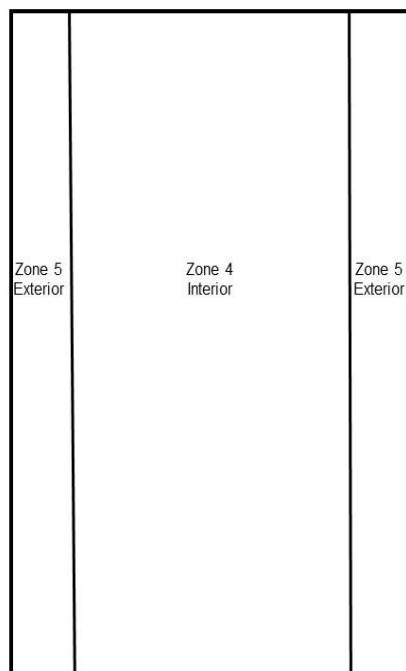


Figure 1-2: Pressure coefficients for ASCE 7-88 (1988) for walls of low-rise and high-rise buildings. This shows the pressure coefficients for positive and negative pressure coefficients based on the size of the cladding and component. The zones are given in Figure 1-1.

ASCE 7-95 (1995) changed the zoning for high-rise buildings, changing the zoning from three zones in high-rise buildings to just two. The reasoning for this change is unclear in the code provisions. Figure 1-3 shows the new zoning for high-rise buildings, which is still used for the current iteration of ASCE 7. ASCE 7-95 (1995) changed the edge zone width to the same requirements as low-rise building with  $a$  increasing to 10% of minimum width opposed to the previous 5%. The zones are now vertical, no longer differentiating zoning for edges along the roof of the building. The naming convention of the zones was changed to be similar to the low-rise building.



*Figure 1-3: Zoning for high-rise building from ASCE 7-95 to present.*

In addition, in ASCE 7-95 the pressure coefficients were decreased in magnitude. The positive pressure coefficients for low-rise buildings and high-rise buildings are much closer in value. Values for the negative pressure coefficients were all decreased significantly through the elimination of zone 7, but also changes in the role of area. Wall edges still have higher negative pressure coefficients. For high-rise buildings, the design pressure coefficients decrease for areas larger than 1.86 m<sup>2</sup>, as opposed to 9.29 m<sup>2</sup> in ASCE 7-88. The values presented in Figure 1-4 would be used for all subsequent ASCE 7 provisions (i.e., for the years 1995, 1998, 2002, 2005 and 2010).

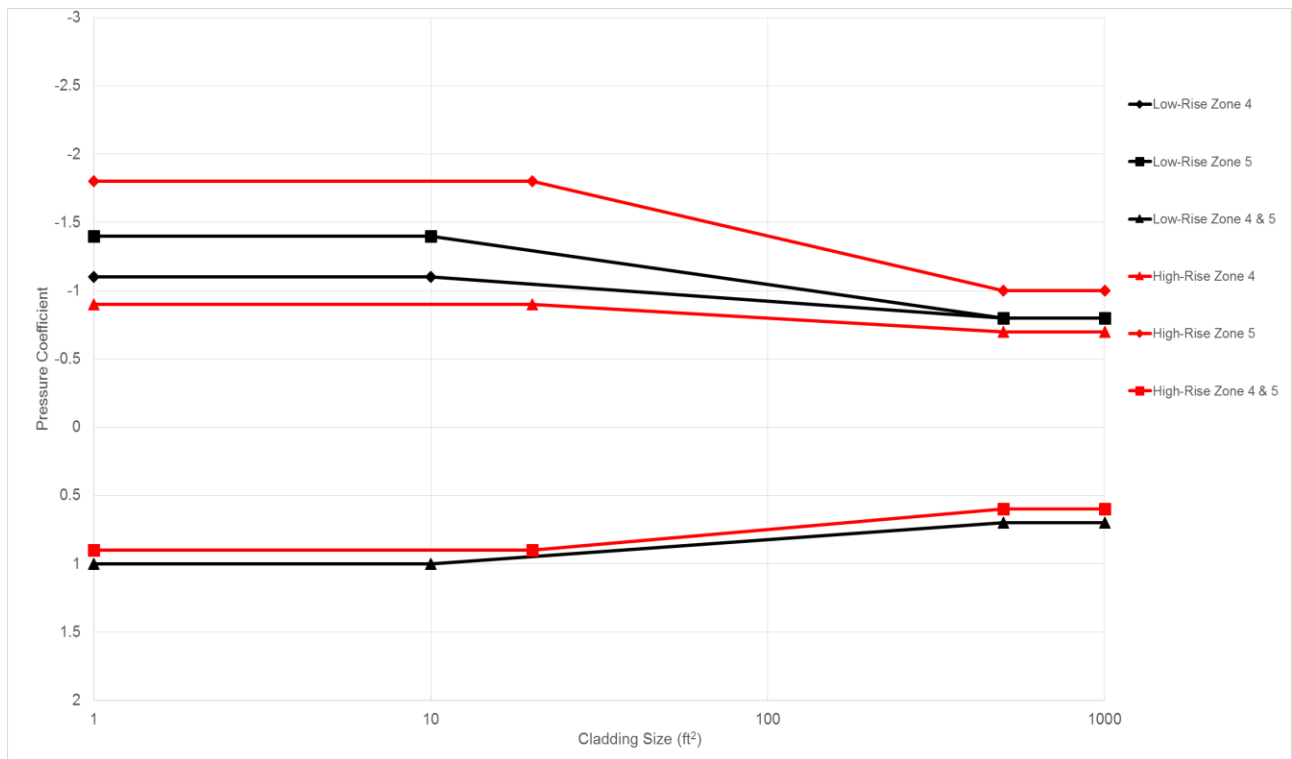


Figure 1-4: Pressure coefficients for ASCE 7-95 (1995) for walls of low-rise and high-rise buildings. This shows the pressure coefficients for positive and negative pressure coefficients based on the size of the cladding and component. The zones are given in Figure 1-1 for low-rise and Figure 1-3 for high-rise. This figure has remained unchanged for later iterations of the ASCE 7 building provisions.



The definition of high-rise and low-rise buildings have been constant for all building codes, with a somewhat artificial boundary at 18.3 m. By the provision's definition, buildings over 18.3 m are considered high-rise buildings while buildings 18.3 m and less are considered to be low-rise buildings. Aerodynamically, buildings that have a height which is less than the least horizontal plan dimensions are "low-rise" as the flows travel over the top of the buildings, whereas buildings with height greater than the plan dimensions are "high-rise", with flows travelling around the sides of the building. The negative pressure coefficients between the two sets of buildings may differ up to 35% between low- and high-rise buildings, as can be seen in Figure 1-4. This causes abrupt changes in the design of cladding and components for buildings around the (artificial) boundary.

## **1.2 Objectives**

The purpose of this investigation is to systematically analyze wall pressure coefficients for buildings from low-rise to high-rise in shape. The hypothesis motivating this work is that the current building code does not adequately represent the aerodynamics because the categorization of buildings as low-rise or high-rise using an artificial boundary may not reflect the physics of the situation. The existing model may be oversimplifying the problem and a systematic study may fill the knowledge gaps. Pressure coefficients have been found to be different in some cases (Gavanski and Uematsu, 2014) and the zoning of cladding elements has changed over time in the ASCE 7 provision. A study using many different configurations will achieve a better understanding of building shape effects of rectangular shaped buildings. With the database of pressure coefficients, the analysis can give insight into the behaviour of wind on these bluff

bodies. Analysis will be performed for different aspect ratios to determine the effects on both the magnitude of pressure coefficients and the spatial patterns (i.e., zones). Ideally, these findings can help formulate recommendations for modified codification, if needed. Due to the high resolution of data, the data set allows for a unique level of detail, which can be used for a variety of purposes.

### **1.3 General Approach**

Experimental tests will be conducted in a wind tunnel to measure pressure coefficients. The set of tests for this study will differ from previous approaches having a much higher density of pressure taps as can be seen in Table 1-1, at least 960 pressure taps for low-rise buildings and up to up to 9600 for high-rise buildings. The larger number of pressure taps provides a higher resolution and minimizes the chance of missing certain pressure patterns. Single tap pressures were used for cladding pressure coefficients in most of the literature, Gavanski and Uematsu (2014) being the notable exception, which oversimplifies the pressure coefficient on larger cladding components, this test will use area averaged pressure coefficient for tributary areas. However, the current tests differ from Gavanski and Uematsu since it involves additional building shapes. The large number of pressure coefficients allow for observing pressure gradients, which is a critical parameter for wind loads on multi-layer wall cladding systems.

The high resolution approach provides much more pressure coefficient information. An example of the high resolution is for the cube, where the present wind tunnel model will use 3840 pressure taps (4 configurations of 960 taps each). Most full-scale testing using the Silsoe cube had between 40-80 pressure taps. On a high-rise building, the number of pressure taps

being used is 1-4 orders of magnitude higher (Maruta et al., 1998) than what is presently being used, as described in the literature review. In all cases, this study's model uses a much larger number of pressure taps than comparable models from Table 1-1. This allows for area averaging to be used in the study which can be described with the equation:

$$C_p = \sum_{i=1}^m \sum_{j=1}^n C_{p_{ij}} \frac{a_{ij}}{A} \quad (1-4)$$

where  $m$  and  $n$  are the number of taps in the area of interest,  $A$ , with  $a_{ij}$  the tributary area of each tap. These dimensions will be marked by the number of pressure taps in the given area, where  $m$  and  $n$  are the vertical and horizontal number of taps, respectively.

The building model has increased flexibility since it can be altered between low-rise and high-rise configurations. This allows for a single model to be used for all tests to examine multiple, different, height configurations and allows for data collection at various heights on the building. This aspect is not commonly used and is another unique aspect of the model. Similar to the categorization of building configurations in Table 1-1, the  $H/W$  ratios were used to compare the buildings. This categorization is seen in Figure 1-5. Of the studies listed in Table 1-1, it is common that each study focused on only one of the building categories. This study aims to connect the low-rise and high-rise buildings better than previously performed studies and should provide correlation between the two types of buildings. A full description of this model can be found in Chapter 2.

#### **1.4 Scope of Project**

The scope of this thesis is to analyze and collect wind tunnel data. Analysis will be completed and patterns will be observed. This study also focuses on interpreting the pressure

coefficients for select building configurations as well as making comparisons with the current ASCE 7-10 (2010) provisions. The analysis will involve examination of the pressure coefficient data and trends between different building configurations. This information will help to refine the current provisions and provide insight into the spatial variations of pressure coefficients on rectangular buildings.

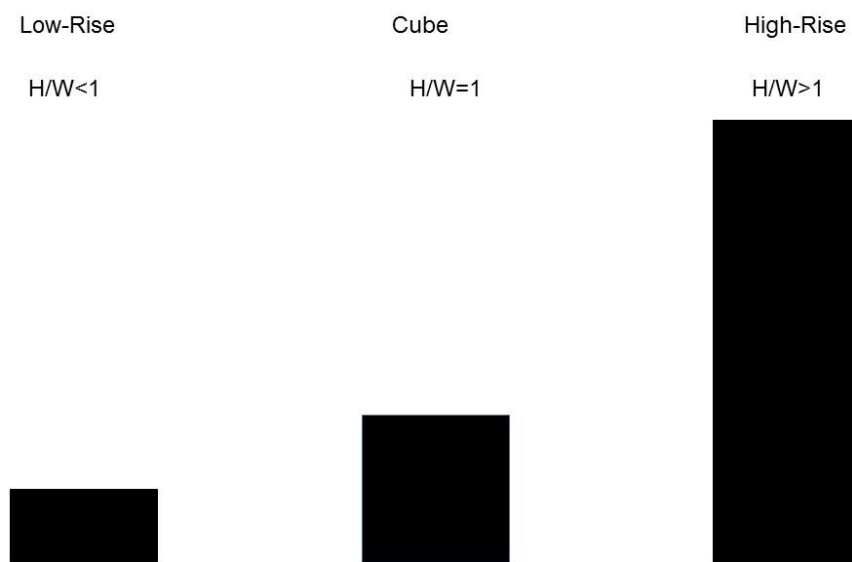


*Figure 1-5: Three building shapes depicting the three categories based on H/W ratios.*

## **1.5 Overview of Thesis**

In this thesis, an experimental study will be presented. Chapter 2 deals with the experimental set-up and methodology. The scaling of the model and wind simulation will be

described along with details of the method of analysis. Chapter 3 will discuss the analysis of the pressure coefficient data. The reliability of the data will be analyzed. Conclusions and recommendations will be discussed in Chapter 4.

## Chapter 2 Methodology and Analysis Procedure

### 2.1 Geometry of the Building Model

A single model was used for all testing at the Boundary Layer Wind Tunnel Laboratory located on the campus of the University of Western Ontario. This model was built by University Machine Services of the University of Western Ontario. Figure 2-1 shows the model in the wind tunnel at the highest height configuration. This model consisted of a rectangular prism with one open side filled with ten removable panels, a roof and an open bottom. As seen in the figure, there are ten removable panels to fill out the open side of the prism. The bottom of the model was open to accommodate the instrumentation required to perform the testing. This model had a square plan, with dimensions of 32.0 cm by 32.0 cm.



*Figure 2-1: Picture of wind tunnel model at tallest H/W configuration with the pressure tap panel 3<sup>rd</sup> from the bottom.*

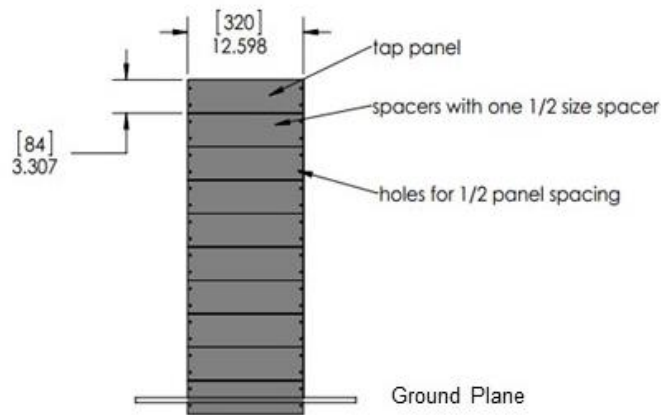


Figure 2-2: Elevation of the building model used displaying the ten panels and the bottom line shows the floor (ground plane). The dimensions shown indicate the side length and panel lengths. The figure shows the units in mm inside the square brackets and inches.

Figure 2-2 shows an elevation view of the model. In the current height configuration, the building has nine panels above the ground plane. One of the panels would contain the instrumentation as the instrumented panel, and the remaining eight panels above the ground plane would be “dummy” panels, containing no instrumentation to finish the wall. The height of the model could be changed by moving the model upwards or downwards through the floor of the wind tunnel. Table 2-1 describes the different heights used and the corresponding  $H/W$  ratios. The different height configurations are separated into three categories: the  $H/W$  ratios above 1 were all considered high-rise buildings;  $H/W=1.08$  was considered to be close to a cube; the remaining buildings ( $H/W<1$ ) were all considered low-rise buildings.

Table 2-1: Configuration heights and H/W ratios.

<b>H (model scale: cm)</b>	<b>Number of Panels</b>	<b>H/W</b>
8.9	1	0.28
16.67	2	0.52
25.72	3	0.8
34.61	4	1.08
42.23	5	1.32
53.18	6	1.66
58.74	7	1.83
67.31	8	2.1
75.4	9	2.35
82.87	10	2.58

Figure 2-3 shows the instrumented panel. This panel contained a total of 960 pressure taps. These taps were arranged in 16 rows by 60 columns, as seen in Figure 2-3. A total of 60 scanners were needed for testing, each scanner being responsible for 16 pressure taps. The tap layout was done so that each scanner would be used for one column of pressure taps, the tap layout is described in Appendix A.

Since the experimentation needed such a large amount of instrumentation, only one panel could be instrumented. To measure pressure coefficients at different positions on the building, the ten panels could be used interchangeably by screwing them in and out to change the order of panel. In Figure 2-1, the instrumented panel is the third panel from the bottom, to measure at a different position on the building the instrumented panel would be moved to a different position and another set of tests would be performed.



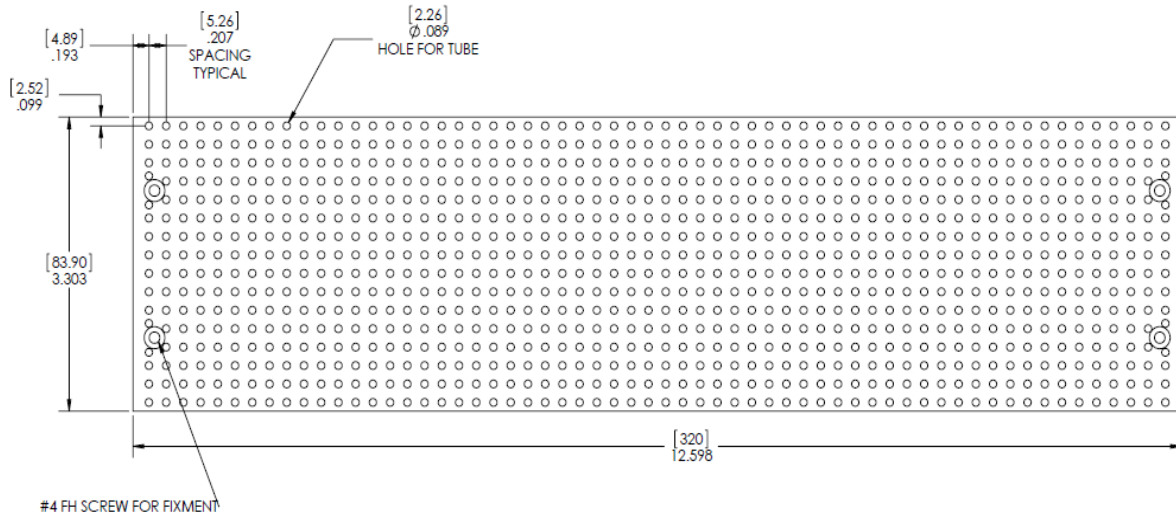


Figure 2-3: Drawing of the high resolution of pressure taps on instrumented panel used on the wind tunnel building model. Square brackets indicate mm dimensions, other dimensions are in inches.

A total of 55 different tests could be conducted, ten different height configurations with the pressure tap panel at any panel position on the building. Figure 2-4 illustrates the model in one particular height configuration. In this figure, the pressure tap panel is located at the top of the building and there are four “dummy” panels above the floor of the wind tunnel. This resembles the H/W ratio of 1.32 described in Table 2-1. In this height configuration, the pressure tap panel could be placed at any of the five positions above the wind tunnel floor. To create different heights, the model was raised and lowered through the floor of the wind tunnel. This process was done by adjusting a series of washers and nuts to the appropriate heights. Additionally, spacers were used to add stiffness to taller models and placed at the bottom of the model, below the wind tunnel floor. As seen in Figure 2-4 , panels are below the wind tunnel, subtracting from the full height of the model. For each panel position, a separate test was performed, i.e., for  $H/W=2.58$  the model was tested ten times, with the instrumented panel at

each height, or  $H/W=1.08$ , four trials in the wind tunnel would have to be run for all positions on the building.

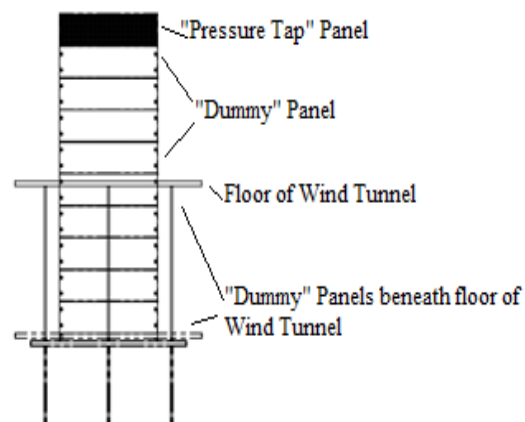


Figure 2-4: Wind tunnel model in configuration of a 5 panel tall building with the pressure tap panel at the top of the building. This yields a  $H/W$  ratio of 1.32.

## 2.2 Wind Tunnel Test Parameters

For the testing an open terrain was used as it would yield higher pressure coefficients than rougher terrains, providing better pressure coefficients for code purposes. Time series data of the wind profile was taken of the terrain and provided following testing. This data collection was performed by C. Wu and A. Fahad at Boundary Layer Wind Tunnel Laboratory. This time series data was used to determine the turbulence intensity, the mean wind profile and the power spectrum.

The testing parameters were the same as the studies conducted in Ho et al. (2005). The pressure tubing was flat to about 200 Hz. The pressure data were taken at 500 samples per

second for 100 seconds for every wind angle. The time for each wind angle was chosen to obtain adequate data for extreme value analysis and the sampling rate was chosen to correspond with the power spectrum data. These data collection parameters yielded 50,000 pressure coefficients for each individual pressure tap at each angle. Wind directions were taken in 10 degree increments over the interval from 0 to 180 degrees, resulting in 19 different wind angles being tested. Data were only taken from 0 to 180 degrees due to the symmetry of the model.



*Figure 2-5: Photograph of the wind tunnel with the model inside facing a 180 degree angle. This image shows the exposure used in the background. This terrain configuration involved the barriers, block heights, scattered nuts and spires. The model is set in a 6 panel high configuration ( $H/W = 1.66$ ).*

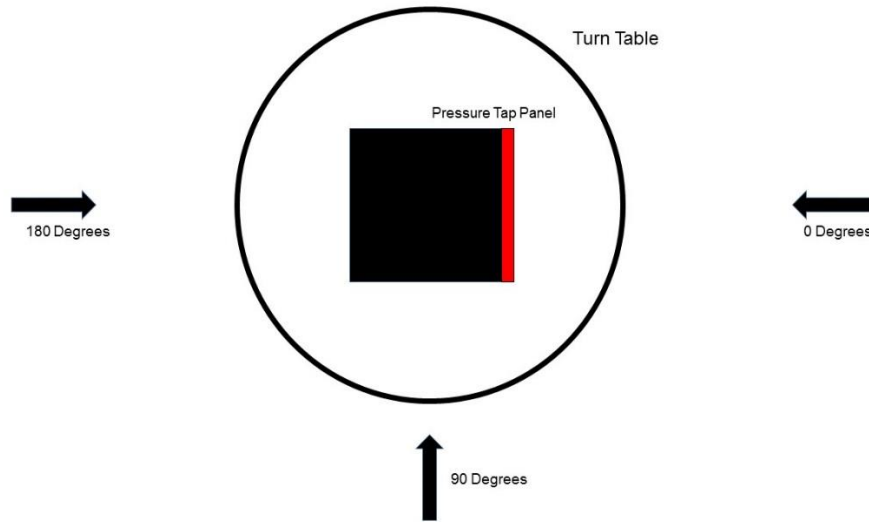


*Figure 2-6: Wind tunnel model with 0°, 90° and 180° indicated on the figure. During testing, the turn table rotated so the wind would be coming from the indicated direction.*

The Pitot-static tubes were set up at a standard height of 147 cm. The Pitot static tubes were set at this height since it was at the gradient height of the wind profile. Pitot static tubes are usually set at the roof height of the building model, however for this study, the roof height changes for different height configurations. The wind profile measurements would be used to normalize the pressure coefficients to the roof height. The wind tunnel reference velocity at 147 cm was set at roughly 13.7 m/s for all tests to be consistent with wind tunnel practice. These conditions were identical (within measurement uncertainty) for all configurations tested. Testing was performed twice and parameters were duplicated for both sets of tests, with repeated runs for a few configurations. During testing, a limited number of pressure taps malfunctioned; less than 1% of the total number of pressure taps. In these cases, the surrounding pressure taps were used to estimate the time series of the failed pressure taps. Due to the large density of pressure taps in the model, this method was deemed satisfactory.

Table 2-2 summarizes the tests performed. These two sets of tests were conducted months apart, with the first set of tests examining some of the cases and the second set of testing used to fill out the matrix. In total, 35 different cases were tested with 14 repeated runs. For six of the  $H/W$  ratios, all panel positions were tested with the instrumented panel.

Table 2-2: Height configurations and positions tested and corresponding set that the testing was performed.

Configuration	Tests Carried Out		
	Set 1	Set 2	
<b><math>H/W=2.58</math> <math>H=82.87</math> cm 10 Panel</b>	1st Panel (Top of Building)	Tested	Retested
	2nd Panel	Tested	Retested
	3rd Panel		Tested
	4th Panel	Tested	Retested
	5th Panel		Tested
	6th Panel		Tested
	7th Panel		Tested
	8th Panel	Tested	Retested
	9th Panel		Tested
	10th Panel (Bottom of Building)		Tested
<b><math>H/W=2.35</math> <math>H=75.40</math> cm 9 Panel</b>	1st Panel (Top of Building)	Tested	
	2nd Panel		
	3rd Panel		
	4th Panel		
	5th Panel		
	6th Panel		
	7th Panel		
	8th Panel		
	9th Panel (Bottom of Building)		
<b><math>H/W=2.10</math> <math>H=67.31</math> cm 8 Panel</b>	1st Panel (Top of Building)	Tested	
	2nd Panel	Tested	
	3rd Panel		
	4th Panel		
	5th Panel		
	6th Panel		
	7th Panel		

	8th Panel (Bottom of Building)		
<b><i>H/W=1.83</i></b> <b><i>H=58.74 cm</i></b> <b>7 Panel</b>	1st Panel (Top of Building)	Tested	Retested
	2nd Panel		Tested
	3rd Panel		Tested
	4th Panel	Tested	Retested
	5th Panel		Tested
	6th Panel		Tested
	7th Panel (Bottom of Building)		Tested
<b><i>H/W=1.66</i></b> <b><i>H=53.18 cm</i></b> <b>6 Panel</b>	1st Panel (Top of Building)	Tested	
	2nd Panel	Tested	
	3rd Panel		
	4th Panel		
	5th Panel		
	6th Panel (Bottom of Building)		
<b><i>H/W=1.32</i></b> <b><i>H=42.23 cm</i></b> <b>5 Panel</b>	1st Panel (Top of Building)	Tested	
	2nd Panel	Tested	
	3rd Panel		
	4th Panel	Tested	
	5th Panel (Bottom of Building)		
<b><i>H/W=1.08</i></b> <b><i>H=34.61 cm</i></b> <b>4 Panel</b>	1st Panel (Top of Building)	Tested	Retested
	2nd Panel	Tested	Retested
	3rd Panel		Tested
	4th Panel (Bottom of Building)	Tested	Retested
<b><i>H/W=0.80</i></b> <b><i>H=25.72 cm</i></b> <b>3 Panel</b>	1st Panel (Top of Building)	Tested	Retested
	2nd Panel	Tested	Retested
	3rd Panel (Bottom of Building)		Tested
<b><i>H/W=0.52</i></b> <b><i>H=16.67 cm</i></b> <b>2 Panel</b>	1st Panel (Top of Building)	Tested	Retested
	2nd Panel (Bottom of Building)	Tested	Retested
<b><i>H/W=0.28</i></b> <b><i>H=8.90 cm</i></b> <b>1 Panel</b>	1st Panel	Tested	Retested
<b><u>Totals</u></b>		22	27 13 new cases 14 retested

### 2.3 Scaling

In wind tunnel experimentation, the flow field and the buildings must be scaled properly for appropriate results. These must be at the same scale since, without the two matching, problems arise in the interpretation of the data. The scaling of the flow field will be discussed first.

The flow fields for experimentation are used to mimic existing terrain conditions. Important characteristics of flow fields include the ratios of wind speeds throughout the height, the eddies and the fluctuations. For wind tunnel testing, the turbulence intensities, mean wind profile and spectral densities are compared to expected full-scale values. These parameters must be taken in the proper ratios to simulate the terrain correctly. Relationships between the target full-scale and model-scale velocities, time and length are considered. For this analysis, the scaling will replicate Engineering Sciences Data Unit (ESDU) models for terrain roughness.

One of the difficulties of this experimentation is the use of a single model and terrain configuration. The same terrain is to be used for multiple different building heights and ideally a single length ratio can be used for all configurations. This complicates the scaling as often times, the requirements of scaling low-rise (Tieleman et al., 2003) and high-rise buildings (Dalglish, 1975) tend to be different. Low-rise and high-rise buildings follow different parameters for simulation, such as the characteristic lengths used; the height for low-rise buildings and the width for high-rise buildings. As a result, there are different governing aerodynamics for different height configurations in the testing. The objective of the scaling was to determine an appropriate scale that could be used for all model heights. For the testing, many of the buildings were considered high-rise buildings. For the purpose of this work, a high-rise building scaling method was used.

### 2.3.1 Definitions

The mean velocity is the time-averaged velocity at a point. The mean wind speed is represented by  $\bar{u}$ . The standard deviation can be determined from a time series using:

$$\sigma = \sqrt{\sum_{i=1}^n \frac{(u-\bar{u})^2}{n}} \quad (2-1)$$

This standard deviation is for the fluctuations in the along wind direction. From the standard deviation of the time series, the turbulence intensity can be determined as:

$$I_u = \frac{\sigma}{\bar{u}} \quad (2-2)$$

The integral length scale is related to the size of the eddies. The integral length scale measures the amount that a time series is correlated with itself and the time that a particle is influenced by a previous position. The autocorrelation can be used to the integral time scale,  $L_t$ :

$$L_t = \int_0^{\infty} \rho_{uu}(\tau) d\tau \quad (2-3)$$

The longitudinal integral length scale,  $L_x$ , is determined using the integral time scale:

$$L_x = \bar{u}L_t \quad (2-4)$$

assuming Taylor's hypothesis of frozen turbulence.



### 2.3.2 Scaling Method

For the scaling, the roughness length,  $z_0$ , and target full scale height,  $z_{fs}$ , could be chosen. The roughness length was determined from the turbulence intensity and wind profile. The height was determined from the scale. For the wind profile, ESDU (1974, 1985) documents were used to simulate the terrain. This process yields target wind speeds and turbulence intensities for full-scale. This study utilized ESDU 74030 (1974) and 85020 (1985). ESDU 74 uses a log-law fit (Oke, 1987) to match the wind speed and the turbulence intensity. ESDU 85 uses a von Kármán spectrum to match the power spectral density.

The measured mean wind speed and turbulence intensity were compared to the theoretical values from ESDU. The fit from the wind profile would yield the roughness length,  $z_0$ . Additionally, a power law fit was used to fit the data. For the mean wind profile, a power law was first used to fit the data. Since the test was intended to model an open terrain, the power law exponent,  $\alpha$ , should be within 0.08 – 0.22 (estimation used for open water to open country terrain). The power law takes the form of:

$$\frac{U}{U_r} = \left(\frac{z}{z_r}\right)^\alpha \quad (2-5)$$

where  $U_r$  is the velocity at the reference height and  $z_r$  is the reference height. For this fit, the reference height was considered to be the largest roof height. To determine  $\alpha$ , the power law was used to match the experimental mean wind speeds. This  $\alpha$  was compared for the different roof heights needed throughout experimentation. Ideally, a single  $\alpha$  value could be used for all of the height configurations. Figure 2-7 shows the power law fit used, using the height of the tallest height configuration as  $H$ . To make this comparison dimensionless, the velocity was plotted as a

ratio of the velocity at the particular height with the normalizing velocity (the velocity at the roof height of the building),  $U/U_H$ .

To determine if the power law fit was a good fit for the given data, a least squares fitting was performed. This method was performed analytically, using the  $\alpha$  with the least deviations, resulting in an  $\alpha$  of 0.10. This is within the range of expected values for an open terrain condition, albeit at the smoother end of the range.

The log-law given in ESDU 85 (ESDU 85020, 1985) is in the form:

$$\frac{U_z}{U_{10}} = \frac{\ln\left(\frac{z}{z_0}\right)}{\ln\left(\frac{10}{z_0}\right)} + 86.25f_0z \quad (2-6)$$

The second term of the equation (i.e.,  $86.25f_0z$ ) is negligible as it is the Coriolis parameter defined as:

$$f_0 = 2\omega \sin \phi \quad (2-7)$$

For the purpose of the analysis,  $\phi$  was set as  $45^\circ$  and the Coriolis parameter was found to be  $1.03 \times 10^{-4}$ . This value is orders of magnitude below the first term and will not affect the  $K_z$  value.

With the value of  $U_z/U_{10}$  the velocities could be compared similar to the power law fit. This can be performed by dividing the  $U_z/U_{10}$  for one height by the  $U_z/U_{10}$  of the reference or normalizing height.

The turbulence intensity was determined using ESDU 85020 (1985) which refers to ESDU 83045 (1983) for simulation of this characteristic. ESDU 83045 (1983) determines the turbulence intensity as the product of several ratios:

$$I_u = \frac{\sigma_{ux} \sigma_u u_* U_z}{\sigma_u u_* U_z U_{zx}} \quad (2-8)$$

where  $I_u$  is the turbulence intensity,  $\sigma_u$  is the standard deviation of the streamwise wind,  $\sigma_{ux}$  is the local standard deviation of the streamwise wind,  $u_*$  is the friction velocity,  $U_z$  is the wind speed at the height and  $U_{zx}$  is the local wind speed at the height. These ratios can be simplified to give the expression in ESDU 85020:

$$I_u = \frac{\sigma_u u_*}{u_* U_z} \quad (2-9)$$

Thus, the turbulence intensity depends on the ratio of the standard deviations to the friction velocity and the friction velocity to the reference wind velocity. ESDU 85 gives the equations for determining these ratios, which are empirically determined. The first ratio can be determined as:

$$\frac{\sigma_u}{u_*} = \frac{(7.5\eta[0.538+0.09\ln(\frac{z}{z_0})]^p)}{1+0.156\ln(\frac{u_*}{f_0 z_0})} \quad (2-10)$$

and the second term is given as:

$$\frac{U_z}{u_*} = 2.5 \left[ \ln\left(\frac{z}{z_0}\right) + \frac{34.5f_0 z}{u_*} \right] \quad (2-11)$$

In Equation 2-10,  $\eta$  and  $p$  are defined as:

$$\eta = 1 - \frac{6f_0 z}{u_*} \quad (2-12)$$

$$p = \eta^{16} \quad (2-13)$$

The friction velocity is a function of the roughness length given as:

$$u_* = \frac{U_{10,model}}{2.5 \cdot \ln\frac{10}{z_0}} \quad (2-14)$$

From these equations, the roughness length is the only parameter that is not known. This roughness length can be used for Equations 2-6 to 2-14. These fits from ESDU 85 will be used to compare the turbulence intensities and mean profiles measured.

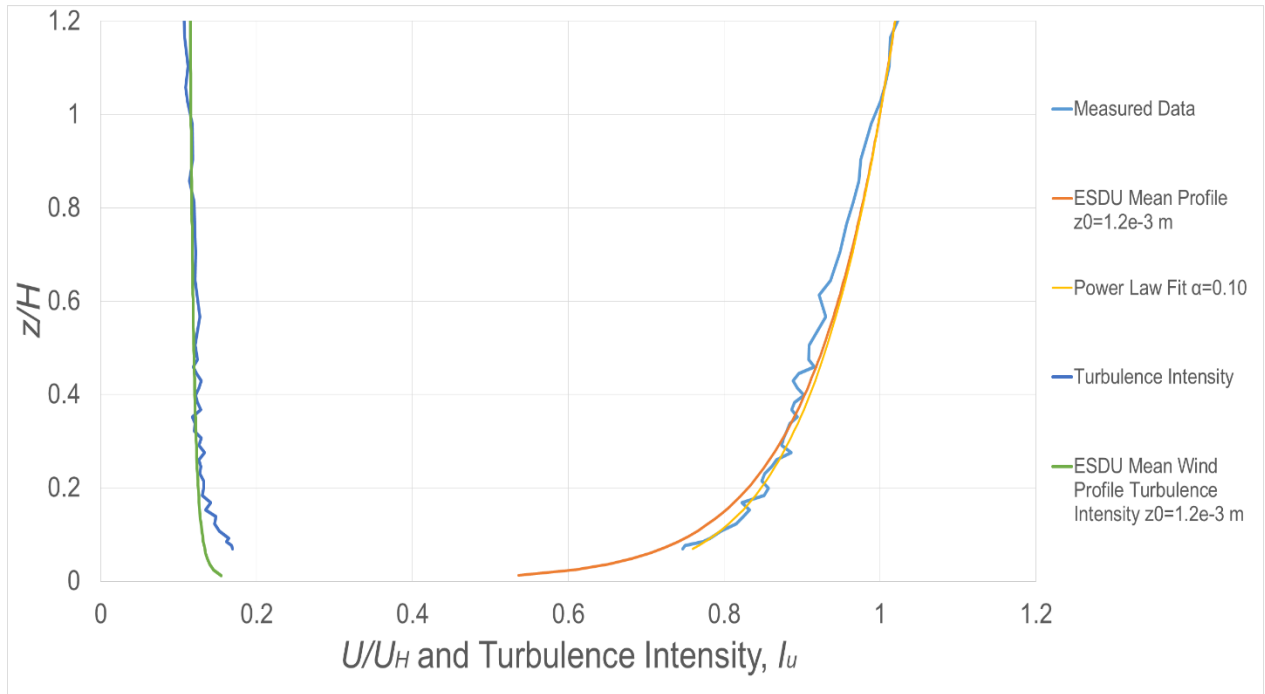


Figure 2-7: Wind profile for a building of  $H/W$  ratio of 2.58. Displaying turbulence intensity and mean wind speeds.

A high-rise scaling was used to determine the roughness length and the tallest  $H/W$  configuration was observed. The mean wind velocity fit is similar to the power law fit. The turbulence intensity and mean wind speeds are in good agreement throughout the building height. There is some scatter towards the bottom of the wind profile, which would only impact the shortest height configuration, with underestimation of turbulence intensities at this height.

The model-scale power spectral density was also observed. Figure 2-8 shows the power spectral density. Using ESDU 74031 (ESDU, 1974) the integral length scale could be determined.

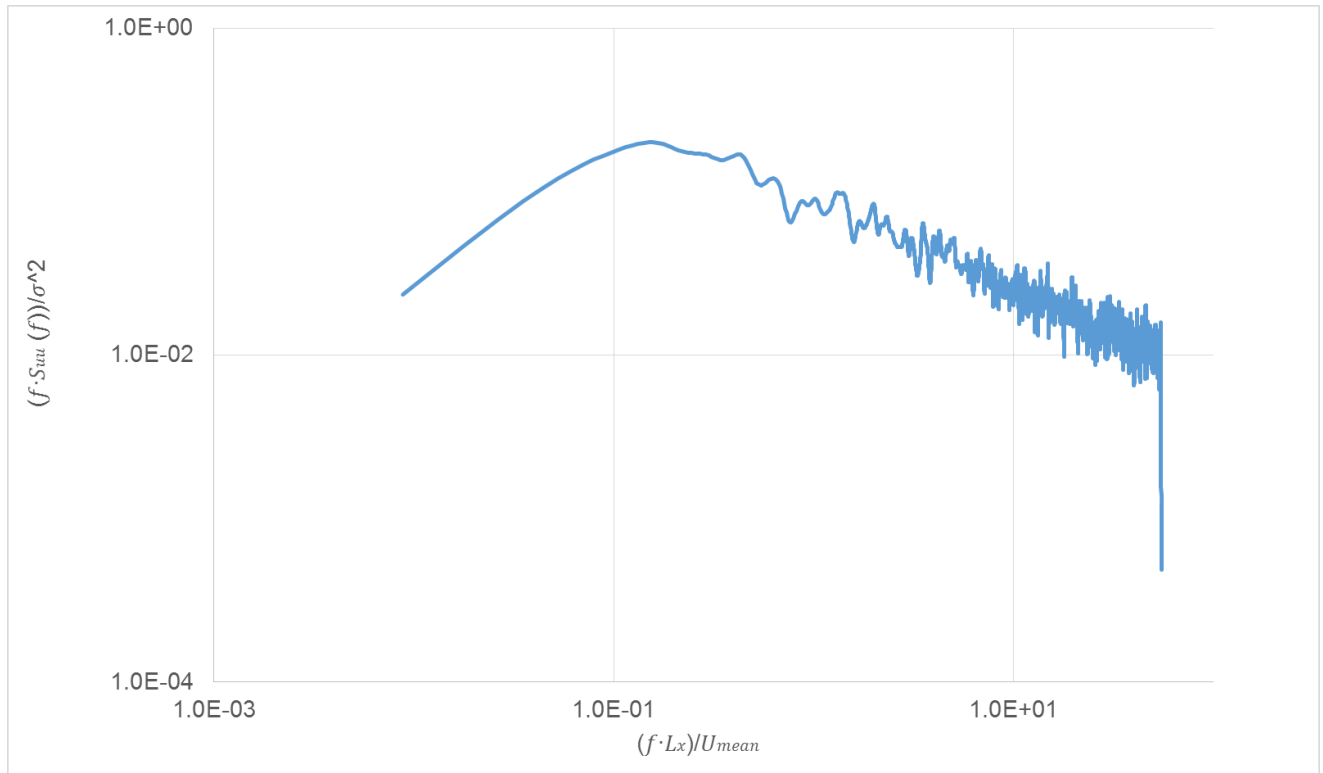


Figure 2-8: Power spectral density for high-rise building at a model-scale height of 0.67m.

For perfect simulation, the turbulence intensity,  $I_u$  and power spectral density,  $f S_{uu} / \overline{U^2}$ , should be matched between model- and full-scale. The power spectral density is a function of the turbulence intensity, which is a function of roughness length. From ESDU 74031, the integral length scale is given as a function of the height and roughness length:

$$L_x = \frac{25z^{0.35}}{z_0^{0.063}} \quad (2-15)$$

The von Kármán spectrum can be determined by:

$$\frac{f S_{uu}}{\sigma^2} = \frac{4 \left( \frac{f L_x}{\bar{U}} \right)}{\left[ 1 + 70.8 \left( \frac{f L_x}{\bar{U}} \right)^2 \right]^{\frac{5}{6}}} \quad (2-16)$$

where  $f$  is the frequency,  $S_{uu}$  is the power spectrum,  $\sigma$  is the standard deviation and  $L_x$  is the integral length scale. The maximum values from Figure 2-8 and yielded values of  $\frac{f S_{uu}}{\sigma^2} = 0.271$  and  $\frac{f L_x}{\bar{U}} = 0.145$ , which can be substituted into Equation 2-16. The maximum  $S_{uu}$  was chosen for the matching and a perfect matching was assumed. Equation 2-16 can be transformed using the turbulence intensity becoming:

$$\frac{f S_{uu}}{\bar{U}^2} = \frac{4 \left( \frac{f L_x}{\bar{U}} \right) I_u^2}{\left[ 1 + 70.8 \left( \frac{f L_x}{\bar{U}} \right)^2 \right]^{\frac{5}{6}}} \quad (2-17)$$

At the chosen point, Equation 2-17 yields:

$$\frac{f S_{uu}}{\bar{U}^2} = 0.271 I_u^2 \quad (2-18)$$

At

$$\frac{f L_x}{\bar{U}} = 0.145, \quad \frac{f W}{\bar{U}} = 0.145 \frac{W}{L_x} \quad (2-19)$$

For perfect fitting, the following relationships should hold:

$$(I_u)_{fs} = (I_u)_{ms}$$

$$\left( \frac{L_x}{W} \right)_{fs} = \left( \frac{L_x}{W} \right)_{ms}$$

$$\lambda_L = \frac{(L_x)_{ms}}{(L_x)_{fs}} = \frac{W_{ms}}{W_{fs}}$$

(2-20)

These conditions scale the model- and full-scale turbulence intensities, integral length scale and building width. For scaling high-rise buildings, the width is used as the characteristic length opposed to the height of the building. Using Equation 2-15 and dividing both sides by the building height:

$$\left(\frac{L_x}{H}\right)_{ms} = \frac{25}{z_0^{0.063} H^{0.65}} \quad (2-21)$$

Using the relationship for model-scale and full-scale:

$$H_{fs} = \left[ \frac{25}{z_0^{0.063} \left(\frac{L_x}{H}\right)_{ms}} \right]^{\frac{1}{0.65}} \quad (2-22)$$

The full-scale height has not been previously set in this equation. The  $z_0$  was determined to be 0.012 m for approximately 15% turbulence intensity, model-scale, integral length scale,  $L_x=0.9047$ , and model-scale height,  $H_{ms}=0.67$ . Using Equation 2-22, the full-scale height is  $H_{fs}=136.78$ .  $\lambda_L=204$  or to one significant figure 200 for the length scale.

## 2.4 Data

The pressure coefficients,  $C_p = (p-p_o)/(0.5 \rho V_H^2)$ , are presented relative to the roof height mean wind speed,  $V_H$ . These pressure coefficients were obtained as a time series, so statistical analyses had to be performed, as described in this section.

### 2.4.1 Area Averaging

An area averaging analysis was carried out. By giving equal weight (because of the tap layout) to all of the pressure taps, the following equation was used:

$$C_p = \sum_{i=1}^m \sum_{j=1}^n C_{p_{ij}} \frac{a_{ij}}{A} \quad (2-23)$$

In ASCE 7-10, there are different tributary areas for differently sized cladding elements, so to replicate this pattern, different areas were examined. For the analysis, the cases can contain overlapping and non-overlapping areas as two separate possibilities. For the purpose of the investigation, cladding sizes were defined by the number of pressure taps involved in particular sizes. All areas used were in square patterns of 1x1, 2x2, 4x4, 8x8 and 16x16 taps. Table 2-3 shows the full-scale tributary areas for these tap arrangements. Only for 8x8 and 16x16 tap areas with overlapping arrangements were used. This process was used on the time series, for example the 4x4 would involve a group of 16 pressure taps in a square and take an average of the pressure coefficient for every point in the time series. This new time series would represent the pressure coefficients for the particular area. The use of this method is significant because only Gavanski and Uematsu (2014) have used area averaging in their studies to determine pressure coefficients on walls. However, it should be noted that the first systematic area-averaging appears to have been conducted by Kopp et al. (2005). With these time series, the extreme value analysis could be performed.



Table 2-3: Full-scale areas used in the analysis, assuming a length scale of 1:200.

Tap Arrangement	Full-Scale Size (m <sup>2</sup> )
1 x1	1.12
2 x2	4.48
4 x4	17.90
8 x8	71.62
16 x16	286.46

### 2.4.2 Extreme Value Analysis

Due to the turbulence in the wind, pressure fluctuations occur with large, intermittent values. Thus, an extreme value analysis is required to determine appropriate peaks in the pressure data (e.g., Gavanski et al., 2016). For the extreme value distribution the Lieblein Best Linear Unbiased Estimator (BLUE) method (Lieblein, 1974) was chosen to analyze the data. This method is an estimator for the Gumbel method. Although other statistical methods could be used, Lieblein BLUE is often used in wind engineering and was chosen to stay consistent with the industry.

For the Lieblein BLUE method, the data set was divided into ten equal subsets of data. These sets contained 10 seconds of wind tunnel testing time. The maximum and minimum values were taken from each of these subsets. The maxima (or minima) are sorted from lowest to great (or greatest to lowest). Then, the following equations can be applied to determine a distribution:

$$u'_n = \sum_{i=1}^{10} a_i \cdot x_i \quad (2-24)$$

$$b'_n = \sum_{i=1}^{10} b_i \cdot x_i \quad (2-25)$$

where  $u'_n$  and  $b'_n$  are the slope and intercept when examining the distribution linearly. The factors  $a_i$  and  $b_i$  are given in Table 2-4.

Table 2-4: Factors used for Lieblein BLUE.

$a_i$	$b_i$
.222867	-.347830
.1623088	-.091158
.133845	-.019210
.112868	.022179
.095636	.048671
.080618	.066064
.066988	.077021
.054193	.082771
.041748	.083552
.028929	.077940

Rearranging the distribution into its original form, the equation is:

$$Prob\{X \leq x\} = e^{-e^{-(x-u'_n)/b'_n}} \quad (2-26)$$

With the distribution, the 78<sup>th</sup> percentile was used (Gavanski et al., 2016). This process was performed at every wind angle and every pressure tap for all time series including the area averages.

### 2.4.3 Conversion Factor for ASCE 7

The peak pressure coefficients need to be adjusted into the form used in ASCE 7-10. As described in St. Pierre et al. (2005), additional factors are needed to interpret wind tunnel data to the code formulation. In St. Pierre et al. (2005) it was determined that:

$$GC_{PF} = F_{WT} C_P \quad (2-25)$$

where  $F_{WT}$  was a factor to convert the wind tunnel test data to full scale, where  $C_P$  was the value from the wind tunnel testing. This parameter,  $F_{WT}$ , is obtained via:

$$F_{WT} = \left( \frac{V_{h,z_0,mean\ hourly}}{V_{10m,z_0=0.03,3\ sec\ gust}} \right)^2 = \left( \frac{V_{10m,z_0=0.03,mean\ hourly}}{V_{10m,z_0=0.03,3\ sec\ gust}} \right)^2 \left( \frac{V_{10m,z_0,3\ sec\ gust}}{V_{10m,z_0=0.03,3\ sec\ gust}} \right)^2 \left( \frac{V_{h,z_0,mean\ hourly}}{V_{10m,z_0,mean\ hourly}} \right)^2 \quad (2-26)$$

These parameters can be summarized as the change from mean-hourly to 3-second gust speeds, the change in roughness and the change in reference heights used. The first parameter to account for was the different reference roof heights used throughout the experiment before applying the  $F_{WT}$  factors. The code pressure coefficients are based on the roof height and gust wind speed. From the wind profile taken, the different roof height wind speeds were used to normalize the pressure coefficient values. To convert the wind-tunnel data to the ASCE 7 formulation, three factors were considered for the 3-second gust, the full-scale 10 m height and the roughness change. The 3-second gust was accounted for by using the "Durst Curve" (ASCE 7-10, 2010).

Table 2-5: Velocity conversion factors for all height configurations

<b>H/W Ratio</b>	<b>Velocity Conversion Factors</b>
0.28	0.5167
0.52	0.6271
0.80	0.6812
1.08	0.7099
1.32	0.7237
1.66	0.7695
1.83	0.8264
2.10	0.8397
2.35	0.8614
2.58	0.8614

Using the wind profile generated, the model-scale to full-scale reference heights could be used to factor the pressure coefficients to account for the difference in reference heights. To convert the wind profile to the necessary reference height, a factor was needed to change values from model-scale to full-scale. This was used to determine at which height 10 m was on the tested profile. The scale used for the analysis was a 1/200 length scale. Since open country terrain was used for the testing, the terrain parameter was considered to be 1 for the analysis. These factors generate the value of  $F_{WT}$  that St. Pierre et al. (2005) described. With these factors considered, the wind tunnel data can be compared to the values found in the current code. Table 2-5 shows the velocity conversion factors using Equation 2-26 for the various height configurations.

## Chapter 3 Analysis of Wall Pressure Coefficients

### 3.1 Reliability of Data

#### 3.1.1 Comparisons between Measured Test Results

The data from the two independent sets of tests were compared. Overall, there is good agreement between the two sets of tests as can be seen in Figure 3-1 and Figure 3-2 showing the peak positive values and peak negative values, respectively, of the pressure coefficients. The figures are similar, in terms of the magnitudes and patterns displayed. Note in Figure 3-1 and Figure 3-2 and throughout this chapter, figures will have  $z/H$  on the vertical axis and  $x/w$  on the horizontal axis.

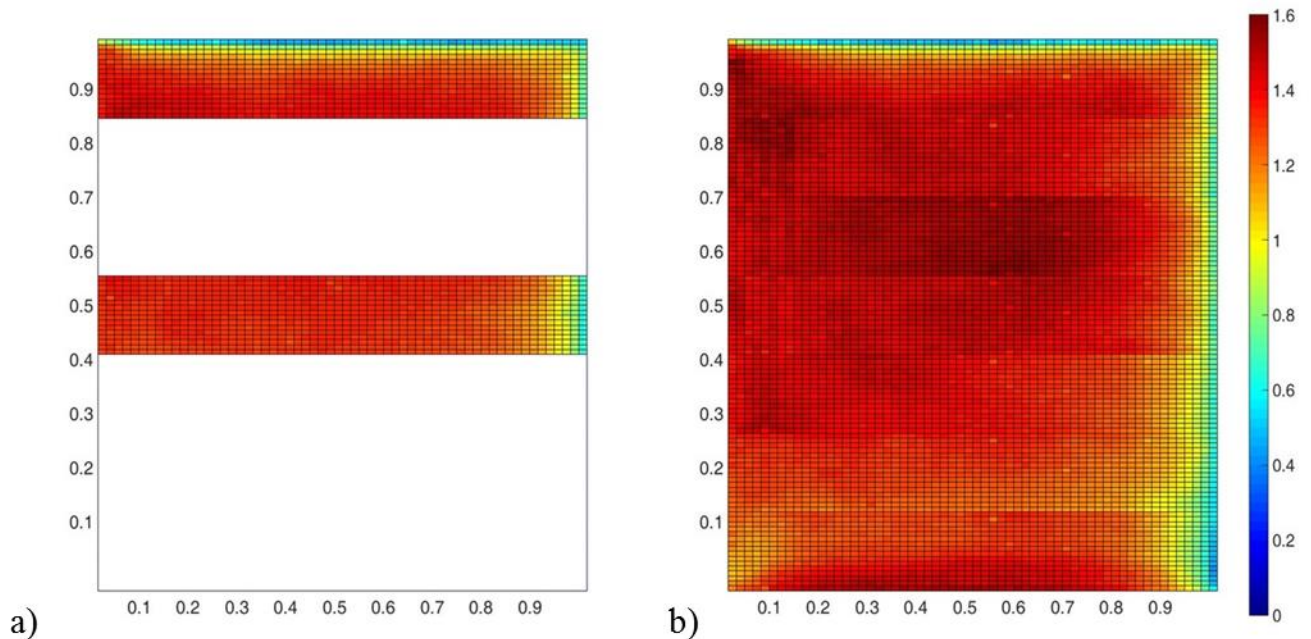


Figure 3-1: Maximum pressure coefficient values,  $G_{Cp}$ , for  $H/W = 1.83$ , enveloped over the measured wind directions, for two separate and independent tests, (a) Set 1, (b) Set 2.

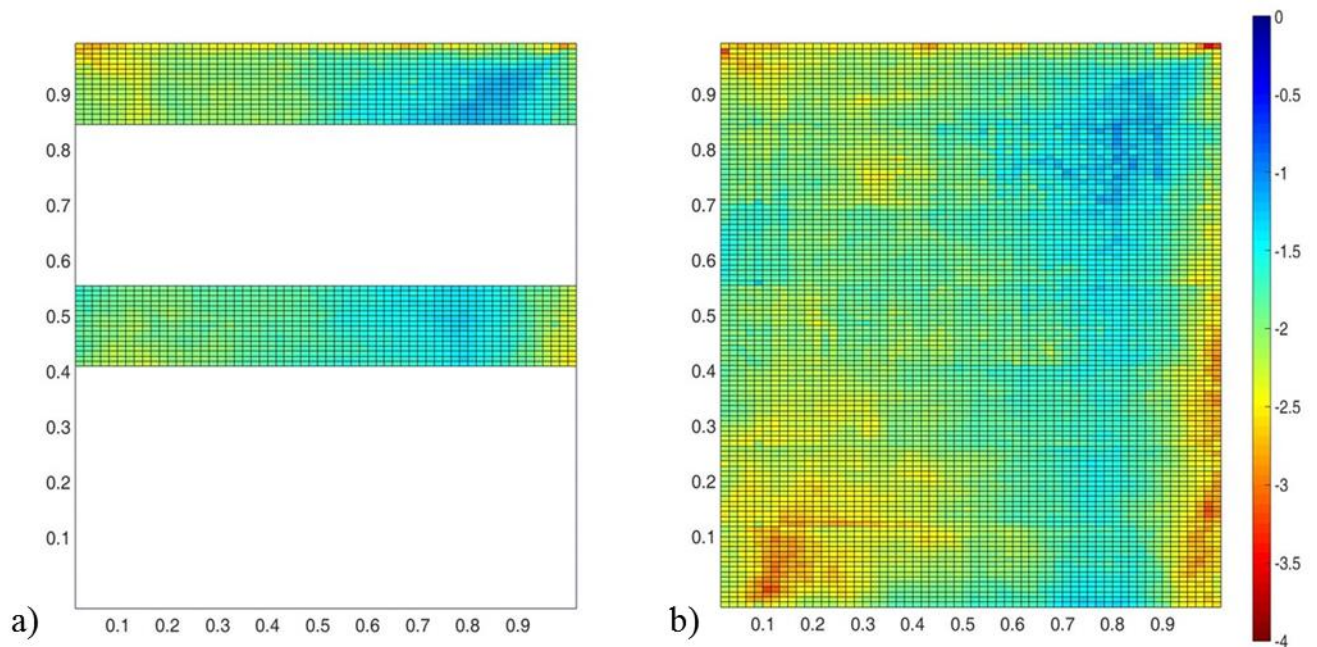


Figure 3-2: Minimum pressure coefficient values,  $GC_p$ , for  $H/W = 1.83$ , enveloped over the measured wind directions, for two separate and independent tests, (a) Set 1, (b) Set 2.

There are some differences in the patterns; however, the shapes are relatively similar. The main difference between the sets of data are the high suction zones towards the top of the building with the second set of tests having a larger zones with higher magnitudes.

Additionally, mean pressure coefficients are compared at every wind direction. Figure 3-3 shows the results for three locations, in the left corner, the middle, and the right edge of the panel (as viewed in Figure 3-1 & Figure 3-2). The figure shows that these pressure taps are in good agreement between the two sets of data, within the measurement uncertainty ( $GC_p$  of 0.1 (Quiroga, 2005)). Further comparison figures can be found in Appendix C.

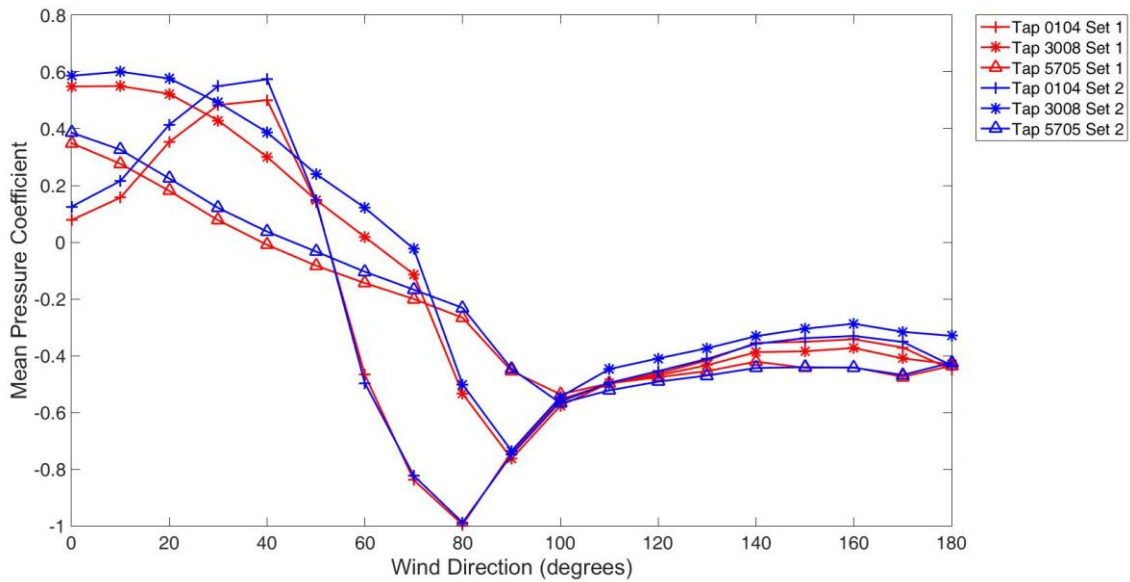
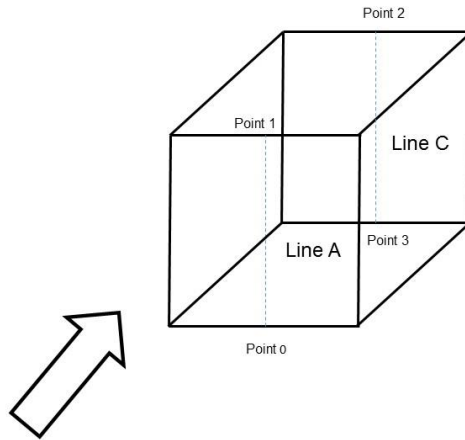


Figure 3-3: Individual pressure tap comparison for  $H/W=2.58$  with the panel at the top most position. The comparison shows Set 1 in red and Set 2 in blue for three different pressure tap locations. The location is indicated by the tap position indicated in Chapter 2.

### 3.1.2 Comparisons with External Data Sets

Existing data from the literature were compared to the current data. Due to the wide availability of data, the cube case was the primary subject for comparisons, including full-scale from the Silsoe cube. The external cases used were Castro and Robins (1977), Hölscher et al. (1998), Richards et al. (2007), and Cóstola et al. (2009).

Figure 3-4 shows the convention used by Castro and Robins (1977) to illustrate the data. Using this convention, the data were compared for wind directions of  $0^\circ$  to  $180^\circ$ . As shown, the windward side of the building is from 0 to 1 and represented by line A and the leeward side of the building is from 2 to 3 represented by line C. The data used for comparison were taken along the centreline of the building (i.e., the cube).



*Figure 3-4: Adaptation Castro and Robins (1977), the convention used for their test of the Silsoe Cube with the wind direction indicated by the arrow. For the comparison, 0 to 1 will be represented by line A going upwards along the height and 2 to 3 will be represented by line C going downwards along the height.*

Figure 3-5 shows the data along the windward and leeward faces of the cube. The positive values in Figure 3-5 (a) are in good agreement. There are some higher pressure coefficients towards the bottom of the building for Set 2, but this data matches the patterns in the literature. The pressure coefficients are of the same magnitude and exhibit the same patterns. All data sets have low pressures near the top of the wall, with higher pressures over the lower 70-80% of the building height, with a decrease at around 20-30% of the building height. There are greater differences in the data for the negative pressure coefficients; however the current data are in good agreement with the published wind tunnel data. The pattern on the leeward wall is of relatively similar magnitude over the full height, although the full-scale field data for the Silsoe



Cube has some differences. Overall, the data set shows good agreement with the data in literature, within the measurement certainty, which are about  $\Delta C_p$  of 0.1 for mean values.

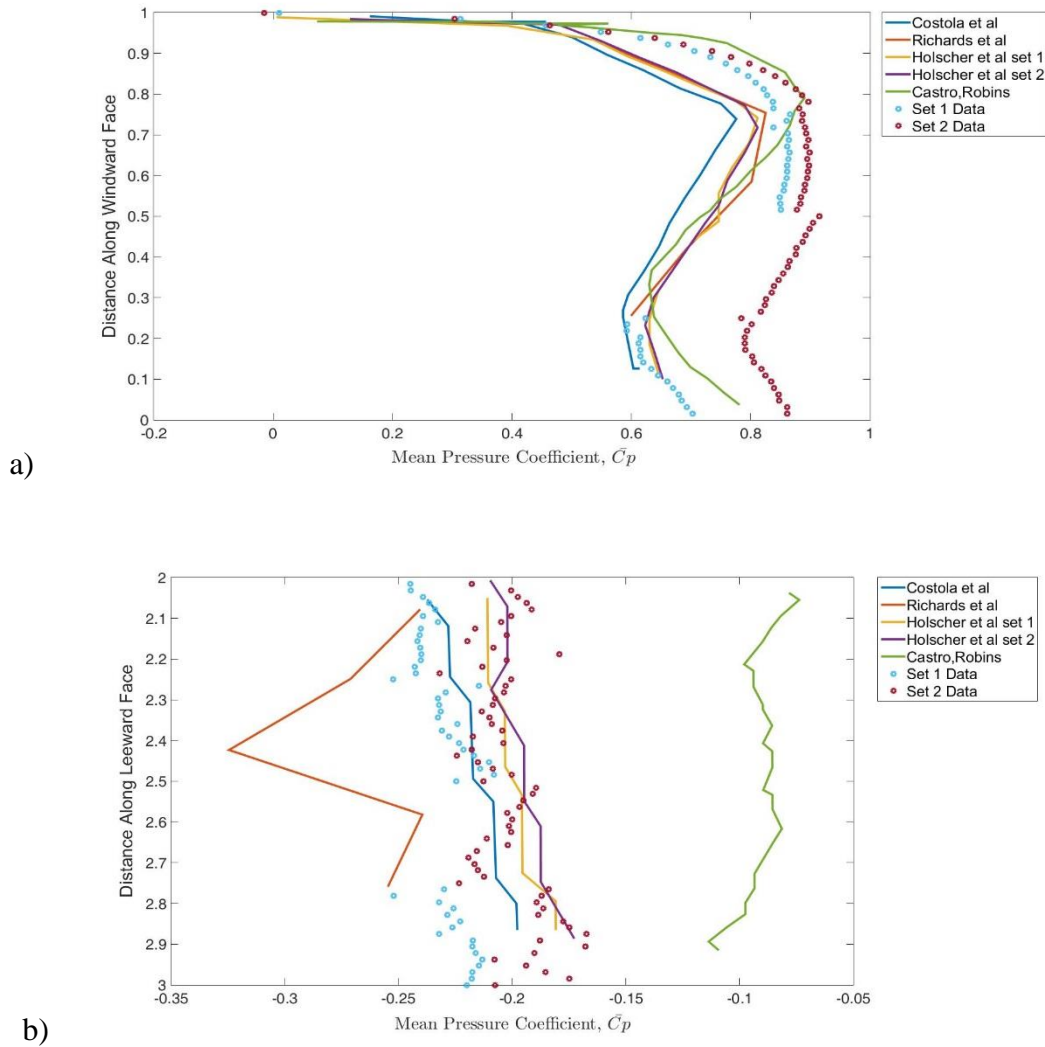


Figure 3-5: a) Comparison of mean pressure coefficients along the windward wall taken for a wind direction of  $0^\circ$ . The vertical coordinate system is with 0 at the bottom of the wall and 1 at the top of the wall, following the nomenclature of Castro & Robins (1977). b) Comparison of mean pressure coefficients along the windward wall taken at a wind direction of  $180^\circ$ . The lengths are taken with 3 at the bottom of the wall and 2 at the top of the wall, following the nomenclature of Castro & Robins.

## 3.2 Pressure Distributions

### 3.2.1 Peak Pressure Coefficients

As discussed in the previous chapter, peak pressure coefficients were found for all wind directions. Figure 3-6 shows the enveloped (non-mirrored) pressure coefficients for a low-rise ( $H/W=0.28$ ) and high-rise ( $H/W=2.58$ ) building. Comparing these two buildings, there are many differences. The magnitude of the pressure coefficients (which are plotted on the same scale in Figure 3-6) vary, with the high-rise building having higher values over the majority of the building. While the high-rise building is more uniform, the low-rise building has lower pressures at the bottom to the middle of the building. However, there are also some similarities, for example the low pressures near the roof edges of the buildings and lower pressures on the right side of each building (for the wind directions examined).

The negative peak pressure coefficients are shown in Figure 3-7. The patterns of the negative peak pressure coefficients differ more significantly between the low-rise and high-rise buildings than the positive pressure coefficients. The negative pressure coefficients are larger in magnitude for the high-rise building, with suction coefficients up to about -4.0 while the low-rise building has highest suction coefficients around -1.5. There are differences between the patterns of pressure coefficients on the buildings too, although both buildings have highest suctions at the upper left corner of the building. The low-rise building has lower magnitude suctions over most of the building, with relatively higher suctions occurring on the windward edge and along the top edge of the building. Further analysis into the causes of these higher suction zones will be discussed in Section 3.2.2.

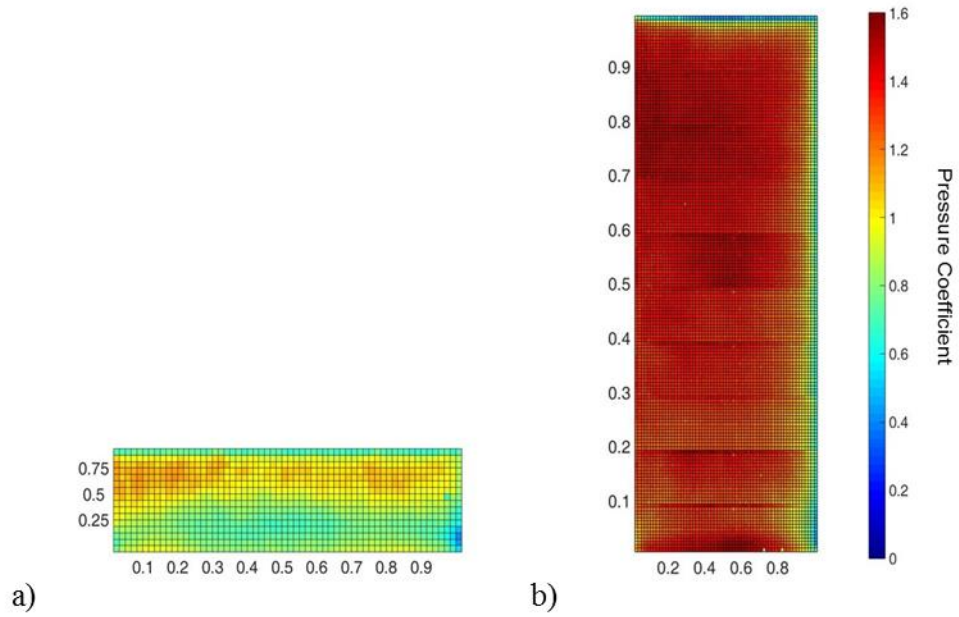


Figure 3-6: Peak positive pressure coefficients for low-rise building (a) and high-rise building (b).

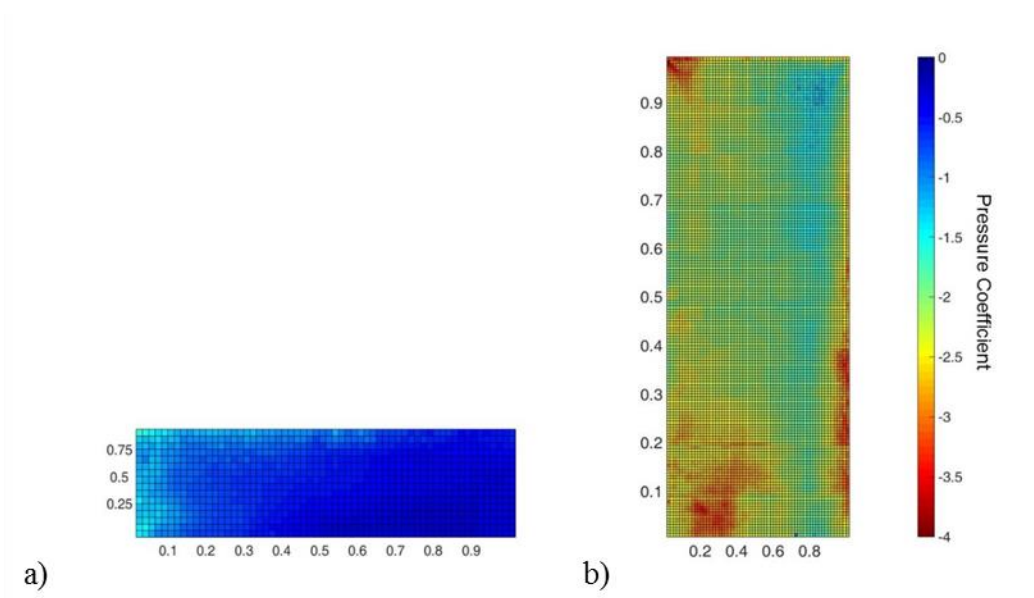
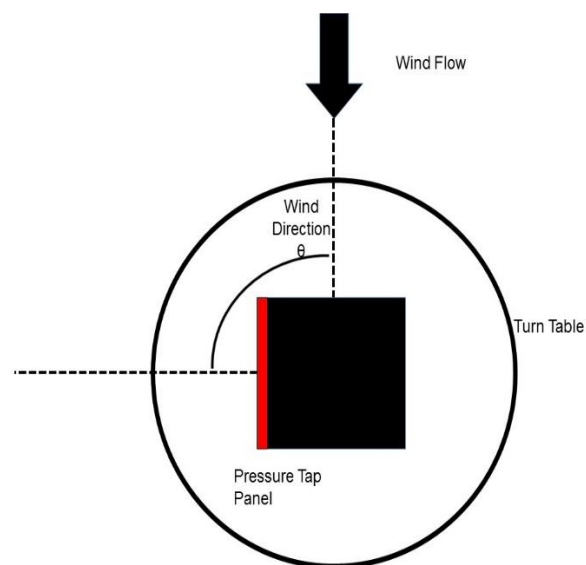


Figure 3-7: Peak negative pressure coefficients for low-rise building (a) and high-rise building (b).

### 3.2.2 Wind Direction Effects

To further examine the pressure coefficient patterns, the patterns for the wind directions were examined. The wind direction is defined, as discussed in Chapter 2, and shown in Figure 3-8. The wind directions causing the extreme pressure coefficients were observed. The pressure distributions for the wind directions were used to predict the wind patterns affecting the building.



*Figure 3-8: Wind direction definition based on the wind flow of the wind tunnel. The initial position of the pressure tap panel faces the wind flow and rotates with the turn table. The presented configuration is of a wind direction of 90°.*

Figure 3-9 shows the wind directions for positive pressure coefficients of a low-rise and high-rise building. The wind directions causing the highest pressures (or suctions) were considered the worst wind directions. These two buildings have similar distributions of the wind directions throughout the building. The wind directions varied from 0 to 50° for the largest pressures. The worst wind directions generally followed the pattern with 0° on the leeward (right on the figure) side of the building. For pressures at locations near the windward edge, oblique

wind directions controlled, usually in the range of 10 -30°. The exception to this is at the top of the wall, where wind directions are at 40 – 50°.

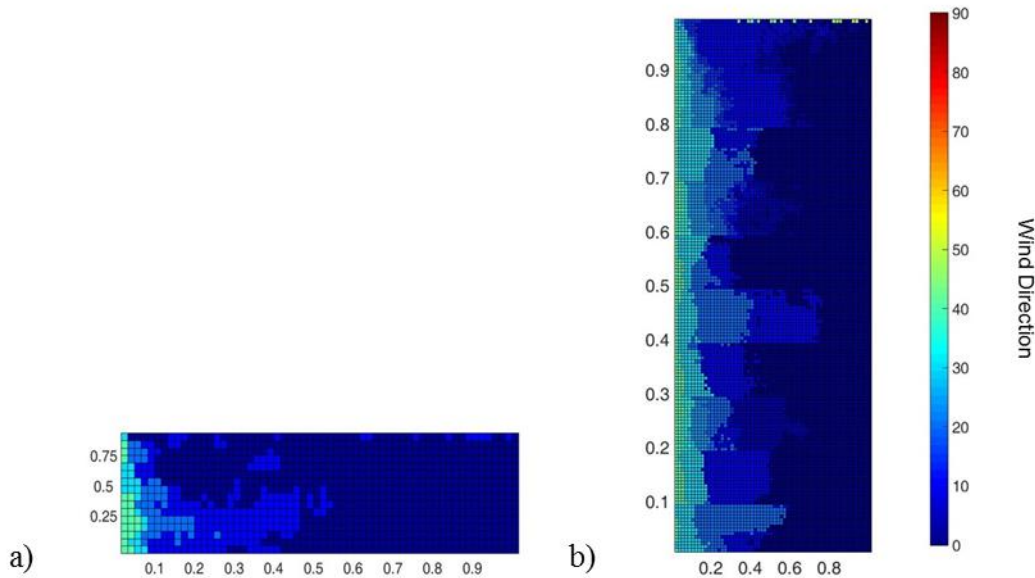


Figure 3-9: Distribution of the critical wind directions causing highest positive pressures for  $H/W=0.28$  (a) and  $H/W=2.58$  (b). The colour legend is for the wind directions.

Figure 3-10 and Figure 3-11 show the critical wind directions for low-rise and high-rise buildings, respectively. As seen in Figure 3-7, there are differences in the behaviours of suctions on low-rise and high-rise buildings. Similarly, the critical wind directions are different on low-rise and high-rise buildings. The majority of critical wind directions were from 90-180°, however there were some between 60-80°. The aspect ratio clearly affects the distribution of critical wind directions, with the two low-rise buildings showing differences in the wind direction patterns.

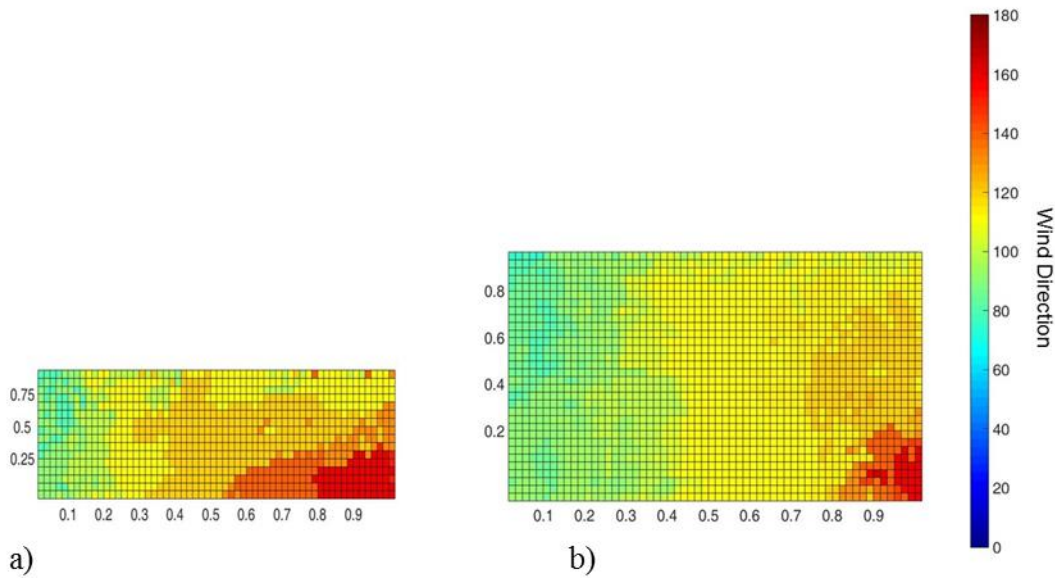


Figure 3-10: Distribution of angles causing the worst suction pressure coefficients for low-rise of  $H/W=0.28$  (a) and  $H/W=0.56$  (b). The colour axis is for the different wind directions.

Figure 3-10 provides the low-rise building critical wind directions. Comparing to Figure 3-7, the low-rise building has highest suctions within 10-20% away on the leading edge. These occur for wind angles between  $70-100^\circ$ . For the lower suctions spanning the right half of the building, corresponds with the wind direction of  $110-120^\circ$ . The critical wind directions of  $160^\circ$  correspond with relatively small suctions values and, when mirroring the pressure coefficients for design, will disappear. The difference between the two low-rise buildings is likely a result of the change to the separation bubble as the  $H/W$  ratio increases, consistent with the aspect ratio effects observed by Akon and Kopp (2016) for roofs. Lower wind directions are governing for a larger portion of the higher aspect ratio, as the separation bubble is larger for the taller building.

Figure 3-11 shows the high-rise building critical wind directions. From Figure 3-7, the highest suctions were on the right side of the building, the top left corner and left bottom corner.

The high suction at the bottom of the building is likely caused by a separation bubble at the bottom of the building. The 70-90° wind directions are critical for roughly 65-70% of the building width. The lower suction zone in Figure 3-7 (70-90% of the building width) is associated with the wind direction of 120°. This is due to a change in the separation bubble thickness.

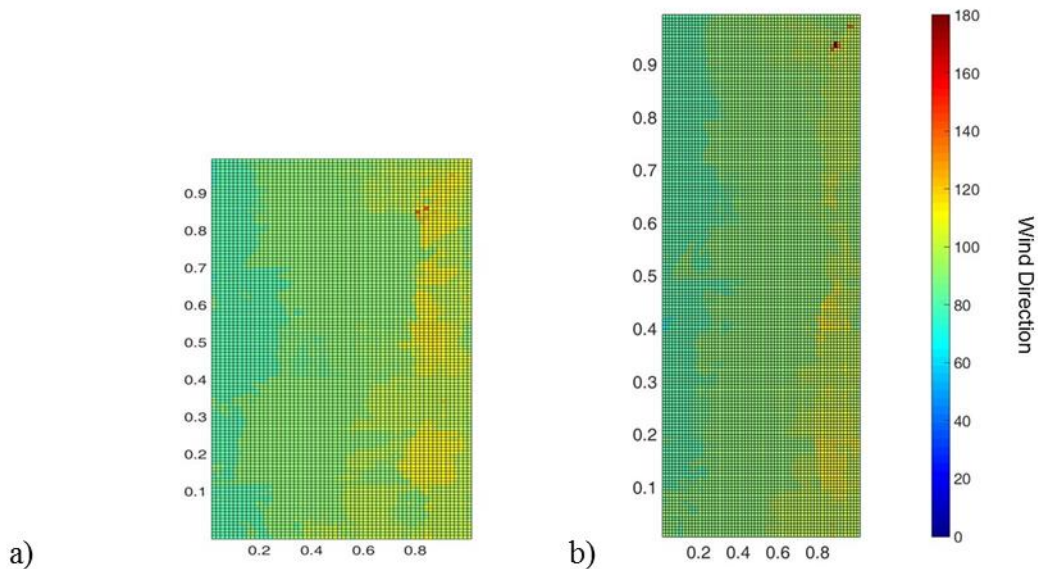


Figure 3-11: Distribution of angles causing the worst suction pressure coefficients for high-rise of  $H/W=1.2$  (a) and  $H/W=2.58$  (b). The colour axis is for the different wind directions.

To examine the changes in separation bubbles, the pressure coefficients for buildings at wind directions of 90° and 120° were examined. Figure 3-12 shows the pressure coefficients for the  $H/W=0.28$  building at these angles. The pressure coefficients for 90° are higher at the leading edge. The separation bubble extends to about 20% of the building width, if the distribution identified by Akon & Kopp (2016) holds for walls. In comparison, at 120° the separation bubble

extends further, as one might expect for the increased angle of attack. However the pressure coefficients on the building are lower at the edge, but extend further along the wall, where larger values are observed for 120°. There are also differences along the height of the building and at the top of the wall which may be due to the flow over the roof.

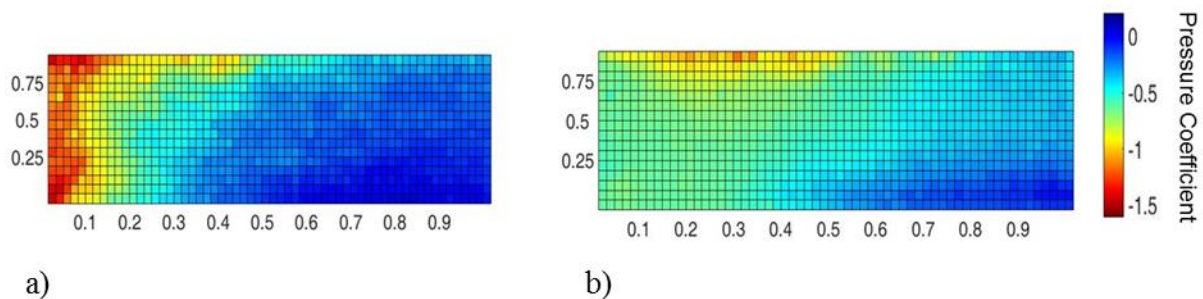


Figure 3-12: Pressure coefficients for low-rise building ( $H/W=0.28$ ) at wind directions of 90° (a) and 120° (b).

The pressure coefficients for the high-rise ( $H/W=2.58$ ) building for wind directions of 90° and 120° can be seen in Figure 3-13. For 90°, the magnitudes of the suctions are larger on both the windward wall and the leeward wall. There is a lower suction zone towards the top of the leeward wall. There is a higher suction zone towards the bottom of the building. In comparison, the 120° wind direction has lower magnitudes throughout the building. The high



suction zone on the leeward wall has decreased in magnitude and does not extend as far up the height of the building. Most of the building is the same magnitude, with low suctions between -1 and -0.5. The separation bubble has increased in size, to around 70-80% of building width for a wind direction of  $120^\circ$ , and there may be reattachment on the wall.

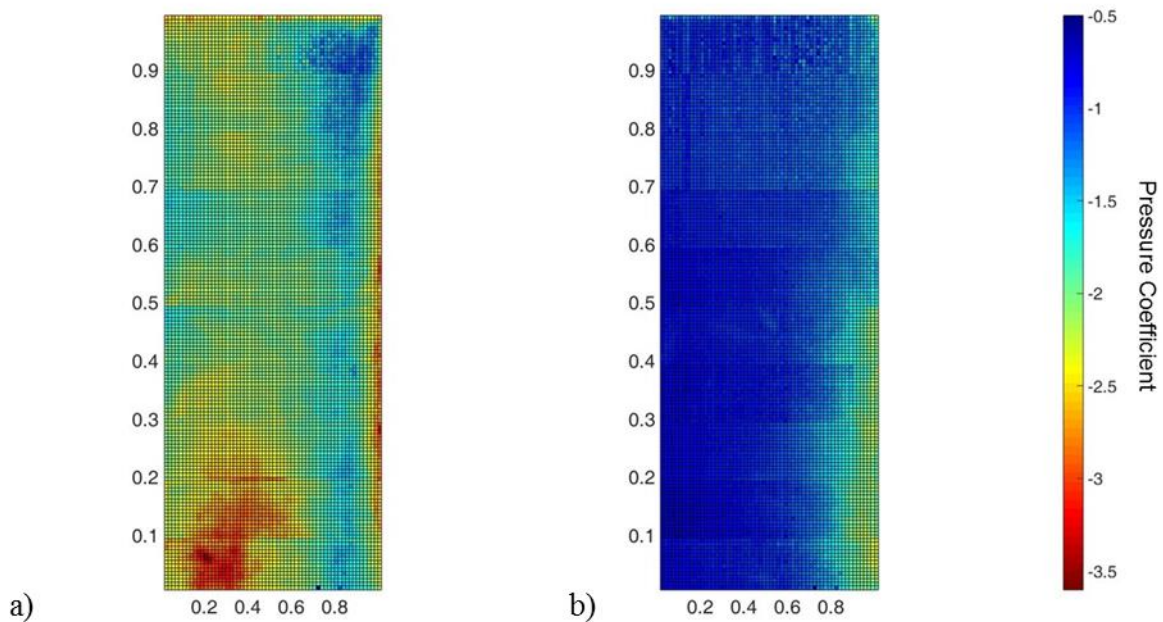


Figure 3-13: Pressure coefficients for high-rise building ( $H/W=2.58$ ) at wind directions of  $90^\circ$  (left) and  $120^\circ$  (right).

Comparing Figure 3-12 and Figure 3-13, the aspect ratio of the building clearly affects the length of the separation bubble, with a larger aspect ratio resulting in a larger separation bubble. The separation bubble effects increase the suctions towards the top of the building for the low-rise building while the high-rise building has increased suctions towards the bottom of the

building. The low-rise building does not have the same effects on the leeward edge as the high-rise building.

### 3.2.3 Mirroring the Pressure Coefficients and Normalizing

Due to the symmetry of the model, the enveloped peak pressure coefficients were mirrored on both sides. During testing, only 180° were tested, 360° degrees would result in symmetric distributions. This was performed for all areas examined. Additionally, the building dimensions were normalized by the building height so that the pressure distributions are easier to compare. Figure 3-14 shows the positive pressure coefficients for the six building aspect ratios. From these figures, similarities in the pattern are observed for the different buildings. For example, all buildings have lower pressures at the top of the building, with the highest pressure coefficients directly beneath these on the walls.

Examining the low-rise buildings,  $H/W < 1$  (Figure 3-14 (a)-(c)), the mirrored pressure contours all have similarities. There are lower pressures along the top edge of the building. The largest pressure values are all around the same  $z/H$ : 0.5-0.9 for  $H/W=0.28$ , 0.4-0.95 for  $H/W=0.52$  and 0.3-0.95 for  $H/W=0.8$ . There is a region of lower pressures towards the bottom of the building. This region is larger than the pressures at the top of the wall. This region is similar among the different  $H/W$  ratio, below  $z/H$  of 0.5 for  $H/W=0.28$ , 0.4 for  $H/W=0.52$  and 0.3 for  $H/W=0.80$ .

The high-rise buildings (Figure 3-14 (e)-(f)) are more uniform throughout the whole building. There are still lower pressures at the top of the wall and towards the bottom of the building. Figure 3-14 (d) is the cube case and is a transition between the low-rise and high-rise

patterns. The lower pressure zone towards the bottom of the building decreases further and the magnitude of pressure values increases further.

These lower pressures near the bottom of the building are likely caused by horseshoe vortices. This flow pattern may be occurring on the windward wall. This characteristic is most prominent on the low-rise building cases. As the  $H/W$  ratio increases, the vortex structure changes and this horseshoe pattern begins to disappear. For the high-rise buildings, there are no lower pressure zones found near the bottom of the building and the flow likely just moves around the building without a strong horseshoe vortex.

Figure 3-15 shows the negative pressure coefficients for the six building configurations. The magnitude of the suction increases as the  $H/W$  ratio increases.  $H/W$  ratio of 0.28 has the lowest suction with higher suction towards the edges of the building. At  $H/W=0.52$  and  $H/W=0.80$ , a pattern begins to emerge. The suction starts to increase along the edges, with the biggest increase occurring at the corners. At  $H/W=0.80$ , the suction along the top of the wall begins to increase. At  $H/W=1.08$ , a high suction zone begins to develop at the bottom of the wall. For the high-rise buildings,  $H/W=1.83$  and  $H/W=2.58$ , the highest suction is near the bottom edge with high suction values along the other edges. At the tallest height configuration,  $H/W=2.58$ , this pattern is even more prominent with suction up to three times larger than those at  $H/W=0.28$ .

Examining these figures, there are differences in the patterns for low-rise and high-rise buildings, which implies different zones would be appropriate. For zoning, considering the effects of the size of cladding should also be examined. Figure 3-16 and Figure 3-17 show the positive and negative pressure coefficients respectively, of  $H/W=2.58$  for various cladding areas.

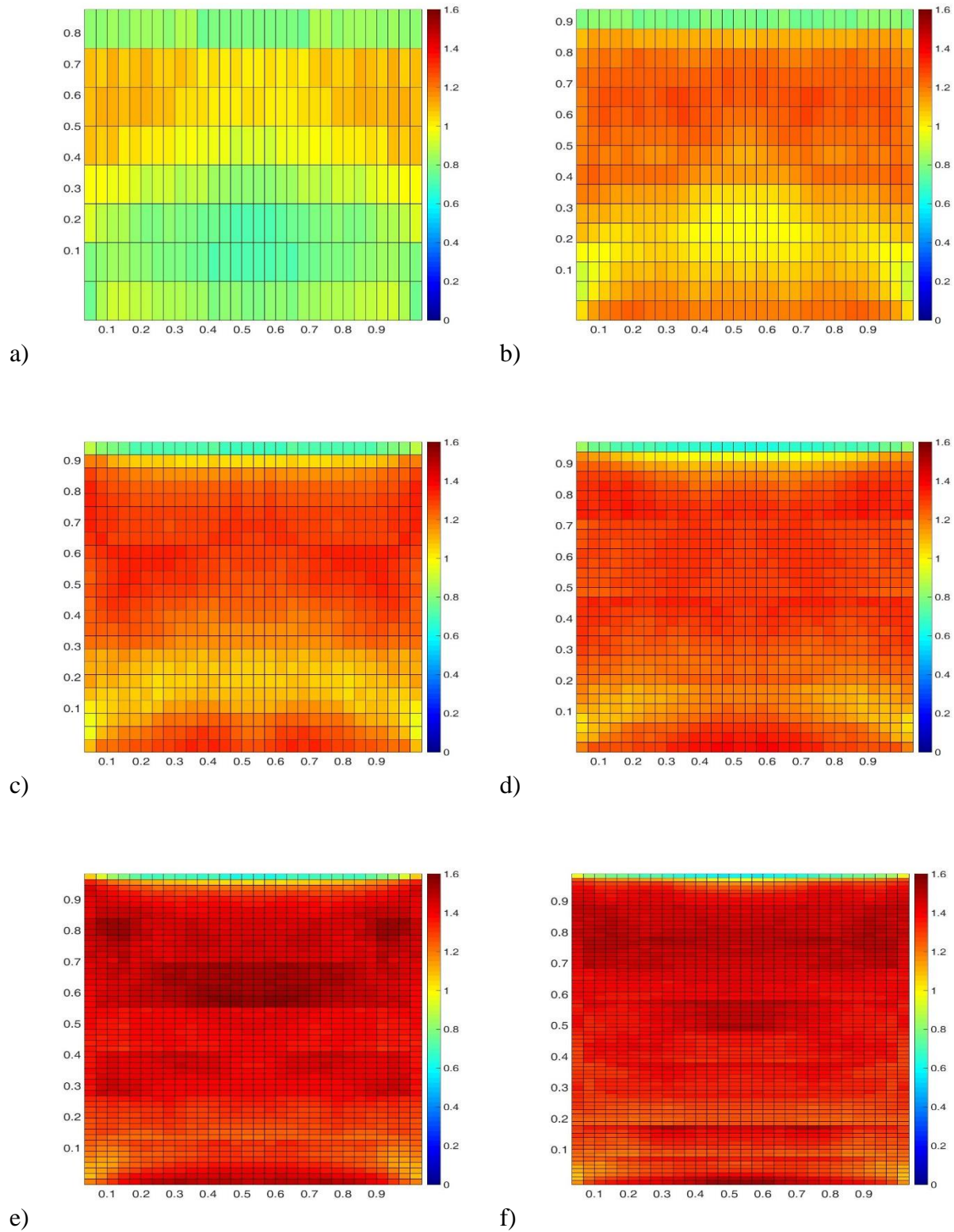


Figure 3-14: Positive pressure coefficients for cladding size of  $4.48 \text{ m}^2$  for a)  $H/W=0.28$  b)  $H/W=0.52$  c)  $H/W=0.80$  d)  $H/W=1.08$  e)  $H/W=1.83$  and f)  $H/W=2.58$ .

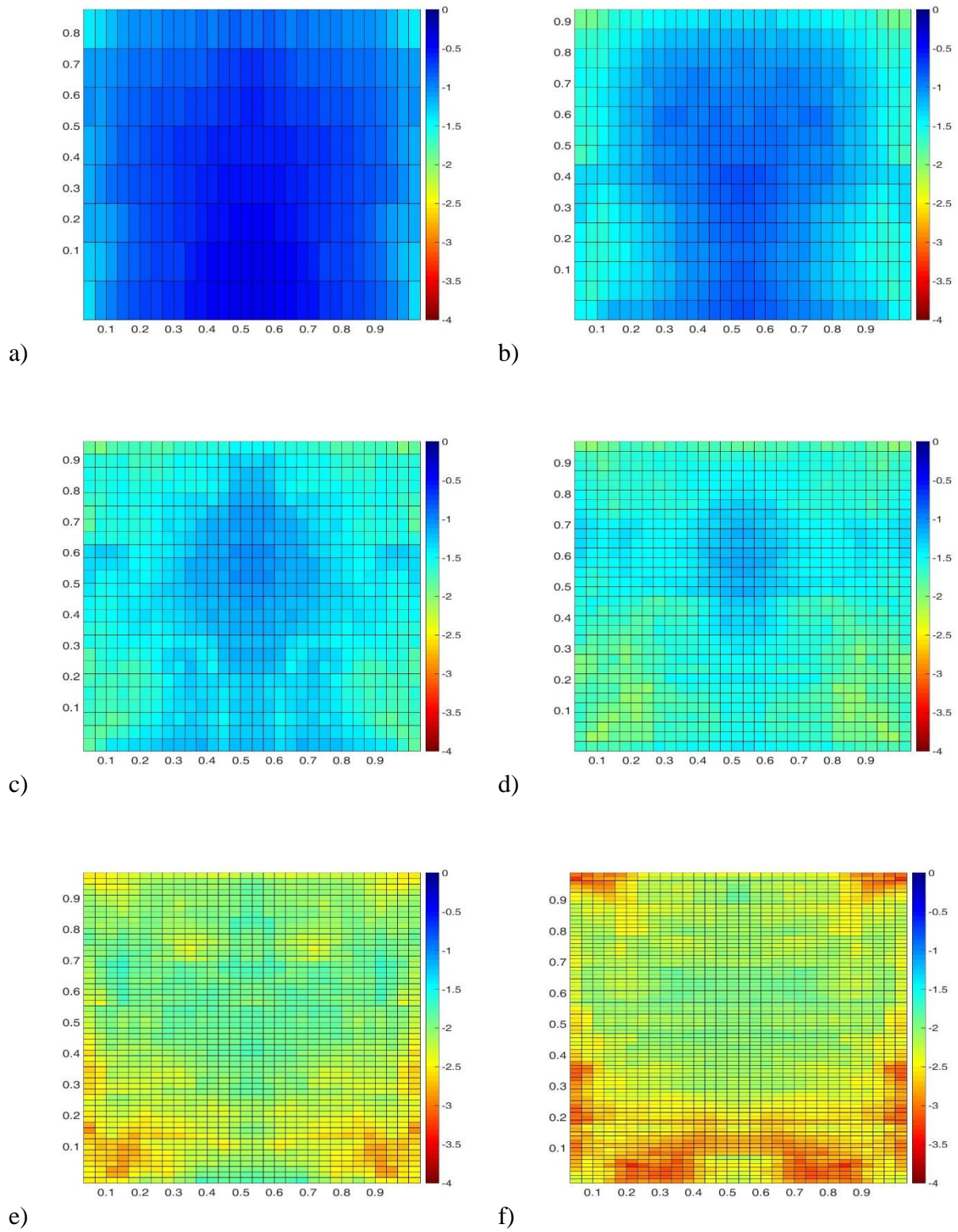
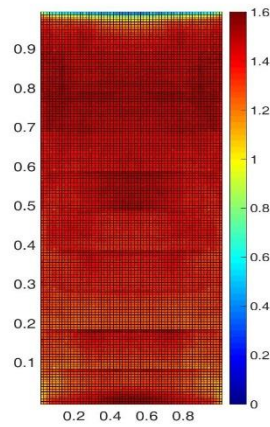
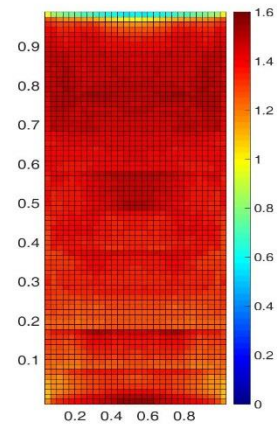


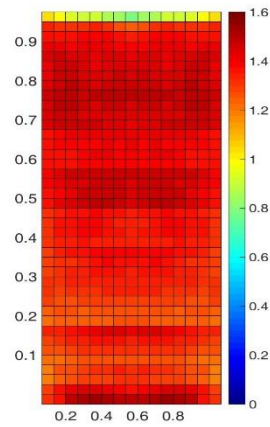
Figure 3-15: Negative pressure coefficients for cladding size of  $4.48 \text{ m}^2$  for a)  $H/W=0.28$  b)  $H/W=0.52$  c)  $H/W=0.80$  d)  $H/W=1.08$  e)  $H/W=1.83$  and f)  $H/W=2.58$ .



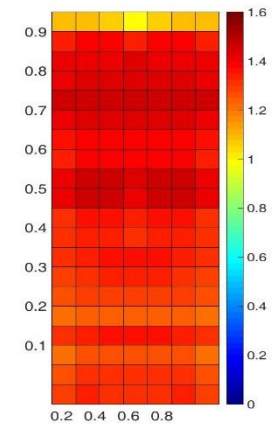
a)



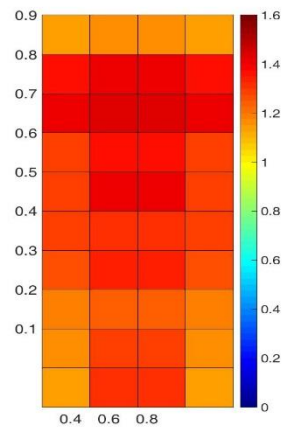
b)



c)

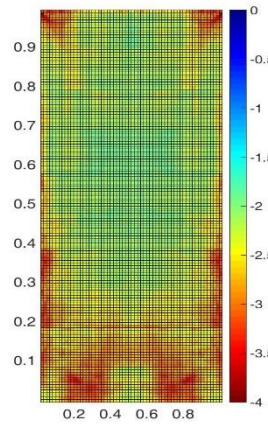


d)

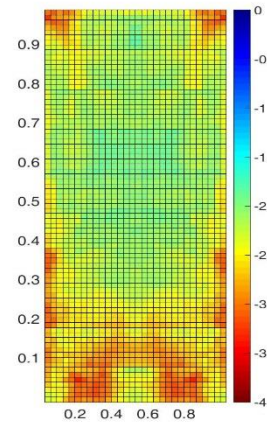


e)

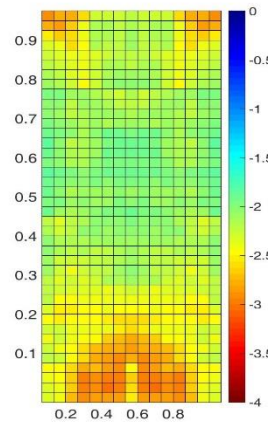
Figure 3-16: Positive pressure coefficients for  $H/W=2.58$  a)  $1.12 \text{ m}^2$  cladding size b)  $4.48 \text{ m}^2$  cladding size c)  $17.90 \text{ m}^2$  cladding size d)  $71.62 \text{ m}^2$  cladding size e)  $286.47 \text{ m}^2$  cladding size.



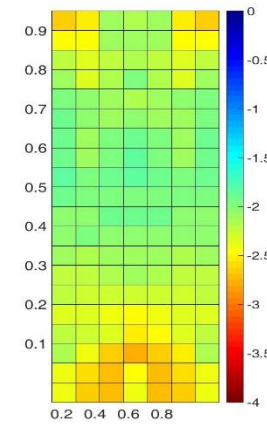
a)



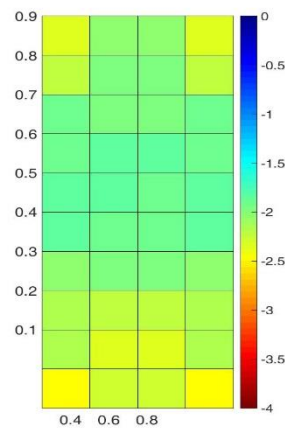
b)



c)



d)



e)

Figure 3-17: Negative pressure coefficients for  $H/W=2.58$  a)  $1.12 \text{ m}^2$  cladding size b)  $4.48 \text{ m}^2$  cladding size c)  $17.90 \text{ m}^2$  cladding size d)  $71.62 \text{ m}^2$  cladding size e)  $286.47 \text{ m}^2$  cladding size.

For all of the different cladding sizes, the patterns are similar. The increase in cladding size smooths the patterns previously observed in Figure 3-15. For the configuration shown,  $H/W=2.58$ , the maximum pressure decreases from 1.56 for tributary area of 1.1 m<sup>2</sup> to 1.43 for tributary area of 286.5 m<sup>2</sup> and the maximum suction decreases from -3.85 for tributary area of 1.1 m<sup>2</sup> to -2.47 for tributary area of 286.5 m<sup>2</sup>.

### **3.3 Cumulative Distribution Functions**

Cumulative distribution functions were used on the data to try and examine the enveloped pressure coefficients in a more statistical manner with respect to the zoning. In this section, the cumulative distribution functions will be shown for the whole building and cumulative distribution functions of different tributary areas will be discussed following that.

#### 3.3.1 Distributions for Different Aspect Ratios

From the pressure coefficient patterns shown earlier, it is clear that the different height configurations have different ranges and distributions of pressure coefficient values. Figure 3-18 shows the positive pressure coefficient cumulative distribution functions for a tributary area of 4.5 m<sup>2</sup>. The positive pressure coefficients are larger for the taller buildings. The two high-rise building cases,  $H/W=1.83$  and  $H/W=2.58$ , are similar in magnitude and distribution. The low-rise buildings have a larger spread in the magnitudes of the pressure coefficients,  $H/W=0.28$  peaks around 1.2, while  $H/W=0.80$  peaks around 1.4. The spread of the pressure coefficient values increases as the aspect ratio decreases, with the lowest aspect ratio having a wider spread in values. The steep distribution shows that there may not be a need for different zones for positive



pressure coefficients. The lower pressure coefficients, seen in Figure 3-18, are at the top of the wall and are all within a small percentile of the distribution.

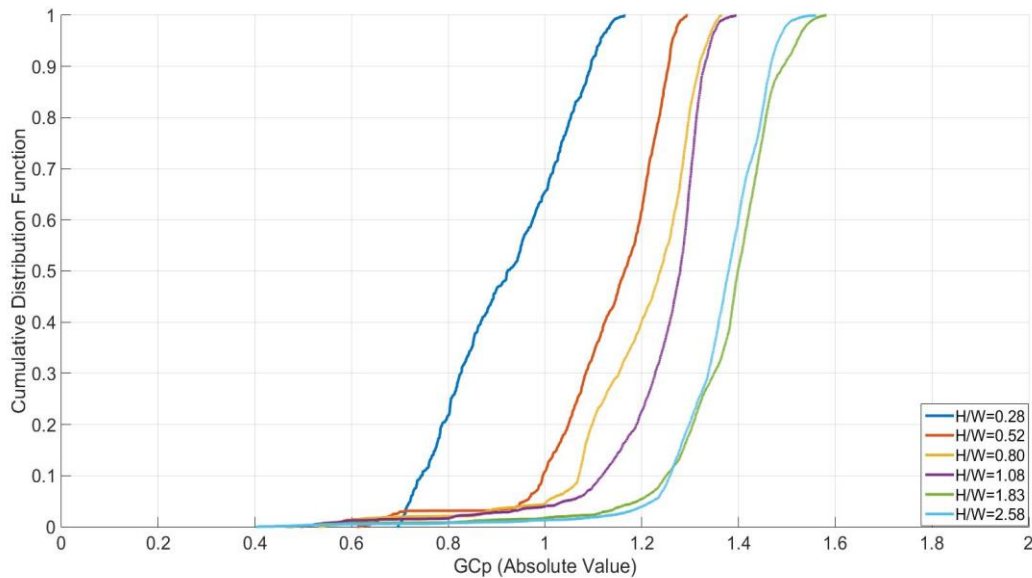


Figure 3-18: Cumulative distribution functions at different H/W ratios for cladding size 4.48 m<sup>2</sup> for positive pressure coefficients.

The cumulative distribution functions for the negative pressure coefficients are shown in Figure 3-19. For these distribution functions, the distribution of pressure coefficients is more spread out. Due to this larger spread of values, different zones may be beneficial based on the cumulative distribution function. The low-rise buildings and high-rise buildings have different magnitudes. There are significant differences between buildings of the same category, comparing pressure coefficients of equal percentiles between height configurations show some large differences. At the 90<sup>th</sup> percentile for the two high-rise buildings, there is a difference of roughly 10%.

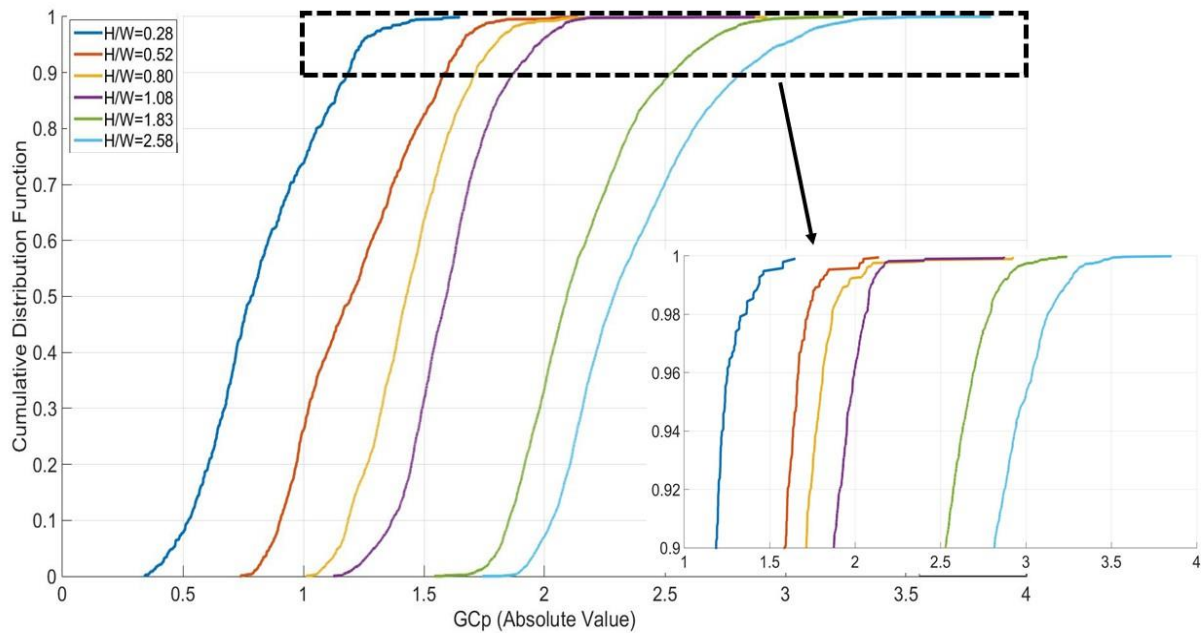


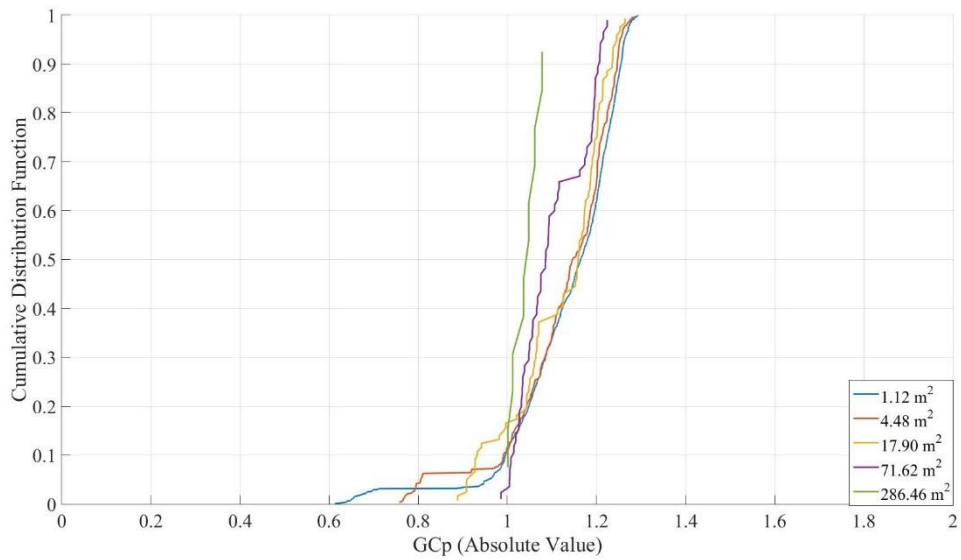
Figure 3-19: Cumulative distribution functions at different H/W ratios for cladding size 4.48 m<sup>2</sup> for negative pressure coefficients. Zoomed in view of 0.9 to 1.0.

### 3.3.2 Comparing Different Tributary Areas

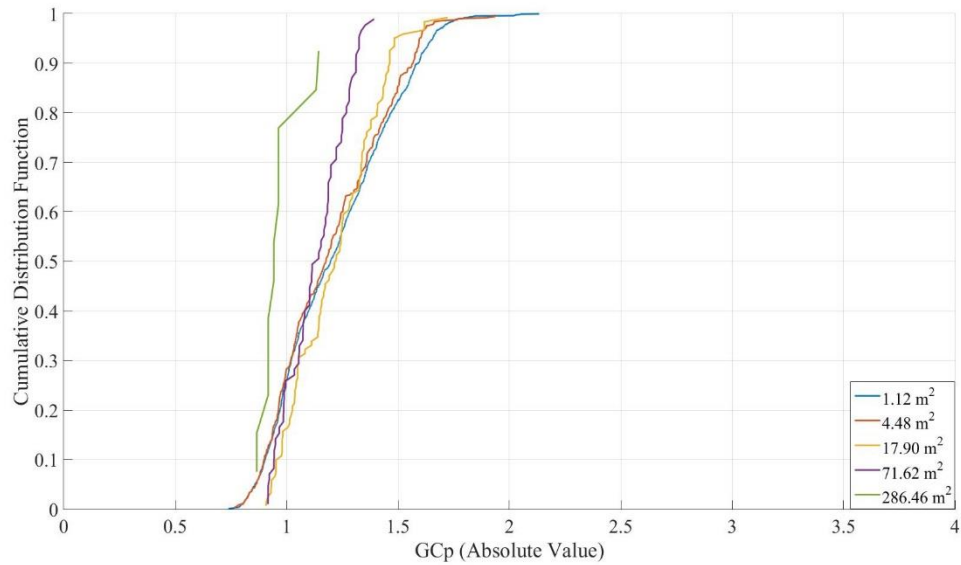
Figure 3-20 and Figure 3-21 show the cumulative distribution functions for different tributary areas. Figure 3-20 (a) and (b) show the low-rise building positive pressure coefficients and negative pressure coefficients respectively. Figure 3-21 (a) and (b) show the high-rise building positive pressure coefficients and negative pressure coefficients respectively.

For the positive pressure coefficients in Figure 3-20 (a), tributary areas from 1.12-17.90 m<sup>2</sup> are the same for most percentiles. At the larger tributary areas, 71.62 and 286.46 m<sup>2</sup>, there are larger decreases in  $GC_p$  with 286.5 m<sup>2</sup> having much lower values above the 45<sup>th</sup> percentile. The negative pressure coefficients have larger differences around the 80<sup>th</sup> percentile. The extreme

values for 71.6 m<sup>2</sup> are lower compared to 1.1-17.9 m<sup>2</sup>. The 286.5 m<sup>2</sup> is significantly lower than the distribution for 71.6 m<sup>2</sup>.

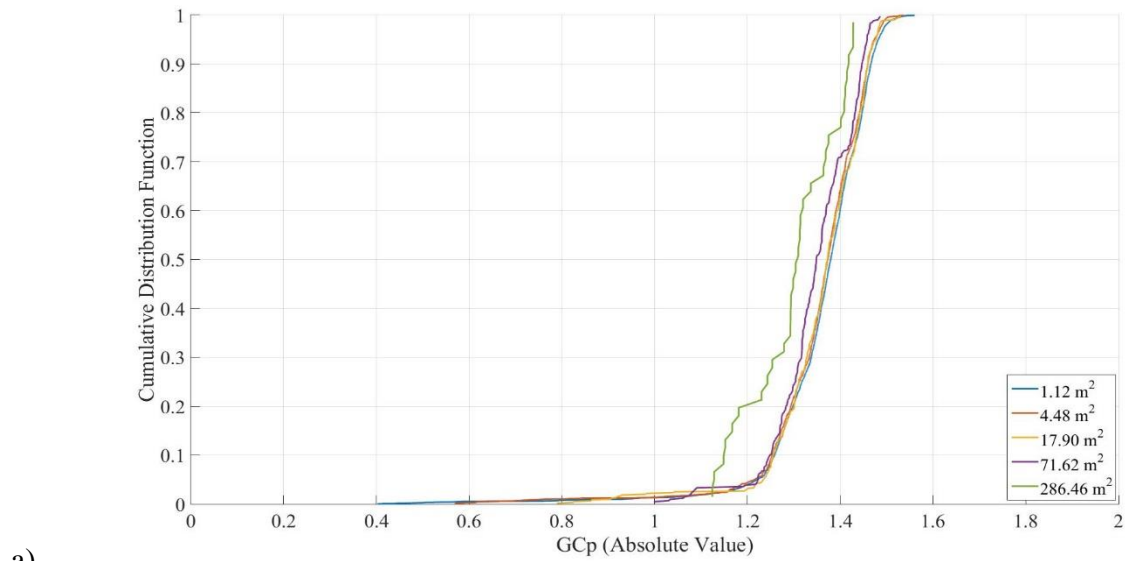


a)

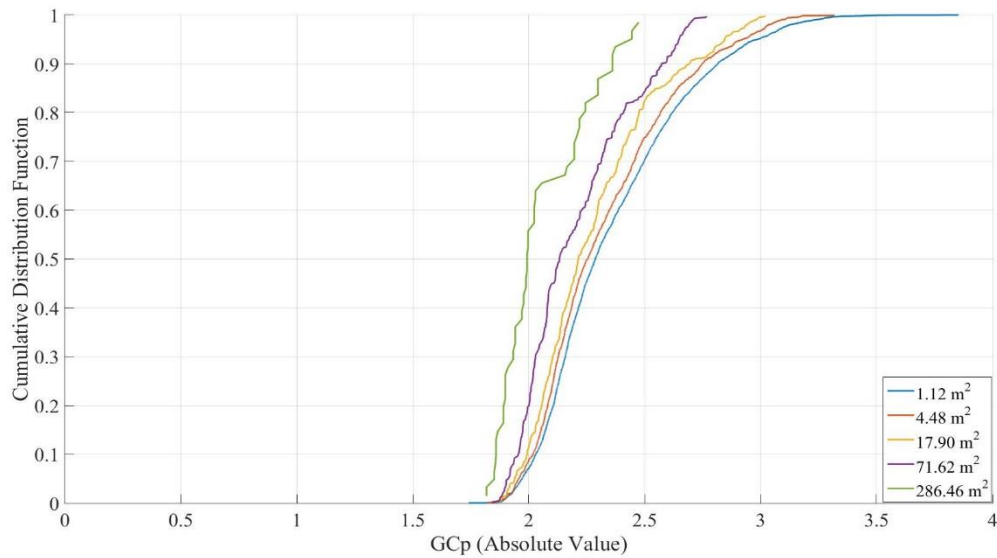


b)

Figure 3-20: Cumulative distribution function for the different cladding sizes of  $H/W=0.52$  for a) positive and b) negative pressure coefficients.



a)



b)

Figure 3-21: Cumulative distribution function for the different cladding sizes of  $H/W=2.58$  for a) positive and b) negative pressure coefficients.

The positive pressure coefficients in Figure 3-21 (a) show similar distributions for cladding sizes 1.1-71.6  $m^2$ . The distribution for 286.5  $m^2$  is lower than the other distributions by approximately 0.1 between the 10<sup>th</sup> and 20<sup>th</sup> percentile and above the 90<sup>th</sup> percentile. Between the

20<sup>th</sup> and 90<sup>th</sup> percentile this difference is lower. The negative pressure coefficients in Figure 3-21 (b) have large differences at the 98<sup>th</sup> percentile. The difference in suctions is largest at these high percentiles and decreases at lower percentiles.

From examining the cumulative distribution functions, the percentile affects the difference in  $GCp$  values. For the highest percentiles, there are larger differences in the  $GCp$  values. For some percentiles, most of the cladding sizes can use the same  $GCp$  value. This impacts the negative pressure coefficients more, positive pressure coefficients have similar distributions for most of the cladding sizes. The decrease in positive pressure coefficients occurs at large areas, with 1.1-17.9 m<sup>2</sup> having similar distributions before decreasing in magnitude at 71.6 m<sup>2</sup>. High-rise buildings have larger differences in  $GCp$  for the higher percentiles whereas low-rise buildings are more similar for different tributary areas.

### **3.4 Pressure Coefficients vs Position**

#### **3.4.1 Comparison of Vertical Position on Building**

To determine where zones might be appropriate, the effects of position on cladding elements were observed. Figure 3-16 and Figure 3-17 showed that the position along the height of the building affected the pressure coefficients. Figure 3-22 shows the pressure coefficients for  $H/W=2.58$ , using the most extreme pressure coefficients shown previously in Figure 3-16 and Figure 3-17. The positive pressure coefficients are uniform throughout the building excluding the top of the wall. At the top of the wall there is a decrease in the pressure coefficients.

There is more scatter for the negative pressure coefficients throughout the height of the building. Figure 3-22 (b) shows that there may be some difficulties in determining zones for the negative pressure coefficients. There are peaks in the suction values at both the top of the building and the bottom of the building. These peak values are around -3.0 to -3.4 and are at  $z/H$  below 0.4 and above 0.9. These regions also have some pressure coefficient values between -2.0 and -2.5. When comparing the lower suction region,  $z/H$  of 0.4 to 0.9, the suctions are generally between -2.0 and -2.5. This makes it difficult to determine an appropriate height to draw this distinction.

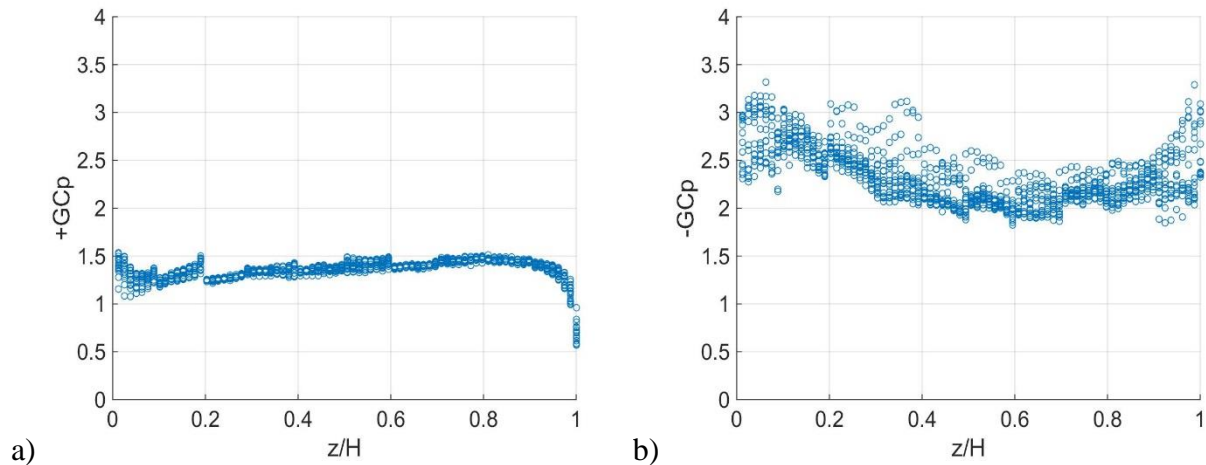


Figure 3-22: Pressure coefficients for  $H/W=2.58$  comparing the pressure coefficients of cladding size  $4.48 \text{ m}^2$  along the height of the building for a) positive pressures b) suctions.

### 3.4.2 Comparisons of Horizontal Position on Building

The effects of the position away from the wall edges were observed. The most extreme pressure coefficients for the cube are shown in Figure 3-23. This plot shows all the pressure

coefficient values for  $H/W=1.08$  for a tributary area of  $4.48 \text{ m}^2$ . The positive pressure coefficients are relatively constant for all distances away from the wall edge. The negative pressure coefficients show higher suction values at the edge of the wall, however this is a small decreasing trend. The suction coefficients from the outer edge to the centre decrease by roughly 0.5.

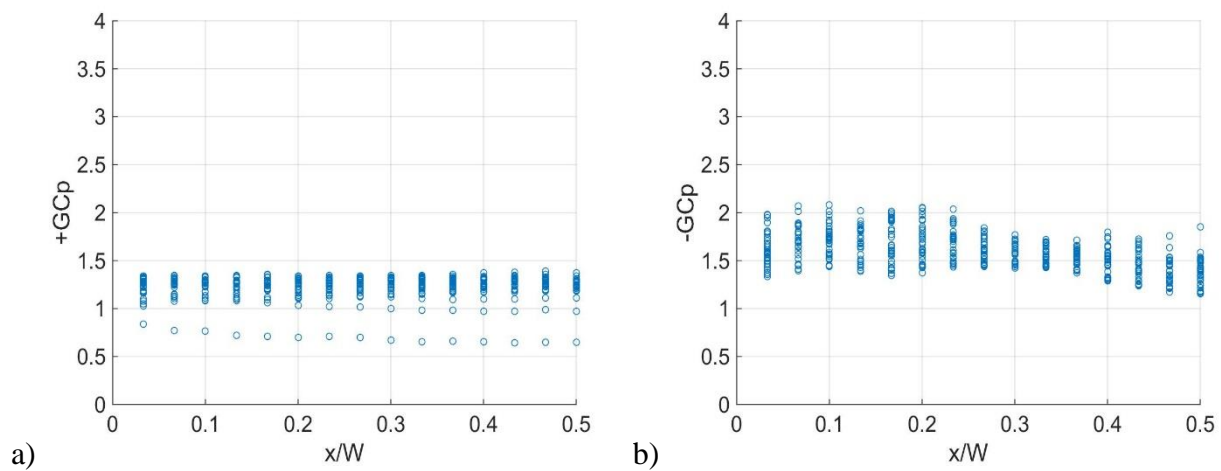


Figure 3-23: Pressure coefficients for  $H/W=1.08$  comparing the pressure coefficients of cladding size  $4.48 \text{ m}^2$  along the width of the building for a) positive pressures b) suction.

Figure 3-24 shows the negative pressure coefficient figures for other height configurations. Figure 3-24 (a) show a low-rise building and Figure 3-24 (b) shows a high-rise building. The low-rise building shows a decrease in pressure coefficient for more inner cladding elements. The worst suction and average pressure coefficients generally decrease as the cladding elements are position more inward. From Figure 3-15 (b), this was seen with all the highest suction values at the sides of the building. There are some higher suction values at the top center of the wall, however these values increase along the top towards the corners. The

suction values from the edge to the center decrease by roughly 0.5. The high-rise building shows less of a trend. There is still some decrease when observing the horizontal position along the wall, however the pressure coefficients values are generally all in the same range, independent of horizontal position. From Figure 3-15 (f), the high negative pressure coefficients (-2.5 to -4.0) are spread throughout the width of the building.

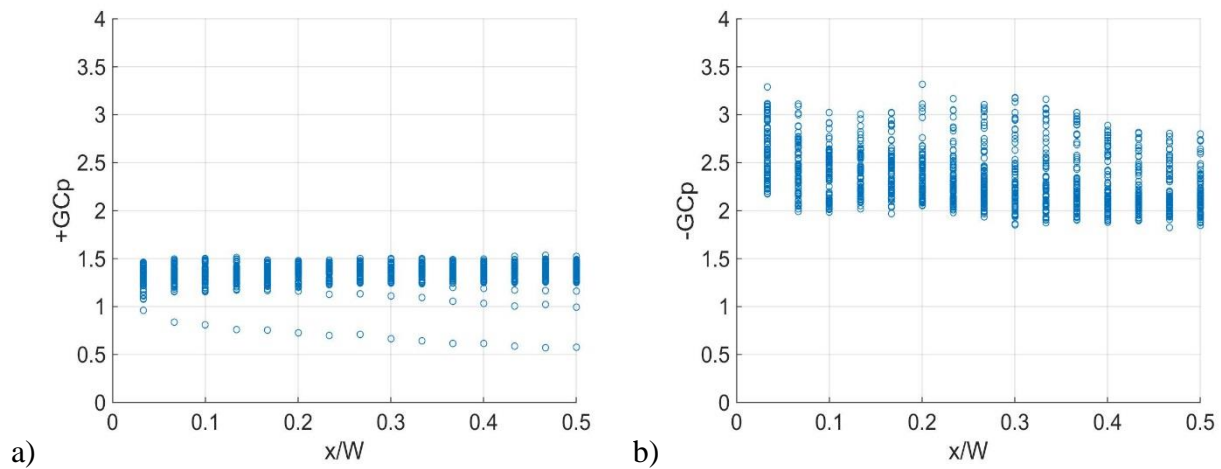


Figure 3-24: Negative pressure coefficients for cladding size  $4.48 \text{ m}^2$  along the width of the building a)  $H/W=0.52$  and b)  $H/W=2.58$ .

There are no trends observed between positive pressure coefficients and their position along the height of the building. The negative pressure coefficients show a trend of decreasing towards the center of the building. This is more prominent for low-rise buildings, with decreases in the worst values and average values around 0.5. For the high-rise building, there are some decreases in suction coefficients, however the suction coefficients are generally not affected by their horizontal position. For zoning purposes, zones with respect to horizontal position would



not be necessary. There may be some need for horizontal zoning for negative pressure coefficients for low-rise buildings, high-rise buildings do not appear to require this same zoning.

### 3.4.3 Comparisons of Position Away from Edges

The pressure coefficients with respect to their position away from all edges of the building is shown in Figure 3-25. This uses an approach similar to ASCE 7-88, seen in Figure 1-1. This comparison considered the distance away from the edge of the wall and the top of the wall. The positive pressure coefficients are constant throughout the building. The lower pressure coefficients were observed previously in Figure 3-22 along the top of the wall. The negative pressure coefficients show a decreasing trend away from the edges, with about a 10% drop after the 6<sup>th</sup> cladding element or at  $x/w=0.10$ .

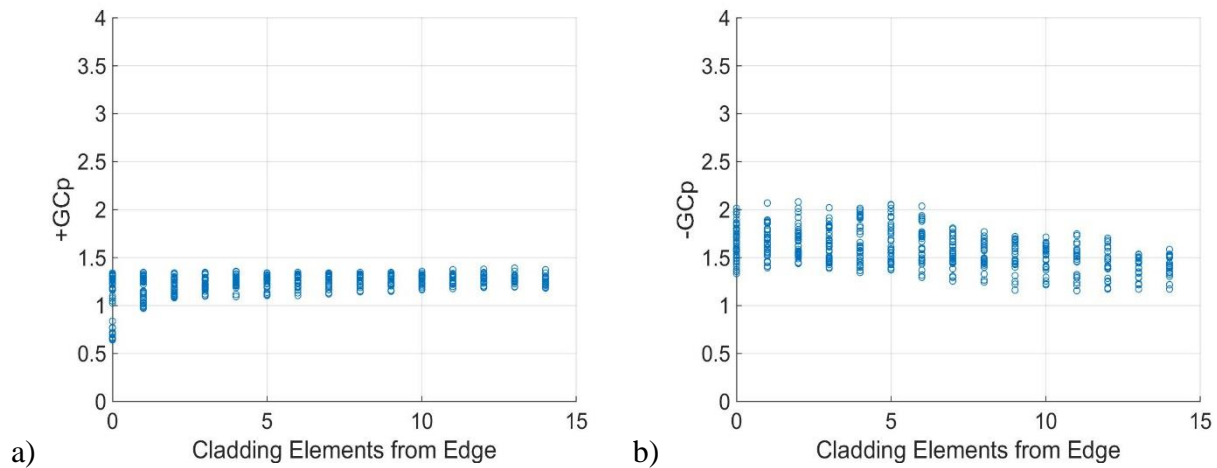


Figure 3-25: Pressure coefficients for  $H/W=1.08$  comparing the pressure coefficients of cladding size  $4.48 \text{ m}^2$  compared by the distance away from the edge of the wall for a) positive pressures b) suction.

Figure 1-1 used the distance from edges for high-rise buildings. Figure 3-26 shows the effect that the position away from edges has on the two high-rise building cases. There is no significant decreasing trend observed for the pressure coefficients. These figures imply that Figure 1-1's zoning for high-rise building was not appropriate to differentiate the suction zones.

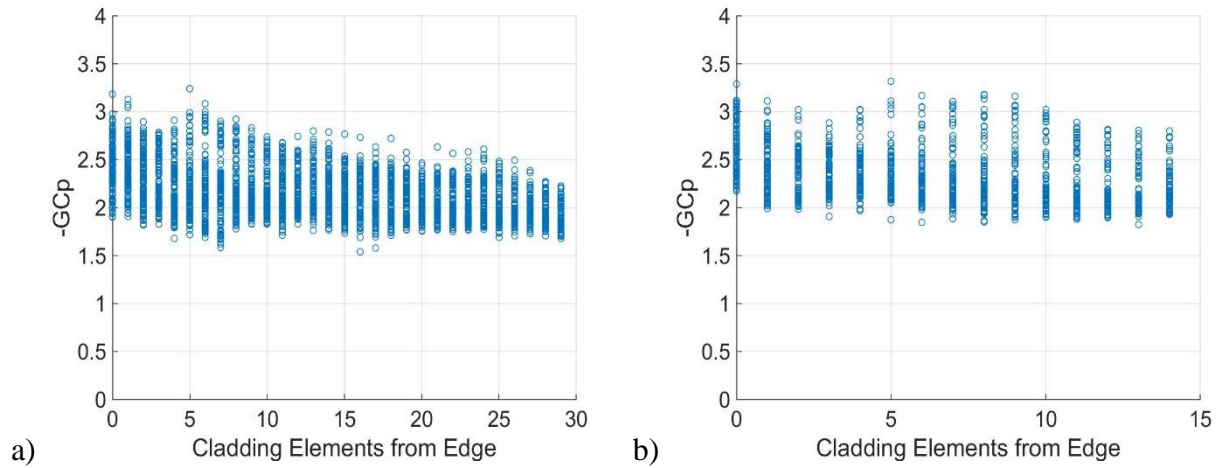


Figure 3-26 Negative pressure coefficients for cladding size 4.48 m<sup>2</sup> along the width of the building a) H/W=1.83 and b) H/W=2.58.

Figure 3-27 shows the negative pressure coefficients with respect to distance away from the edges for low-rise buildings. These figures show that zoning using distance away from edges may be better suited for low-rise buildings. There is a decreasing trend in the pressure coefficients away from edges. Using the distance away from the edge only works for the low-rise suction zones, in all other cases there are no observed trends.

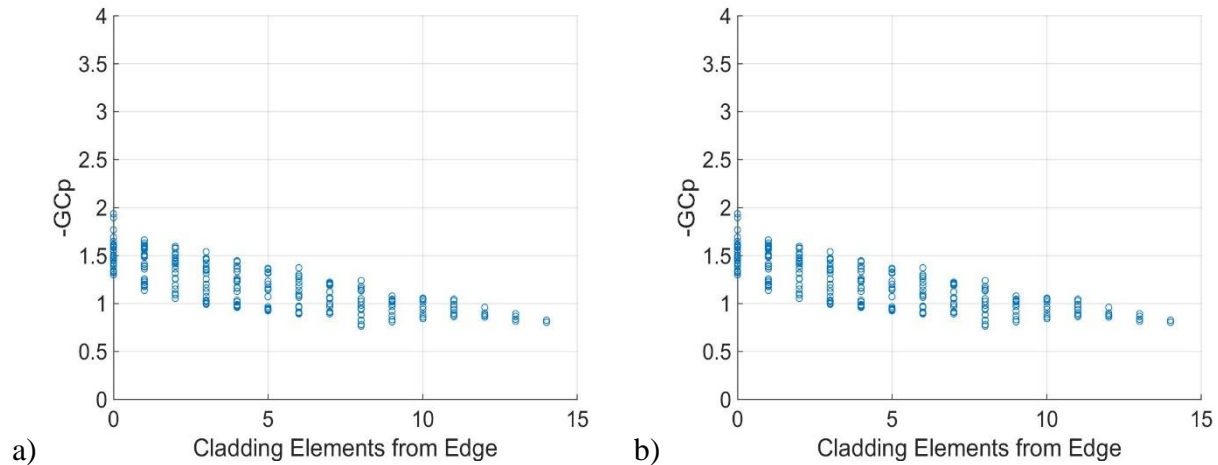


Figure 3-27 Negative pressure coefficients for cladding size  $4.48 \text{ m}^2$  along the width of the building a)  $H/W=0.52$  and b)  $H/W=0.28$ .

### 3.5 Current ASCE Building Code Comparison

The current study results were compared with the ASCE 7-10 (2010) provisions. Comparisons could be made for both the low-rise and high-rise data. These comparisons used the current zoning, although some of the current zoning provision patterns are not in good agreement with the data collected.

Figure 3-28 shows the data for high-rise buildings. The positive and negative values are all underestimated, with the lowest observed extreme values for smaller cladding areas being the closest to the current code provisions. With the two different observed height configurations, there are some magnitude differences between the pressure coefficient magnitudes. Overall, with the observed data, there is not good agreement between the magnitudes of the suctions and pressure values.

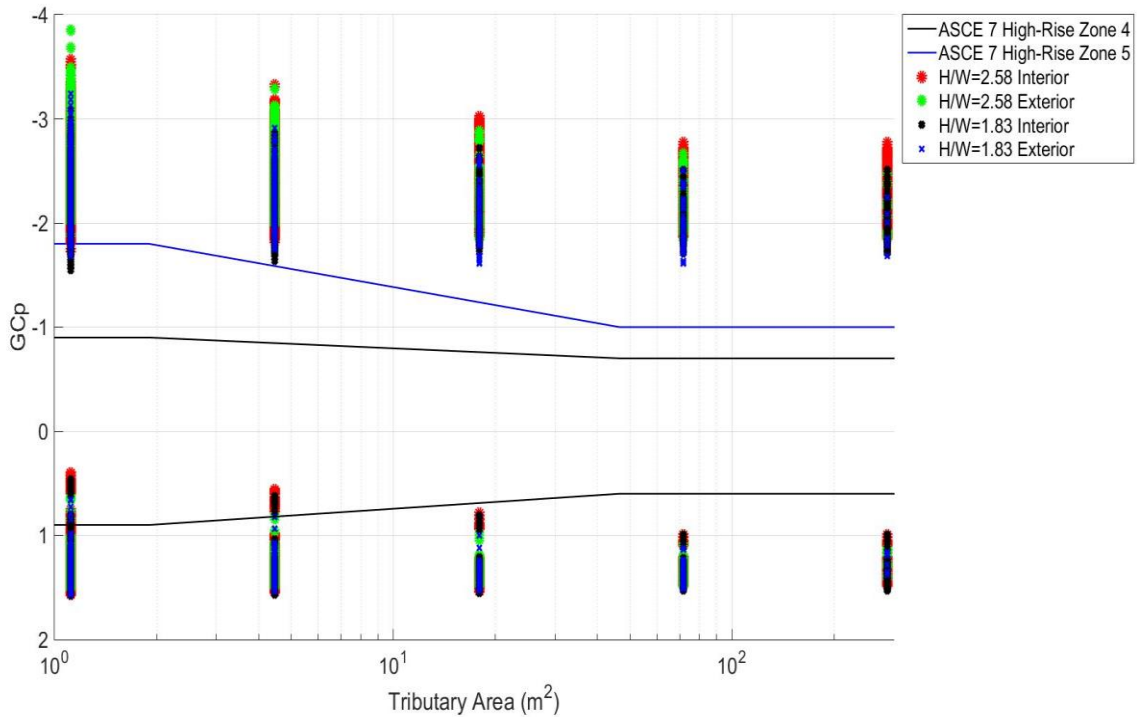


Figure 3-28: Comparison between the code and collected pressure coefficient values for high-rise buildings. The code values are from ASCE 7-10.

Figure 3-29 shows the comparison for low-rise buildings. The low-rise building data are closer in magnitude with the code values than the high-rise building data. The data still shows that the higher  $H/W$  ratios tend to have higher magnitude of pressure coefficient values. The negative pressure coefficient values are in good agreement for the lowest building tested. Figure 3-30 and Figure 3-31 show the comparison of the two lowest building configurations, with the current configuration being well suited for  $H/W=0.28$  but not as well suited for  $H/W=0.52$ . From the observed data, the decrease in the pressure coefficient for larger cladding elements is not as dramatic as the current code provisions suggest. The exterior zone pressure coefficients for larger cladding elements are similar, in many cases lower, than their interior zone counterparts as suggested in the current ASCE 7 code provisions.

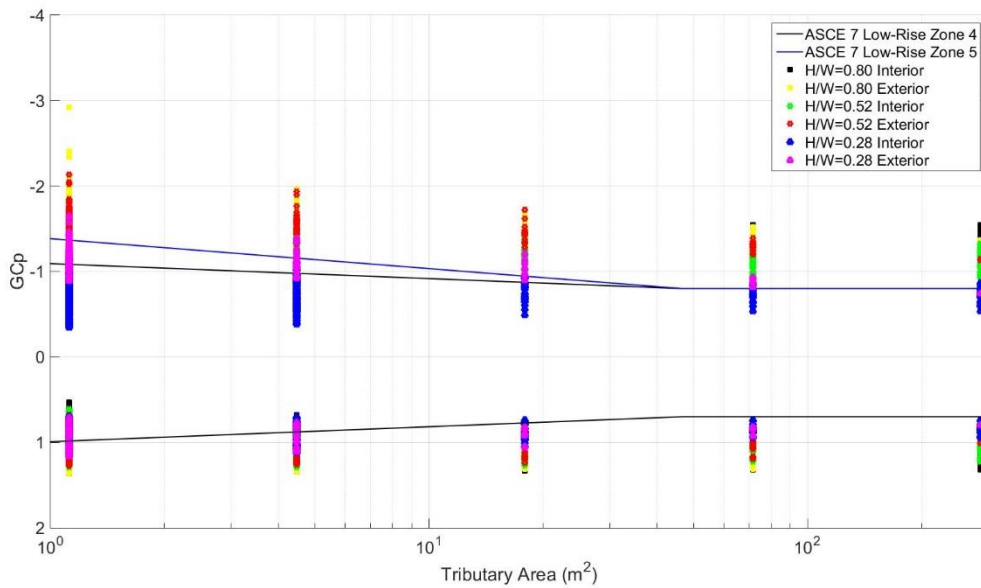


Figure 3-29: Comparison between the code and collected pressure coefficient values for low-rise buildings. The code values are from ASCE 7-10.

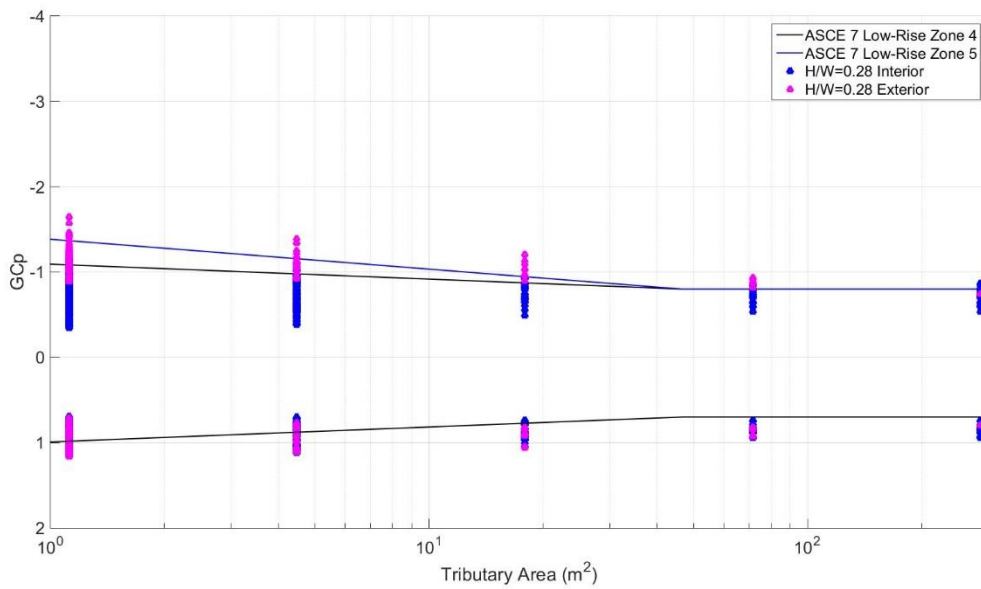


Figure 3-30: Comparison of the code provisions and observed data for  $H/W=0.28$ . The code values are from ASCE 7-10.

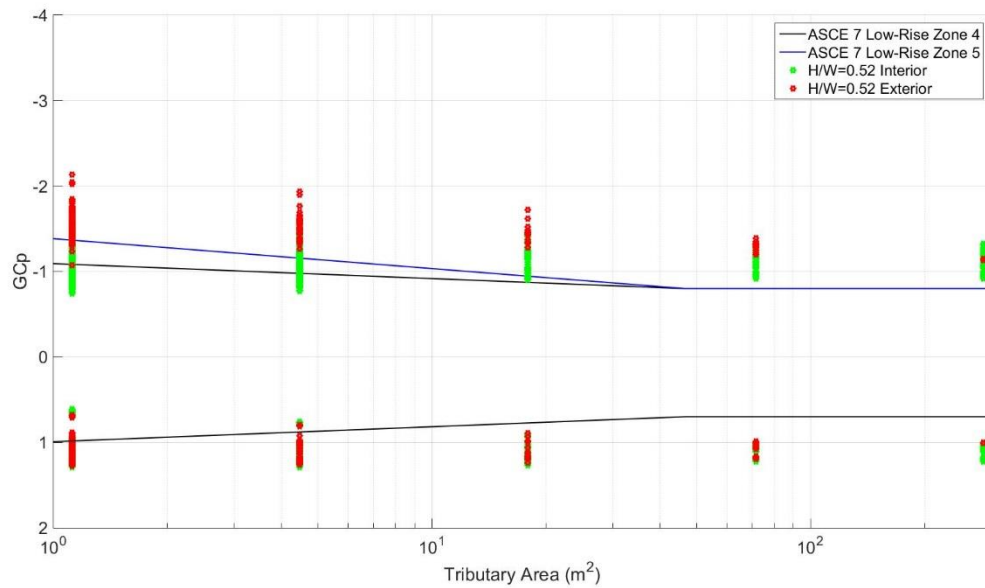


Figure 3-31: Comparison of the code provisions and observed data for  $H/W=0.52$ . The code values are from ASCE 7-10.

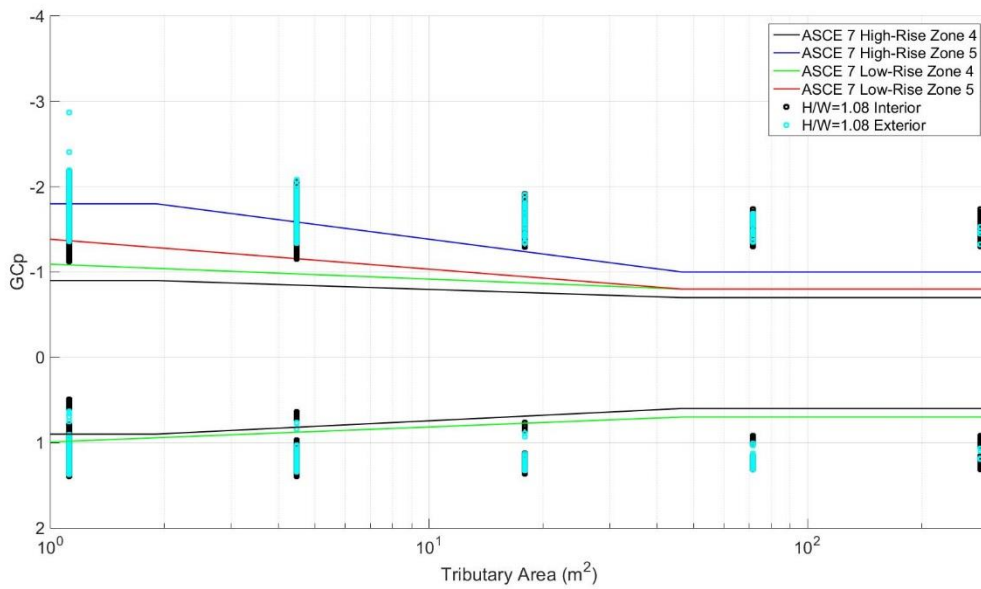


Figure 3-32: Code comparison for high- and low-rise compared with the cube configuration ( $H/W=1.08$ ). The code values are from ASCE 7-10.

Figure 3-32 shows the comparison for the cube ( $H/W \sim 1$ ). The positive pressures are better for smaller cladding sizes but underestimated for larger tributary areas. The high-rise provisions are better for this building configuration, the low-rise provisions only estimate and lower pressure coefficient values for the exterior zone. The interior zone provisions underestimate the observed data. Overall, neither of the two provisions are well suited to the observed data.

The low-rise data can also be compared to Gavanski and Uematsu (2014). Their study compared the negative pressure coefficients for ASCE 7 zone 4 and 5, as well as the positive pressure coefficients. Figure 3-33 shows the comparison of the positive pressure coefficients. The peaks from Gavanski and Uematsu's data is higher for smaller tributary areas, while for larger tributary areas the current study has larger values. These peaks decrease more in Gavanski and Uematsu's study and are relatively constant in the current study. Both sets of data are higher than the ASCE 7-10.

Figure 3-34 shows a comparison of the interior zones. The magnitude of the maximum suction is similar between Gavanski and Uematsu and the current study. In Gavanski and Uematsu's study, the pressure coefficients do not decrease until  $4 \text{ m}^2$ . The decrease is larger in their study; the suction at  $1 \text{ m}^2$  are less than -2 and at  $100 \text{ m}^2$  are around -1. The current study has similar pressure coefficients for smaller areas but the pressure coefficients at tributary areas  $>80 \text{ m}^2$  are not in good agreement, with the current study having pressure coefficients around -1.5.

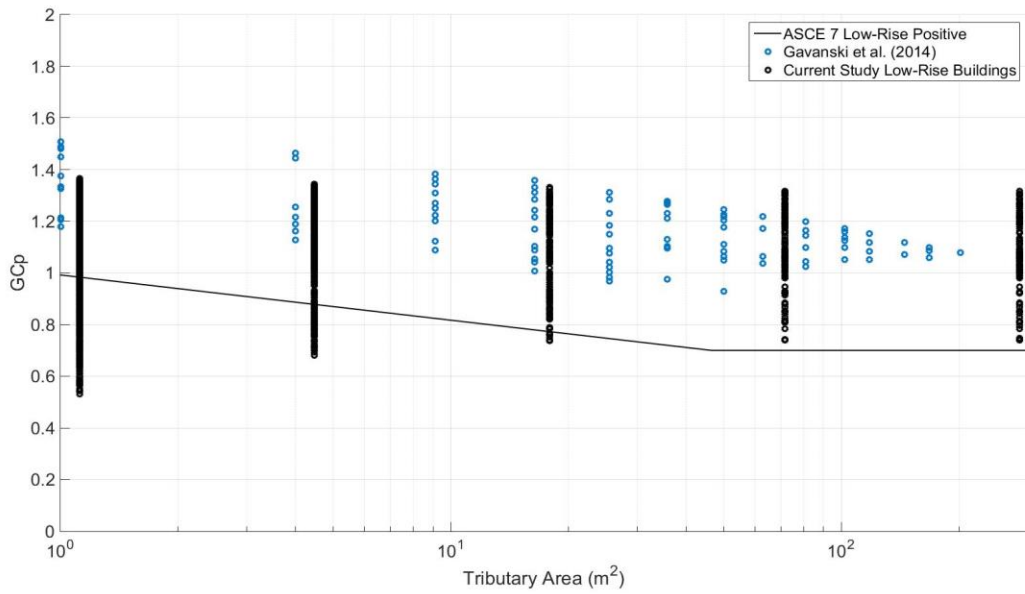


Figure 3-33: Comparison of positive pressure coefficients for low-rise buildings between ASCE 7, Gavanski and Uematsu (2014) and the current study ( $H/W=0.28$ ,  $H/W=0.58$ ,  $H/W=0.80$ ).

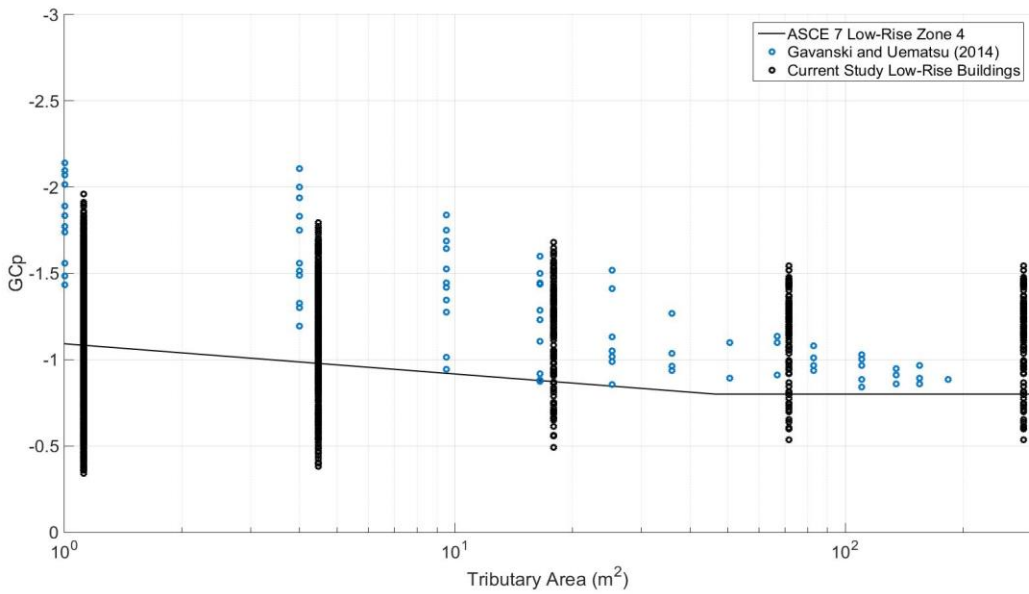


Figure 3-34 Comparison of interior zone negative pressure coefficients for low-rise buildings between ASCE 7 (Zone 4), Gavanski and Uematsu (2014) and the current study ( $H/W=0.28$ ,  $H/W=0.58$ ,  $H/W=0.80$ ).



Figure 3-35 shows the comparison of the low-rise buildings to the edge zone. These pressure coefficients are in better agreement than the positive pressure coefficients and Zone 4. The peaks of the current study are higher than Gavanski and Uematsu's data. There are still higher peaks in the current study, however the lower edge zone values are similar to their Gavanski and Uematsu's data.

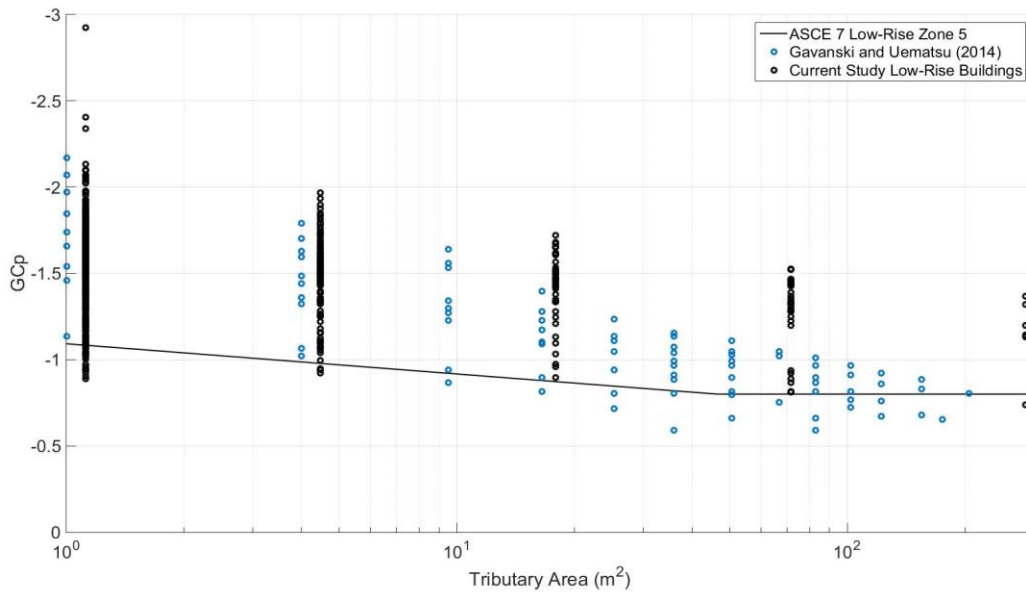


Figure 3-35: Comparison of edge zone negative pressure coefficients for low-rise buildings between ASCE 7 (Zone 5), Gavanski and Uematsu (2014) and the current study ( $H/W=0.28, 0.58, 0.80$ ).

Figure 3-36 shows the same comparison as Figure 3-35 with only the data for  $H/W=0.28$ . This height configuration is similar in magnitude for the larger tributary areas. The peaks for smaller tributary areas are higher for Gavanski and Uematsu's data than the current data set. The largest tributary area of the current study follows the trend of Gavanski and Uematsu's pressure coefficients.

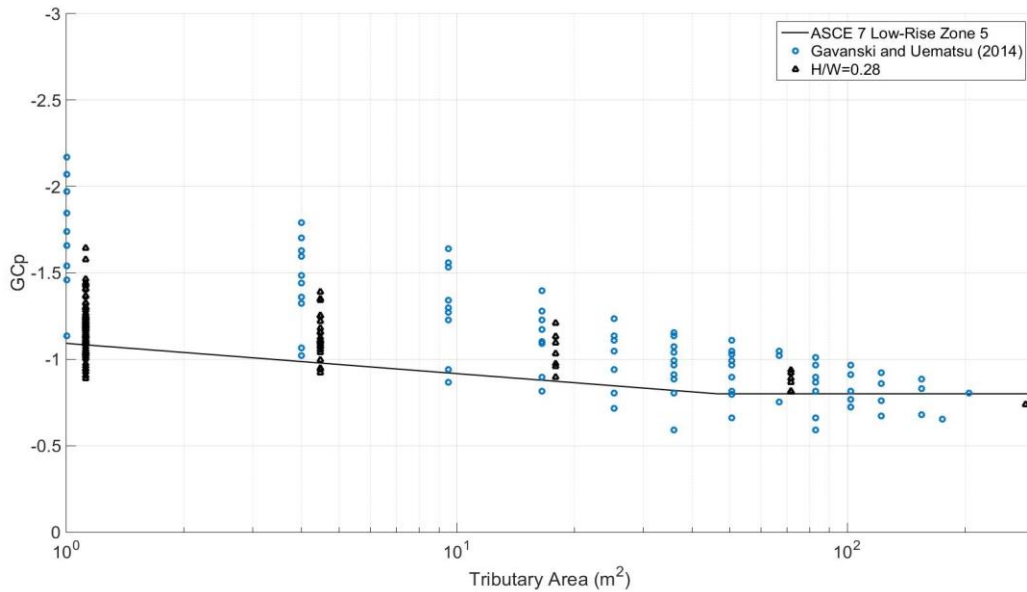


Figure 3-36: Comparison of edge zone negative pressure coefficients for low-rise buildings between ASCE 7 (Zone 5), Gavanski and Uematsu (2014) and  $H/W=0.28$ .

From these comparisons, similar conclusions can be made as Gavanski and Uematsu (2014) such as lower pressure coefficients for larger tributary areas and the differences in observed pressure coefficients and ASCE 7-10. The pressure coefficients observed for lower tributary areas were higher than the provisions in ASCE 7-10. In Gavanski and Uematsu (2014), the pressure coefficients for larger tributary areas were found to be overestimated in ASCE 7-10. The current study observes overestimations for  $H/W=0.28$  but at larger aspect ratios, these values are found to be underestimated.

### 3.6 Implications

From the data, there are some differences between the current results and ASCE 7-10. For design purposes, improvements can be made to the existing provisions. Some of the information in the current code provisions was supported in the findings. The negative pressure coefficients were found to be larger for the taller buildings. The positive pressure coefficients are uniform and unaffected by position on the building. There are decreases at larger cladding sizes and the exterior and interior pressure coefficients for these larger cladding sizes converge.

From the pressure patterns on the building, the behaviours of the flow fields around low-rise and high-rise buildings are quite different. The flow around the building may be better characterized by the aspect ratio of the building than estimating based on building height. These flow patterns show a continuously changing pattern from low-rise to high-rise buildings. This shows that the artificial boundary may not be the most effective way in determining building categorization and cladding zoning. The high suction values are caused by flow affects that behave differently for different aspect ratios. With the two high-rise building cases analyzed, the pressure zones are more developed in the taller  $H/W$  ratio. These results may mean the aspect ratio should be considered when categorizing a building.

For determining pressure coefficient values, the percentile chosen for design affects the magnitude of the pressure coefficient value. When comparing the pressure coefficients for different sizes of cladding, the largest differences are at higher percentiles. For lower percentiles, two cladding sizes may be designed to similar pressure coefficients. When comparing buildings of different height configurations, the pressure distributions were similar but at different magnitudes.

The current zones may not be the most efficient at determining the current design pressure coefficient values. The positive pressure coefficients have shown to be unaffected by position on the building, excluding the top of the wall which yields lower pressure coefficient values. The low-rise building negative pressure coefficients may be better zoned by using the distance away from all edges, the roof and sides of the building. The distances of such zones would depend on the percentiles chosen and the allowance for the overdesign of more interior cladding elements. The high-rise building pressure coefficients are more difficult to zone. Most of the higher suction zones are towards the bottom of the wall, the sides of the wall and the top of the building. The lower suction values are around the  $z/H$  of 0.4 to 0.9. From Figure 3-17 (e) and (f), there are higher suction regions identified. Characterizing and zoning these regions may result in zones that include the top corners of the building, the sides of the building and the bottom of the building.

## Chapter 4 Conclusion and Recommendations

### 4.1 Conclusions

The immediate aim of this study was to extend the current knowledge regarding the wind loading on walls of buildings with different aspect ratios. The motivation of this work was determining if the artificial boundary between low-rise and building heights at 60 ft. properly represent the physics or if a continuous trend could be determined. Additionally, the data provide a database of pressure coefficients for square planned buildings. These results may help refine the current wind load provisions and fill in some gaps in knowledge.

The study used a flexible model that allowed multiple building configurations to be studied. A scaling method was investigated that could be used for all building configurations. The reliability of the wind tunnel data was determined by comparing the collected data to data in the literature. The flow patterns on the building were identified based on the pressure patterns. Using area-averaging, pressure coefficients for tributary areas were determined. The Lieblein BLUE method was used to determine statistics related to the pressure coefficient values.

The following conclusions can be made:

- The wall aspect ratio affects the length of the separation bubble on the walls of the building. Many of the extreme suctions resulted from the flow separations for wind directions between 90° and 120°. These patterns are compressed spatially for smaller  $H/W$  ratios.
- For positive pressure coefficients, the lower magnitudes are found at the top of the building. For the low-rise buildings, there are zones of different pressure values; (i) there is a zone of higher pressure from the mid-height of the wall to the upper part of

the wall, with (ii) a lower pressure zone towards the bottom of the wall. The lengths of these zones differ, depending on the aspect ratio. For high-rise buildings, the pressures are more uniform over the full height of the building.

- For the suction coefficients, a continuously varying pattern was observed. The magnitudes of pressure coefficients are lower for the lower height configurations. Edge zones begin to develop as the aspect ratio (i.e., height) is increased at the wall edges and top. For high-rise buildings, strong suction develops near the bottom edge of the building.
- Low-rise building suction coefficients are better differentiated by the distance away from all edges. The positive pressure coefficients may not require zoning, the pressure patterns are mostly uniform excluding the top of the building. The top of the building has a lower pressure coefficient. High-rise buildings are harder to zone with the highest suction occurring at the top corners, the sides and bottom of the building. The size of these zones varies with aspect ratio, making them difficult to determine

The results show that there are some differences between the current code provisions and the observed data set. The current provisions use the height of the building as the parameter to set the pressure coefficients. Building aspect ratio may be a more effective parameter, this study examined the effects of the aspect ratio and its influence on the pressure patterns.

## 4.2 Recommendations

This study examined ten different height configurations. Although these height configurations examined low-rise and high-rise buildings, only building configurations were of a square plan. For a more thorough investigation, building configurations of rectangular plan should be investigated. Different plan shapes may affect the flow on some of the walls, causing different pressure coefficient magnitudes and patterns.

From the data, flow field patterns were observed. Further work could determine the mechanisms causing the change in separation bubbles for the different building configurations. Examination using particle image velocimetry (PIV) could be used to determine how the wind flows around the building. This analysis may help determine what factors affect the separation bubble thickness and intensity. These factors could be useful in determining the zones for code purposes.

## References

- Akon, A. F., Kopp, G. A., “Mean pressure distributions and reattachment lengths for roof-separation bubbles on low-rise buildings”, *Journal of Wind Engineering and Industrial Aerodynamics* Vol. 155 pp 115-125, 2016
- Baker, B., “Experiments on Wind Pressure”, *Engineering* Vol. 60, pp 787, 1895
- I.P. Castro, A.G. Robins, “The flow around a surface mounted cube in uniform and turbulent streams”, *Journal of Fluid Mechanics* Vol. 79, pp 307-335, 1977
- Dagnew, A. K., Bitsuamalk, G., Merrick, R., “Computational evaluation of wind pressures on tall buildings”, *11th Americas Conference on Wind Engineering*, Conference, 2009
- Dalgliesh, W. A., "Comparison of model/full-scale wind pressures on a high-rise building", *Journal of Wind Engineering and Industrial Aerodynamics* Vol. 1, pp 55-66, 1975
- Davenport, A. G., “Past, present and future of wind engineering”, *Journal of Wind Engineering and Industrial Aerodynamics* Vol. 90 Issue 12-15, pp 1371-1380, 2002
- Dhillion, S., Tait, C., Gray, J., Van Preat, N., Nelson, J., “The \$125-billion question”, *The Globe and Mail*, 21 March 2016, <http://www.theglobeandmail.com/news/where-will-125-billion-in-infrastructure-spendinggo/article28228477/>, Accessed Feb 1, 2017
- Cóstola, D., Blocken, B., Hensen, J. L. M. “Overview of pressure coefficient data in building energy simulation and airflow network programs”, *Building and Environment* Vol. 44, pp 2027-2036, 2009
- ESDU 74030, “Characteristics of atmospheric turbulence near the ground. Part I: definitions and general information”, 1974, CD, Engineering Science Data Unit
- ESDU 83045, “Strong Winds in the Atmospheric Boundary Layer”, 1983, CD, Engineering Science Data Unit
- ESDU 85020, “Characteristic of Atmospheric Turbulence near the Ground, Part II: single point data for strong winds (neutral atmosphere)”, 1985, CD, Engineering Science Data Unit
- Gavanski, E., Gurley, K. R., Kopp, G. A., “Uncertainties in the estimation of local peak pressures on low-rise buildings by using the Gumbel distribution fitting approach”, *Journal of Structural Engineering* Vol. 142 Issue 11, 2016
- Gavanski, E., Uematsu, Y., “Local wind pressures acting on walls of low-rise buildings and comparisons to the Japanese and US wind loading provisions”, *Journal of Wind Engineering and Industrial Aerodynamics* Vol. 132 pp 77-91, 2014



Higgins, M., “Keeping skyscrapers from blowing in the wind”, *The New York Times*, August 7, 2015, [https://www.nytimes.com/2015/08/09/realestate/keeping-skyscrapers-from-blowing-in-the-wind.html?\\_r=0](https://www.nytimes.com/2015/08/09/realestate/keeping-skyscrapers-from-blowing-in-the-wind.html?_r=0), Accessed Feb 1, 2017

Ho, T. C. E., Surry, D., Morrish, D., Kopp, G. A. “The UWO contribution to the NIST aerodynamic database for wind loads on low buildings: Part 1. Archiving format and basic aerodynamic data”, *Journal of Wind Engineering and Industrial Aerodynamics* Vol. 93, pp 1-30, 2005

Holmes, J. D., *Wind Loading of Structures*, Boca Raton, Florida CRC Press Taylor & Francis Group, 3<sup>rd</sup> Edition, 2015

Hölscher, N., Niemann, H. J. “Towards quality assurance for wind tunnel tests: A comparative testing program of the Windtechnologische Gesellschaft”, *Journal of Wind Engineering and Industrial Aerodynamics* Vol. 74-76, pp 599-608, 1998

Hui, Y., Tamura, Y., Yoshida, A., “Mutual interference effects between two high-rise building models with different shapes on local peak pressure coefficients”, *Journal of Wind Engineering and Industrial Aerodynamics* Vol. 104-106 pp 98-108, 2012

Hui, Y., Tamura, Y., Yoshida, A., Kikuchi, H., “Pressure and flow field investigation of interference effects on external pressures between high-rise buildings”, *Journal of Wind Engineering and Industrial Aerodynamics* Vol. 115 pp 150-161, 2013

Hussain, M., Lee, B. E., “A wind tunnel study of the mean pressure forces acting on large groups of low-rise buildings”, *Journal of Wind Engineering and Industrial Aerodynamics* Vol. 6 Issue 3-4, pp 207-225

Irtaza, H., Beale, R. G., Godley, M. H. R., “A wind-tunnel investigation into the pressure distribution around sheet-clad scaffolds”, *Journal of Wind Engineering and Industrial Aerodynamics* Vol. 103, pp 86-95, 2012

Irwin, P. A., Cicci, M. D., Lankin, J. B., “Variability of cladding pressures caused by adjacent buildings”, *Journal of Wind Engineering and Industrial Aerodynamics* Vol. 77-78 pp 147-156, 1998

Kim, Y., Tamura, Y., Yoshida, A., “Interference effects on local peak pressures between two buildings”, *Journal of Wind Engineering and Industrial Aerodynamics* Vol. 99 pp 584-600, 2011

Kim, Y., Yoshida, A., Tamura, Y., “Characteristics of surface wind pressures on low-rise building located among large group of surrounding buildings”, *Engineering Structures* Vol. 35 pp 18-28, 2012

Kopp, G. A., Morrison, M. J., Henderson, D. J., “Full-scale testing of low-rise, residential buildings with realistic wind loads”, *Journal of Wind Engineering and Industrial Aerodynamics* Vol. 104-106, pp 25-39, 2012

Kopp, G. A., Surry, D., Mans, C., “Wind effects on parapets of low buildings: Part 1. Basic aerodynamics and local loads”, *Journal of Wind Engineering and Industrial Aerodynamics* Vol. 93 Issue 11 pp 817-841, 2005

Kumar, K. S., “Pressure equalization of rainscreen walls: a critical review”, *Building and Environment* Vol. 35 Issue 2, pp 161-179, 2000

Lee, K. H., Rosowsky, D. V., “Fragility assessment for roof sheathing failure in high wind regions”, *Engineering Structures* Vol. 27 pp 857-868, 2005

Lieblein, J., “Efficient methods of extreme-value methodology”, *NBSIR 74-602*, Washington D.C. U.S., October 1974, CD

Lin, N., Letchford, C., Tamura, Y., Liang, B., Nakamura, O., “Characteristics of wind forces acting on tall buildings”, *Journal of Wind Engineering and Industrial Aerodynamics* Vol. 93 pp 217-242, 2005

Maruta, E., Kanda, M., Sato, J., “Effects on surface roughness for wind pressure on glass and cladding of buildings”, *Journal of Wind Engineering and Industrial Aerodynamics* Vol. 74-76, pp 651-663, 1998

Mehta, K. C., “Wind Load History: ANSI A58.1-1972 to ASCE 7-05”, *2010 Structures Congress*, 2010, CD

Oke, T. R., *Boundary Layer Climates*, U.K., Methuen & Co. Ltd., 2<sup>nd</sup> Edition, 1987

Ramponi, R., Angelotti, A., Blocken, B., “Energy saving potential of night ventilation: Sensitivity to pressure coefficients for different European climates”, *Applied Energy* Vol. 123, pp 185-195, 2014

Quiroga, P., “A study of wind effects for Milan Lombardi Government Center,” BLWT Report SS21-2005, 2005

Richards, P. J., Hoxey, R. P., Connell, B. D., Landar, D. P., “Wind-tunnel modelling of the Silsoe Cube”, *Journal of Wind Engineering and Industrial Aerodynamics* 95, pp 1384-1399, 2007

Richardson, G. M., Hoxey, R. P., Robertson, A. P., Short, J. L., “The Silsoe Structures Buildings: Comparisons of pressures measured at full scale and in two wind tunnels”, *Journal of Wind Engineering and Industrial Aerodynamics* Vol. 72, pp 187-197, 1997

Stathopoulos, T., “Turbulent Wind Action on Low-Rise Buildings”, Doctoral Thesis, University of Western Ontario, 1979

Stathopoulos, T., “Wind loads on low-rise buildings: a review of the state of the art,” *Engineering Structures* Vol. 6, Issue 2, pp 119-135, 1984

St. Pierre, L. M., Kopp, G. A., Surry, D., Ho, T. C. E., "The UWO contributions to the NIST aerodynamic database for wind loads on low buildings: Part 2. Comparison of data with wind load provisions", *Journal of Wind Engineering and Industrial Aerodynamics* Vol. 93 pp 31-59, 2005

Tamura, Y., Kikuchi, H., Hibi, K., "Extreme wind pressure distributions on low-rise building models", *Journal of Wind Engineering and Industrial Aerodynamics* Vol. 89 pp 1635-1646, 2001

Tieleman, H. W., "Wind tunnel simulation of wind loading on low-rise structures: a review", *Journal of Wind Engineering and Industrial Aerodynamics* Vol 91 Issues 12-15, pp 1627-1649, 2003

Tieleman, H. W., "Roughness estimation for wind-load simulation experiment", *Journal of Wind Engineering and Industrial Aerodynamics* Vol. 91 Issue 9, pp 1163-1173, 2003

Tieleman, H. W., Reinhold, T. A., Hajj, M. R., "Importance of turbulence for the prediction of surface pressures on low-rise structures", *Journal of Wind Engineering and Industrial Aerodynamics* Vol. 69-71, pp 519-528, 1997

Tieleman, H. W., Hajj, M. R., Reinhold, T. A., "Wind tunnel simulation requirements to assess wind loads on low-rise buildings", *Journal of Wind Engineering and Industrial Aerodynamics* Vol. 75-76, pp 675-685, 1998

Uemastu, Y., Isyumov, N., "Wind pressures acting on low-rise buildings", *Journal of Wind Engineering and Industrial Aerodynamics* Vol. 82 pp 1-25, 1999

Wind Loads Components and Cladding, ASCE-07-88, U.S.

Wind Loads Components and Cladding, ASCE-07-95, U.S. CD

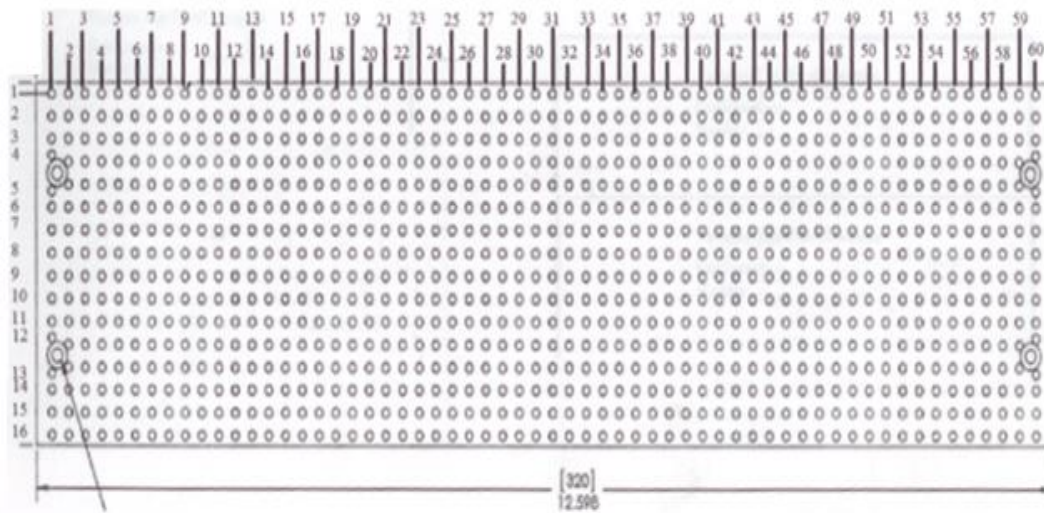
Wind Loads Components and Cladding, ASCE-07-10, U.S., 335-355, 2010, CD

Welch, P. D., "The use of the Fast Fourier Transform for the estimation of power spectra: A method based on time averaging over short, modified periodograms", *IEEE Transactions on Audio and Electroacoustics* Vol 15 Issue 2 pp 70-73, 1967

Zhang, A., Gu, M., "Wind tunnel tests and numerical simulation of wind pressures on buildings in staggered arrangement", *Journal of Wind Engineering and Industrial Aerodynamics* Vol. 96, pp 2067-2079, 2008

# Appendices

## Appendix A



Labeled as a grid:

Across from left to right, 1-60 for the column numbers. Vertically, labeled with 1 being at the top and 16 being at the bottom for the row numbers. Cells named with the convention of column numbers used then row number, with single digit row numbers being proceeded with a 0. Example pressure tap in column 31, row 4 would be 3104.

Figure A1: Excerpt from wind tunnel log. Depicts the naming convention of individual pressure taps on the pressure tap panel.

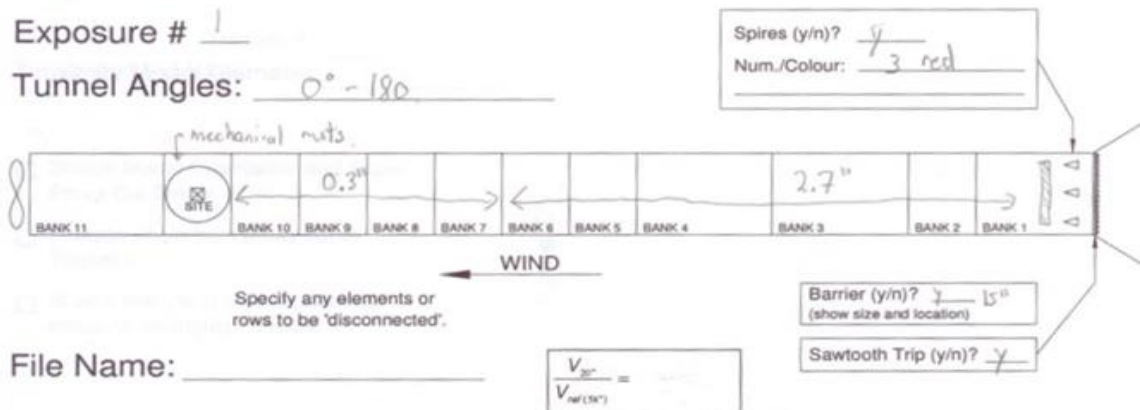


Figure A2: Description of the terrain simulation and the placement of various blocks and obstacles to create the desired terrain. Excerpt taking from wind tunnel log.

Appendix B

Speed: 10000 fps		Exp. d/a	
Freq: 10000 Hz		Exp. d/a	
Sample Time: 1000 seconds		Exp. d/a	
Bagtest Filename: _____		Exp. d/a	
Configuration: _____		Exp. d/a	
1	0-180	1	7
1	0-180	2	8
1	0-180	3	9
1	0-180	4	10
1	0-180	5	11
1	0-180	6	12

Exposure	Tunnel Angle (°)	File Name	Exposure	Tunnel Angle (°)	File Name
1	0-180	GAKP1100-1 Exp R01			
1	0-180	GAKP1100-1 Exp R01			
1	0-180	GAKP1100-1 Exp R01			
1	0-180	GAKP1100-1 Exp R01			
1	0-180	GAKP1100-1 Exp R01			
1	0-180	GAKP1100-1 Exp R01			
1	0-180	GAKP1100-1 Exp R01			
1	0-180	GAKP1100-1 Exp R01			
1	0-180	GAKP1100-1 Exp R01			
1	0-180	GAKP1100-1 Exp R01			
1	0-180	GAKP1100-1 Exp R01			
1	0-180	GAKP1100-1 Exp R01			
1	0-180	GAKP1100-1 Exp R01			
1	0-180	GAKP1100-1 Exp R01			
1	0-180	GAKP1100-1 Exp R01			
1	0-180	GAKP1100-1 Exp R01			
1	0-180	GAKP1100-1 Exp R01			
1	0-180	GAKP1100-1 Exp R01			
1	0-180	GAKP1100-1 Exp R01			
1	0-180	GAKP1100-1 Exp R01			
1	0-180	GAKP1100-1 Exp R01			
1	0-180	GAKP1100-1 Exp R01			
1	0-180	GAKP1100-1 Exp R01			
1	0-180	GAKP1100-1 Exp R01			
1	0-180	GAKP1100-1 Exp R01			
1	0-180	GAKP1100-1 Exp R01			
1	0-180	GAKP1100-1 Exp R01			
1	0-180	GAKP1100-1 Exp R01			
1	0-180	GAKP1100-1 Exp R01			
1	0-180	GAKP1100-1 Exp R01			
1	0-180	GAKP1100-1 Exp R01			
1	0-180	GAKP1100-1 Exp R01			
1	0-180	GAKP1100-1 Exp R01			
1	0-180	GAKP1100-1 Exp R01			
1	0-180	GAKP1100-1 Exp R01			
1	0-180	GAKP1100-1 Exp R01			
1	0-180	GAKP1100-1 Exp R01			
1	0-180	GAKP1100-1 Exp R01			
1	0-180	GAKP1100-1 Exp R01			
1	0-180	GAKP1100-1 Exp R01			
1	0-180	GAKP1100-1 Exp R01			
1	0-180	GAKP1100-1 Exp R01			
1	0-180	GAKP1100-1 Exp R01			
1	0-180	GAKP1100-1 Exp R01			
1	0-180	GAKP1100-1 Exp R01			

Figure B1: Excerpt from wind tunnel log displaying the data logs taken for the wind tunnel tests

## Appendix C

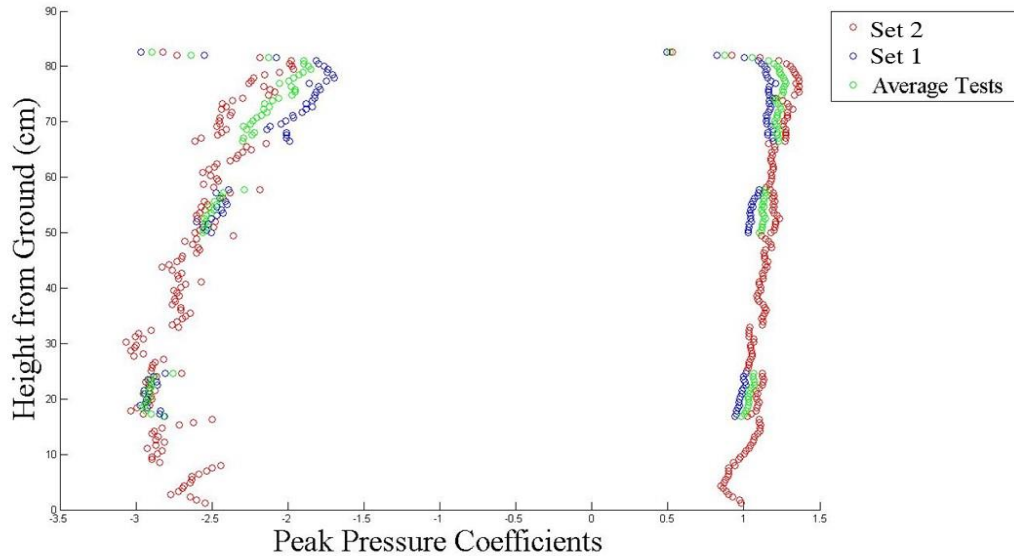


Figure C1: Comparison along the leeward side of  $H/W=2.58$  building. Data are along the height of the building from bottom to the top. The figure compares the peak pressure coefficient values from all wind directions.

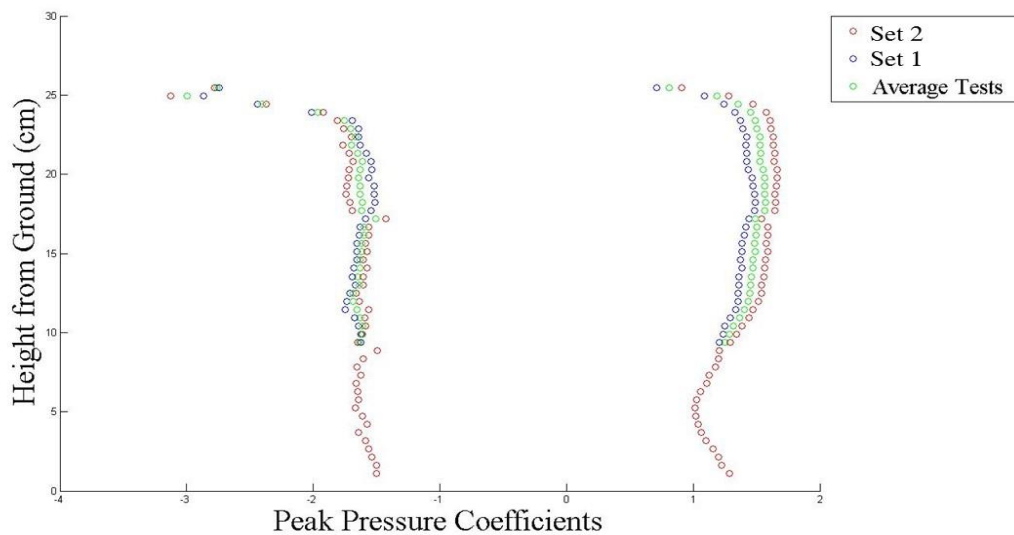


Figure C2: Comparison along the leeward side of  $H/W=0.80$  building. Data are along the height of the building from bottom to the top. The figure compares the peak pressure coefficient values from all wind directions.

## Curriculum Vitae

Name: Emilio S. Hong

Post-Secondary Education and Degrees: University of Western Ontario  
London, Ontario, Canada  
2011-2015, Bachelor of Engineering Science

University of Western Ontario  
London, Ontario, Canada  
2015-2017, Masters of Engineering Science

Honours and Awards: Admission scholarship 2011  
Dean's Honour list 2012, 2013, 2014, 2015  
NSERC USRA 2012, 2013, 2014  
Alan G. Davenport Memorial Scholarship Award 2016

Employment: Undergraduate Researcher 2012-2014  
Teaching Assistant 2015-2017  
Research Assistant 2015-2017

### Journal Publications:

Kopp, G. A., Hong, E., Gavanski, E., Stedman, D., Sills, D. M. L., "Assessment of wind speeds based on damage observations from the Angus (Ontario) Tornado of 17 June 2014", *Canadian Journal of Civil Engineering* Vol. 44 pp 37-44 (2017)

McMillian, A., Dell, M., Zeller, M. P., Cribby, S., Martz, S., Hong, E., Fu, J., Abbas, A., Dang, T., Miller, W., Reid, G., "Disruption of urogenital biofilms by lactobacilli. *Colloids and Surface B: Biointerfaces*". Vol. 86 Issue 1 pp 58-64 (2011)

### Conference Publications:

Hong, E., Kopp, G. A., "Pressure Coefficient Variation on Low, Medium and High Rise Buildings." *2016 CSCE Annual Conference*. CSCE Annual Conference 2016. London, Canada. June – (2016)

Hong, E., Kopp G. A., "Variation of Wall Pressure Coefficients for Low, Medium and High-Rise Buildings." *ICWE Conference Proceedings*. 14<sup>th</sup> International Conference of Wind Engineering, Porto Alegre Brazil. June – (2015)

Hong, E., Stedman, D., Kopp G. A., (2015). "Observations of the wind damage in the Angus (Ontario) tornado of June 17, 2014." *2015 CSCE Annual Conference*. CSCE Annual Conference 2015. Regina, Canada. May – (2015)

### Previous Dissertations:

Hong, E., Variation of wall pressure coefficients on low-rise and high-rise buildings. Bachelor's Thesis, Civil and Environmental Engineering, University of Western Ontario (supervised by G. A. Kopp) (2015)